ULTRASONIC DETECTION OF SIMULATED CORROSION IN 1 INCH DIAMETER STEEL TIEBACK RODS

By

KARL R. OLSEN

A dissertation submitted in partial fulfillment of
the requirements for the degree of

DOCTOR OF PHILOSOPHY

WASHINGTON STATE UNIVERSITY
Department of Civil and Environmental Engineering

August 2009

To the Faculty of Washington State University:

The members of the Committee appointed to examine the dissertation of KARL R. OLSEN find it satisfactory and recommend that it be accepted.

David Pollock, Ph.D. (Chair)

David McLean, Ph.D.

Donald Bender, Ph.D.

William Cofer, Ph.D.

Acknowledgements

"For by him all things were created: things in heaven and on earth, visible and invisible, whether thrones or powers or rulers or authorities; all things were created by him and for him."

Colossians 1:16

First and foremost I would like to thank my parents. Dad, without your encouragement to see beyond my trials I would have given up long ago. I consider it an honor to have you as a father, a mentor and a friend. Mom, thank you your unwavering love, regardless of my accomplishments or failures. I am proud to be your son and thankful for every smile and hug that awaits me every time I see you.

Dr. Pollock, I have learned as much from watching you as I have from listening to your feedback. Your care for your students above your self is evident, and an inspiration. To all those that helped keep me sane throughout this process and remind me that there is more to life than a dissertation: Alan, Neil, Mike, Chuck, Jacob, Rebekah, Jessie, Laura, and Kristina your friendship means more than you know.

Also, this dissertation would not have been possible without funding for this project, which was provided by the U.S. Department of Transportation (USDOT), Transportation Northwest (TransNow) Regional Research Center through contract number 430820. The commercial all-thread tieback rods were provided by Williams Form Engineering Corporation.

ULTRASONIC DETECTION OF SIMULATED CORROSION IN 1 INCH DIAMETER STEEL TIEBACK RODS

Abstract

By Karl R. Olsen
Washington State University
August 2009

Chair: David G. Pollock

The research presented investigates the use of pulse-echo ultrasonic techniques to identify simulated corrosion in steel rods. The primary objective was to quantify loss of cross section due to corrosion of steel tieback rods in earth retention systems. Current techniques require excavation of rods for inspection; however this proposed nondestructive method utilizes the end of the rod protruding from the embankment in conjunction with an ultrasonic pulse-echo system to estimate the reduction in load capacity of the rod. An ultrasonic wave was initiated with a piezoelectric transducer coupled to the end of the rod. The same transducer converted the returning wave into an ultrasonic signal which was used to determine the physical geometry of simulated corrosion. The ultrasonic signal could identify the location of simulated corrosion on the rod using the time between the main bang and the first flaw echo. The diameter of simulated corrosion could be determined from the time between the back echo and the first trailing echo. The length of the corroded region was correlated with the ratio of the first trailing echo and the back echo. Flaw echoes from simulated corrosion could be detected for all transition angles down to 5^{o}. A decrease in the transition angle resulted in a time delay in the arrival of the flaw echo up to 23.8 μs for the 5° transition, which corresponds

to 5.5 in. in steel rods. Williams all-thread commercial tieback rods were tested. Ultrasonic signals generated in Williams rods embedded in various soils showed negligible attenuation of signal amplitude. Simulated corrosion geometry, including location, diameter, and length were inspectable in 1.0 in. diameter Williams tieback rods. Testing showed that ultrasonic testing could be used detected in rod lengths up to 40 feet.

Contents

List of Figures

List of Tables

1 Introduction and Objectives

In 2002, just east of downtown Cleveland, Ohio, several tieback rods in a sheet pile earth retaining wall failed (Esser & Dingeldein, 2007). The failure was due to corrosion and caused a near collapse of the wall. Corrosion in structural steel tieback rods causes a decrease in cross-sectional area, limiting tensile load capacity. Tieback rods are typically buried in soil, eliminating the option of visual inspection without excavation. The research in this study evaluated ultrasonic testing as a method of detecting simulated corrosion in steel rods.

1.1 Tieback Rods

Tieback rods are a vital component of sheet pile retaining walls. The rods connect the outer support structure to anchors (or "deadman") buried in the soil (Figure 1.) The first tieback rods

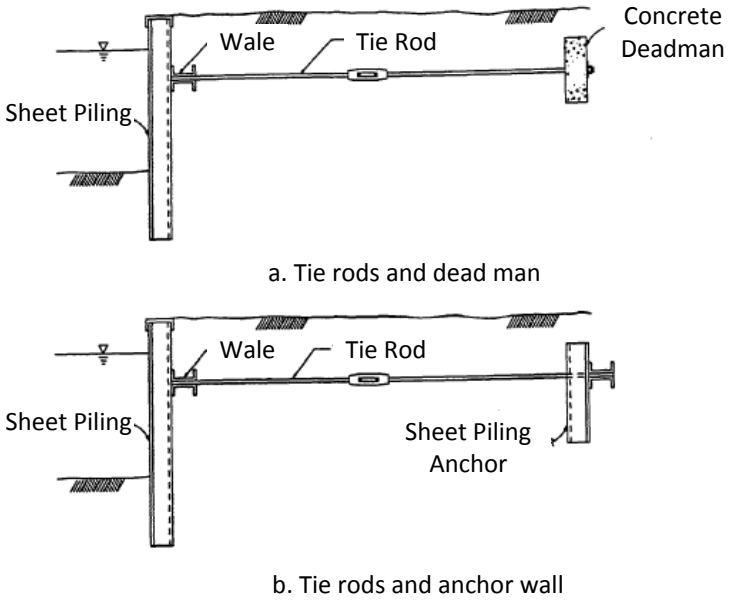

Figure 1. Sheet pile earth retention walls (US Army Corps of Engineers, 1994)

used in commercial construction consisted of A36 (36 ksi yield strength) round stock with upset threads at each end. The majority of rods used in current construction practices, including the Williams Form Corporation tieback rods used in this research, are an all-thread rod with a yield stress of 75 ksi. Developments in corrosion technology have introduced several improvements to tieback rods. Numerous methods for corrosion resistance have been developed (Williams Form Engineering Corp, 2008):

- Epoxy coating
- Pre-grouted rods
- Hot dip galvanizing
- Extruded polyethylene coating
- Coal tar epoxy
- Corrosion inhibiting wax or sheath with grease
- Heat shrink tubing

The selection of rods and corrosion resistance techniques is typically determined by a geotechnical engineer depending upon site conditions (US Army Corps of Engineers, 1994).

1.2 Problem Statement

Older tieback rods are susceptible to corrosion, which may compromise the structural integrity of confined earth embankment systems supporting transportation structures and facilities. Corrosion in buried metal tieback rods is difficult to detect, and the magnitude of associated cross-section loss is particularly difficult to quantify. Since the exposed heads of tieback rods (at the sheet piling face) are typically accessible, an ultrasonic pulse-echo inspection technique has potential for detecting and quantifying cross-section loss due to corrosion. Previous ultrasonic pulse-echo research of steel rods has investigated several geometric properties. This

ultrasonic characterization must be expanded to address a more comprehensive characterization of the rod to accurately assess the reduction in load capacity of a commercial tieback rods.

1.3 Research Objectives

The objectives for this research were divided into two categories. First, use ultrasonic inspection to assess the physical geometry of simulated corrosion in steel rods. Second, evaluate Williams all-thread tieback rods.

1.3.1 Detect Physical Geometry of Simulated Corrosion in Steel Rods

The first set of objectives involved the use of ultrasonic signals to detect the critical physical geometries of a steel rod with simulated corrosion. In previous research, several physical geometries have been detected, including location of flaws, curvature of the rod, diameter of the flaw, and the effect of angled cuts at the end of the rod. The following research objectives were investigated to confirm previous research and develop new techniques to detect other physical geometries.

1. Detect the location of simulated corrosion.
2. Detect the diameter of simulated corrosion.
3. Detect the length of simulated corrosion.
4. Investigate the effect of simulated corrosion transitions on the flaw echo in ultrasonic signals.
5. Develop a normalized amplitude method for assessing attenuation in the transition of simulated corrosion.

1.3.2 Evaluate Threaded Williams Tieback Rods

The second set of objectives involved evaluating Williams tieback rods. The all-thread surface and the surrounding soil affect the ultrasonic wave as it travels through the rod. The following research objectives were investigated to characterize the ultrasonic signal in Williams tieback rods.

1. Determine if ultrasonic response signal can be identified in commercial threaded tieback rods.
2. Determine the effect of various soils on attenuation of ultrasonic signals in commercial threaded tieback rods.
3. Identify simulated corrosion in threaded tieback rods.

1.4 Outline of Dissertation Contents

This dissertation consists of seven chapters. Some background regarding ultrasonic waves is provided in the second chapter. Starting with the fundamentals of wave propagation, the theory is developed and presented, with applications to nondestructive testing. Previous research regarding ultrasonic waves in rods is also summarized in Chapter two. The third chapter describes the experimental setup used in the research presented in the dissertation. Transducer coupling and basic wave velocity tests are included in Chapter three. Chapter four examines the physical geometries of simulated corrosion detectable with ultrasonic pulse echo methods. This includes location, length, diameter, and transition characterization. Chapter five investigates the use of ultrasonic waves in threaded Williams tieback rods. Signal attenuation in soils, maximum detectable rod length, and simulated corrosion in Williams rods are

evaluated. Chapter six addresses guidelines for developing an ultrasonic inspection strategy for use by a state Department of Transportation (DOT). Finally, conclusions are presented in the seventh chapter.

2 Background and Literature Review

This chapter presents a background of ultrasonic waves. An overview of fundamental wave propagation provides the basis for understanding ultrasonic waves. The use of ultrasonic waves in nondestructive testing (NDT) is presented, including previous research pertaining specifically to steel rods.

2.1 Pressure Wave Properties

A wave is a disturbance that propagates through time and space. Energy is transferred from one point to another via waves. A single frequency bulk wave is characterized mathematically by the wavelength (λ) and amplitude (A) of the signal (Figure 2). The wavelength is the distance between two adjacent peaks in the wave cycle and the amplitude is the maximum displacement of the disturbance from the undisturbed position. The frequency (f) of the wave is defined as

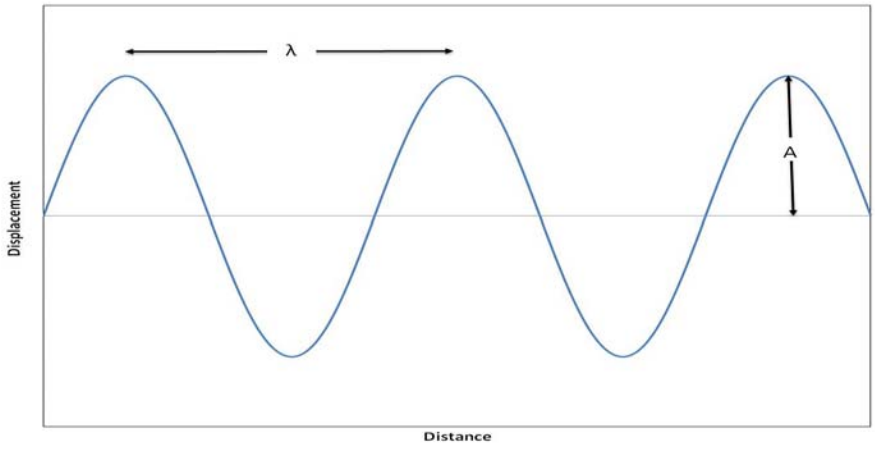

Figure 2. Mathematical wave characterization

the number of oscillations that occur in one second and the period (T) is the time to complete one oscillation.

Phase Velocity

The speed at which the bulk wave travels though a medium is called the phase velocity (v_p) and is calculated with the following equation (Main, 1988).

$$\boldsymbol{v_p = \frac{\lambda}{T}} \qquad \textbf{Equation 1}$$

The phase velocity is dependent upon the type of wave traveling in the medium. Longitudinal and shear waves will be considered in this research. Longitudinal waves exhibit particle motion in the direction of wave propagation. Shear waves exhibit particle motion orthogonal to the direction of wave propagation.

Snell's Law

When a longitudinal wave encounters a boundary surface, longitudinal and shear waves are reflected back into the medium at angles determined by Snell's Law (Figure 3). The resulting longitudinal wave reflects at an angle equal to the incident angle. The reflected shear wave has

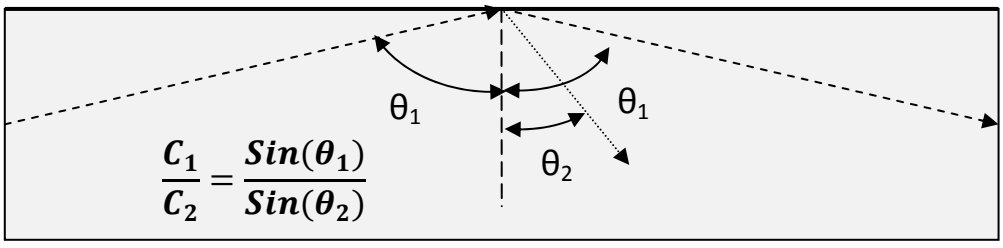

Figure 3. Diagram of Snell's Law

a reflected angle (θ_2) that is dependent upon the incident angle (θ_1), the incoming longitudinal wave speed (c_1), and the reflected shear wave speed (c_2).

Attenuation

As a wave propagates through a medium, the wave displacement decreases with distance due to scattering and absorption. Scattering is the reflection of the wave in directions other than its original direction of propagation. Absorption is the conversion of the wave energy to other forms of energy. Attenuation is the decay rate of the wave as it propagates through material due to scattering and absorption. The attenuation of displacement in a wave as it travels through a medium is characterized by Equation 2, where w_o is the initial displacement, α is the coefficient of attenuation, and x is the distance along the rod (Kolsky, 1963).

$$w = w_o e^{\alpha x} \quad \textbf{Equation 2}$$

2.2 Two methods for Solving the Wave Equation

In a bounded medium, such as the steel rods used in this research, waves are reflected from the boundaries. Solutions can be found by solving the wave equation with cylindrical boundaries. The wave equation, in cylindrical coordinates, in an unbounded medium is defined as follows:

$$\rho \frac{\partial^2 u_r}{\partial t^2} = (l + 2\mu) \frac{\partial \Delta}{\partial r} - \frac{2\mu}{r} \frac{\partial \omega_z}{\partial \theta} + 2\mu \frac{\partial \omega_\theta}{\partial z} \quad \textbf{Equation 3}$$

$$\rho \frac{\partial^2 u_\theta}{\partial t^2} = (l + 2\mu) \frac{\partial \Delta}{r \partial \theta} - 2\mu \frac{\partial \omega_r}{\partial z} + 2\mu \frac{\partial \omega_z}{\partial r} \quad \textbf{Equation 4}$$

$$\rho \frac{\partial^2 u_z}{\partial t^2} = (l + 2\mu) \frac{\partial \Delta}{\partial z} - \frac{2\mu}{r} \frac{\partial (r\omega_\theta)}{\partial r} + \frac{2\mu}{r} \frac{\partial \omega_r}{\partial \theta} \quad \textbf{Equation 5}$$

where z is the axis of the waveguide, ρ is the density of the medium, u_r, u_θ, u_z, are the local displacements of the medium along each axis, r is the radius, t is time, l and μ are Lame's constants. The dilatation (Δ) and elements of the rotation tensor (ω_r, ω_θ, ω_z) are given by:

$$\Delta = \frac{1}{r} \frac{\partial (a u_r)}{\partial r} + \frac{1}{r} \frac{\partial u_\theta}{\partial \theta} + \frac{\partial u_z}{\partial z} \quad \textbf{Equation 6}$$

$$\omega_a = \frac{1}{2} \left[\frac{1}{r} \frac{\partial u_z}{\partial \theta} - \frac{\partial u_\theta}{\partial z} \right] \quad \textbf{Equation 7}$$

$$\omega_\theta = \frac{1}{2} \left[\frac{\partial u_r}{\partial z} - \frac{\partial u_z}{\partial r} \right] \quad \textbf{Equation 8}$$

$$\omega_z = \frac{1}{2r} \left[\frac{\partial (r u_\theta)}{\partial r} \frac{\partial u_r}{\partial \theta} \right] \quad \textbf{Equation 9}$$

The stress in the rod is used as a boundary condition. At the surface of the rod, the three stress components (σ_{rr},$\sigma_{r\theta}$,σ_{rz}) must equal zero. The stress-deformation relations are as follows:

$$\sigma_{rr} = l\Delta + 2\mu \frac{\partial u_r}{\partial r} \quad \textbf{Equation 10}$$

$$\sigma_{r\theta} = \mu \left[\frac{1}{r} \frac{\partial u_r}{\partial \theta} + r \frac{\partial}{\partial r} \left(\frac{u_\theta}{r} \right) \right] \quad \textbf{Equation 11}$$

$$\sigma_{rz} = \mu \left(\frac{\partial u_r}{\partial z} + \frac{\partial u_z}{\partial r} \right) \quad \textbf{Equation 12}$$

General solutions to the wave equations are considered for harmonic waves with exponential propagation in the z direction along a rod. For the general case of vibration, the equations for displacements are as follows:

$$u_r = U(r)\cos n\theta e^{i(kz-\omega t)} \quad \textbf{Equation 13}$$

$$u_\theta = V(r)\sin n\theta e^{i(kz-\omega t)} \quad \textbf{Equation 14}$$

$$u_z = W(r)\cos n\theta e^{i(kz-\omega t)} \quad \textbf{Equation 15}$$

For longitudinal waves the displacement is a function of z and r, therefore the derivative with respect to θ is zero. The displacement u_θ is also zero due to symmetry. Therefore, Equation 3, Equation 4 and Equation 5 reduce to:

$$\frac{\partial^2\Delta}{\partial r^2} + \frac{1}{r}\frac{\partial\Delta}{\partial r} + h'^2\Delta = 0 \quad \textbf{Equation 16}$$

$$\frac{\partial^2\omega_\theta}{\partial r^2} + \frac{1}{r}\frac{\partial\omega_\theta}{\partial r} + \frac{\omega_\theta}{r^2} + \kappa'^2\omega_\theta = 0 \quad \textbf{Equation 17}$$

where:

$$h'^2 = \frac{\rho p^2}{(l+2\mu)} - \gamma^2 \quad \textbf{Equation 18}$$

$$\kappa'^2 = \frac{\rho p^2}{\mu} - \gamma^2 \quad \textbf{Equation 19}$$

Where the frequency of the waves is p/2π and the phase velocity is given by p/γ Since h' and κ' are constants, setting r' = h'r and r'' = κ'r converts Equation 16 and Equation 17 into zero order and first order forms of the Bessel equation, respectively.

$$\frac{\partial^2 \Delta}{\partial r'^2} + \frac{1}{r'}\frac{\partial \Delta}{\partial r'} + \Delta = 0 \quad \text{Equation 20}$$

$$\frac{\partial^2 \omega_\theta}{\partial r''^2} + \frac{1}{r''}\frac{\partial \omega_\theta}{\partial r''} - \frac{\omega_\theta}{r''^2} + \omega_\theta = 0 \quad \text{Equation 21}$$

At this point two separate methods are available for solving the wave equation. These include the mode and the ray approach. Each of the methods are described below.

Mode Approach (Dispersion Diagrams)

The solution to the wave equation using the Bessel function subject to appropriate boundary conditions results in a number of solutions that form continuous propagating modes of vibration. The velocity-frequency relationship of the individual modes can be displayed as a set dispersion curves (Figure 4). Each line in the diagram represents a different mode of vibration.

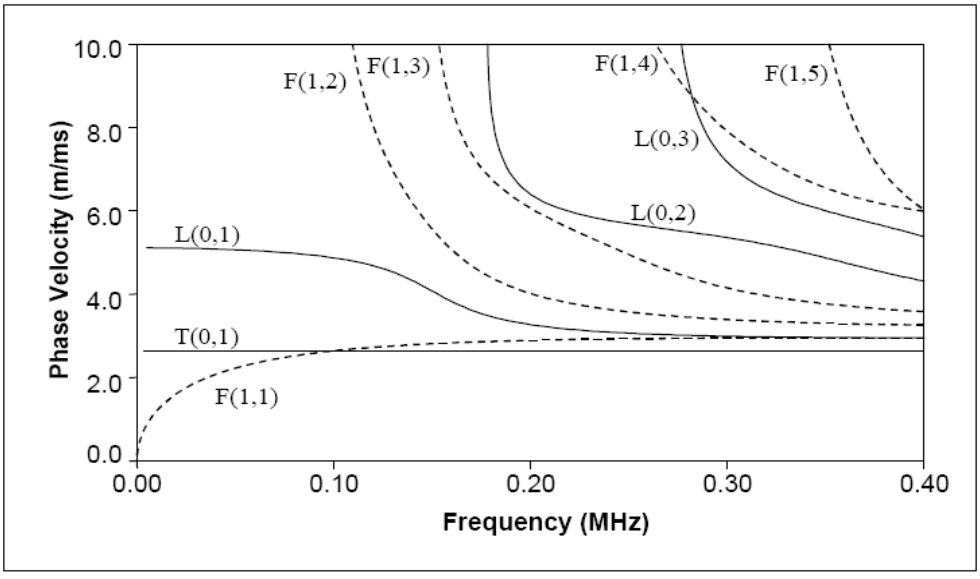

Figure 4. Dispersion diagram for a 0.79 in. diameter steel rod in a vacuum (Beard, Lowe, & Cawley, 2001)

Flexural modes are noted by "F", longitudinal modes are noted by "L", and the torsional mode is noted by "T". This facilitates determination of the frequency to generate in order to initiate specific modes. The frequency of the ultrasonic signal generated in the following research is in the range that will initiate hundreds of modes of vibration.

Ray Approach

The second approach for solving the wave equation is the ray approach. This method involves a simplification of Equation 20 using a differentiation by parts identity.

$$\frac{1}{r'}\frac{\partial}{\partial r'}\left(r'\frac{\partial \Delta}{\partial r'}\right) + \Delta = 0 \quad \text{Equation 22}$$

Assume that Δ varies rapidly compared to changes in r'. Then r' can be pulled outside the derivative. The simplification is based on the assumption that the wavelength of the ultrasonic signal is significantly smaller than the diameter of the rod.

$$\frac{\partial^2 \Delta}{\partial r'^2} + \Delta = 0 \quad \text{Equation 23}$$

The solution for this equation is given as:

$$\Delta = e^{\pm i r'} \quad \textbf{Equation 24}$$

This solution approximates the wave as a bulk wave. Also, since the wavelength is assumed to be significantly smaller than the diameter of the rod, the surface of the rod can be approximated as a flat plate. Assuming a point source for the generation of the wave, Figure 5

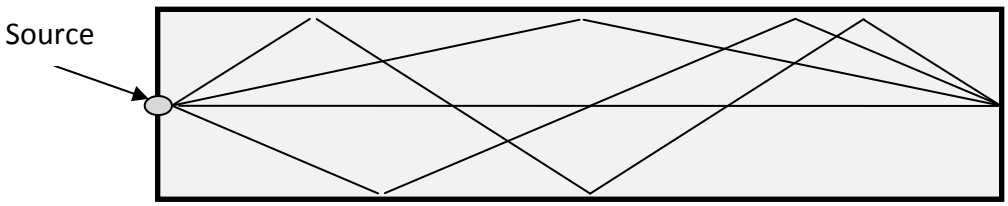

Figure 5. Ray approach for solution of wave equation

represents four of the paths with the shortest travel distance the wave can take from the source to a common point at the end of the rod for longitudinal wave propagation. This depiction allows insight into how the wave propagates through the rod.

The research presented uses the ray approach as opposed to the mode approach for two reasons. First, the pulse-echo method generates a pulse in the steel rod rather than a continuous vibration. Second, the diameter of the steel rods inspected (1.0 in.) is approximately 20 times greater than wavelength generated by the 5MHz ultrasonic transducer in steel. This allows for the assumption used in the ray approach.

2.3 Background in Ultrasonic Waves in Rods

Ultrasonic waves are defined as cyclic pressure waves with a frequency greater than the threshold of human hearing. Although human hearing varies from person to person, the ultrasonic range is considered to include all pressure waves above 20 kHz. The following section presents some fundamental concepts and terminology from previous literature. This

will establish the theoretical foundation that will be built upon to compile a more complete understanding of ultrasonic waves in rods.

2.3.1 Ultrasonic Wave

Ultrasonic waves can be initiated in steel rods using a piezoelectric transducer. An electric signal was sent to the transducer converting electrical energy to mechanical energy in the form of a pressure wave. When coupled to the end of a steel rod the wave is generated in the steel rod and proceeds to travel the length of the rod. At this point a receiving transducer can detect the signal at the other end of the rod, or if the end of the rod is not accessible, the wave reflects from the end surface of the rod and travels back to the transducer. As the wave returns to the front end, the transducer converts the mechanical energy into electrical energy, and the electrical signal is recorded by the computer. The ultrasonic signal for a straight rod without any flaws is shown below (Figure 6). The main bang represents the generation of the ultrasonic wave. The small signal following the main bang is a ringing out of the piezoelectric transducer. The next signal that appears is the first back echo, which represents the front of

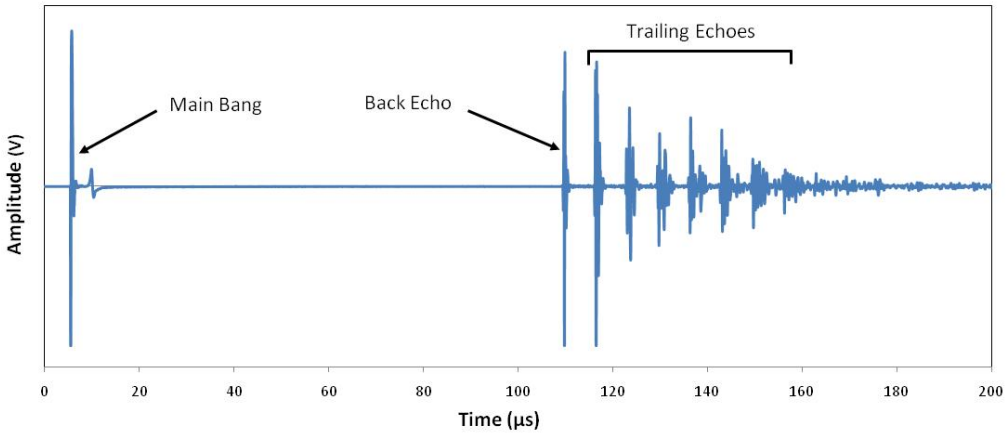

Figure 6. Standard ultrasonic signal from 1.0 ft. long 1.0 in. diameter circular rod

the pressure wave that reflected from the end of the rod and returned to the transducer. Several trailing echoes follow the first back echo, and these will be discussed later in more depth. For a rod with a flaw, an early echo will appear in the signal dependent upon the location of the flaw along the rod. A portion of the ultrasonic wave will reflect from the flaw and return to the transducer before the back echo (Figure 7). Further inspection of the ultrasonic signal reveals a consistent spacing between the trailing echoes after the back echo (Figure 8). Research has shown (Light & Joshi, 1987) that the spacing is due to mode

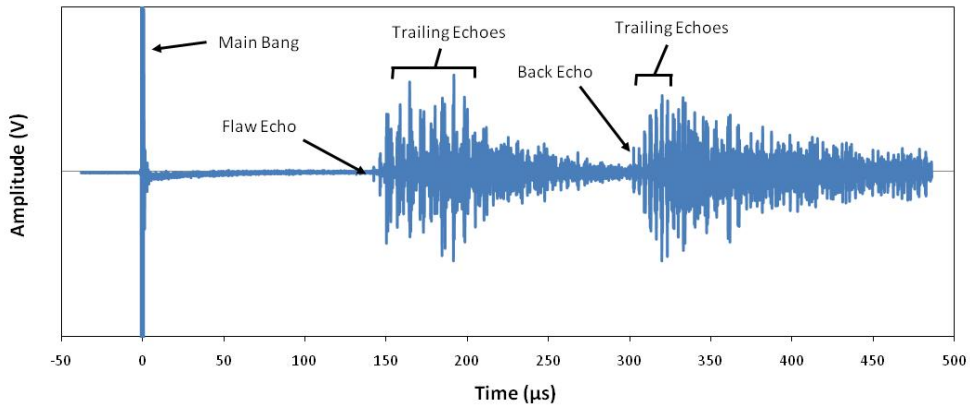

Figure 7. Ultrasonic Signal for 3.0 ft. long 1.0 in. diameter rod with a 2.0 in. length of 0.5 in. reduced diameter starting at 17.0 in. from the transducer

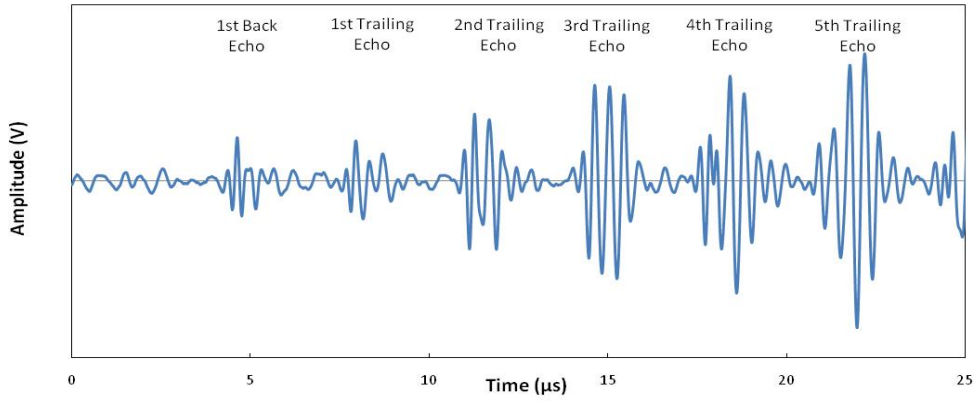

Figure 8. Spacing of trailing echoes for 3.0 ft. long 1.0 in. diameter rod with a 2.0 in. length of 0.5 in. diameter simulated corrosion

conversion when the wave reflects from the cylindrical surface of the rod. Each time a wave is reflected at a boundary, the reflected energy produces a transverse wave as well as a longitudinal wave (Figure 9). Since the transverse wave travels at approximately half the speed of the longitudinal wave and reflects at a steeper angle, the result is a delay in the signal after the first echo. The time delay is dependent upon the diameter of

$$\Delta t = \frac{D\sqrt{C_1^2 - C_2^2}}{C_1 C_2} \quad \textbf{Equation 25}$$

the rod as well as the ratio of wave speeds. Light and Joshi reported Equation 25 correlating the diameter of the rod (D) to the time between echoes (Δt), based upon the speed of longitudinal wave propagation (C_1) and the speed of transverse wave propagation (C_2). This delay repeats itself, as the reflected transverse wave mode converts into a longitudinal wave on the opposite side.

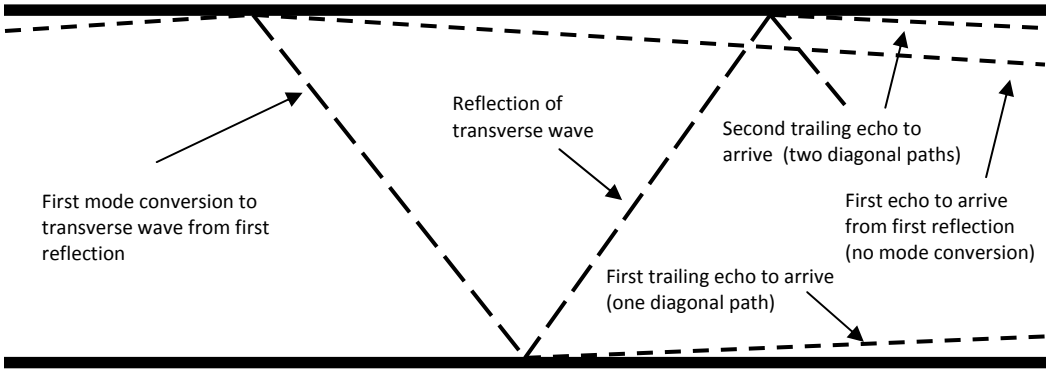

Figure 9. Trailing echoes reflection diagram

2.4 Ultrasonic Applications

Ultrasonic waves have different applications in the natural world and are utilized in an array of current technologies. Ultrasound is used by many animals, including bats and dolphins. Humans have harnessed the use of ultrasonic signals for a broad range of technologies. These include medical ultrasound, cleaning techniques, cool mist humidifiers, real time locating systems (RTLS), as well as nondestructive testing techniques.

2.4.1 Previous Ultrasonic Research

Wave propagation in a free rod was first studied quantitatively in the late 19th century by Pochhammer (Pochhammer, 1876). The study of fundamental longitudinal and flexural modes in solid circular cylinders was studied in the 1940's by Hudson (Hudson, 1943) and Davies (Davies, 1948). Further research has focused on specific aspects of ultrasonic waves in steel rods. This includes location of flaws and cracks, section loss due to corrosion, attenuation due to the end condition of the rod, and curvature of the rod.

Location of Flaws

Pulse-echo techniques are often implemented to detect the length of a rod by generating a wave with an ultrasonic transducer and recording the time required for the pulse to reflect from the back surface and return to the transducer. The wave velocity is then used to convert the time to the length of the material. Similarly when an ultrasonic pulse is reflected from an internal flaw, the stress wave returns to the transducer in less time than the echo from the back

surface. This time to the flaw or crack can be used to determine the length from the transducer to the flaw location (Bray & Stanley, 1989).

Section Loss

The Baltimore Gas and Electric Company developed a technique for evaluating the integrity of anchor bolts (Niles, 1996). This method used ultrasonic nondestructive evaluation to monitor section loss of anchors used to guy steel transmission poles. Specifically, the cylindrically guided wave technique (CGWT), developed by Light and Joshi (Light & Joshi, 1987), was used. This technique correlates the spacing of trailing echoes in the ultrasonic signal with the diameter of the region with reduced cross section. This method is described in more detail in Chapter 4.

End Condition of Rods.

A research group at the University of London used a guided ultrasonic inspection technique to monitor several geometric characteristics of steel post-tensioned cables, and rock bolts in mines (Beard, Lowe, & Cawley, 2001). One of the geometries investigated was the cut angle at the end of the rod and the resulting loss in amplitude of the ultrasonic signal. The end angle was cut with a circular bench saw and with a variation in the angle from 0° to 55^{o} measured from the axis normal to the longitudinal axis of the cable or bolt. The signal (Figure 10) experienced a near linear loss in signal strength from 0^{o} to 10^{o}. At 10° the maximum loss of 40 dB was reached. After the initial loss, the signal maintained consistent signal strength for angle

cuts between 10° and 55°. This shows that the signal was detectable regardless of end condition angle up to 55°.

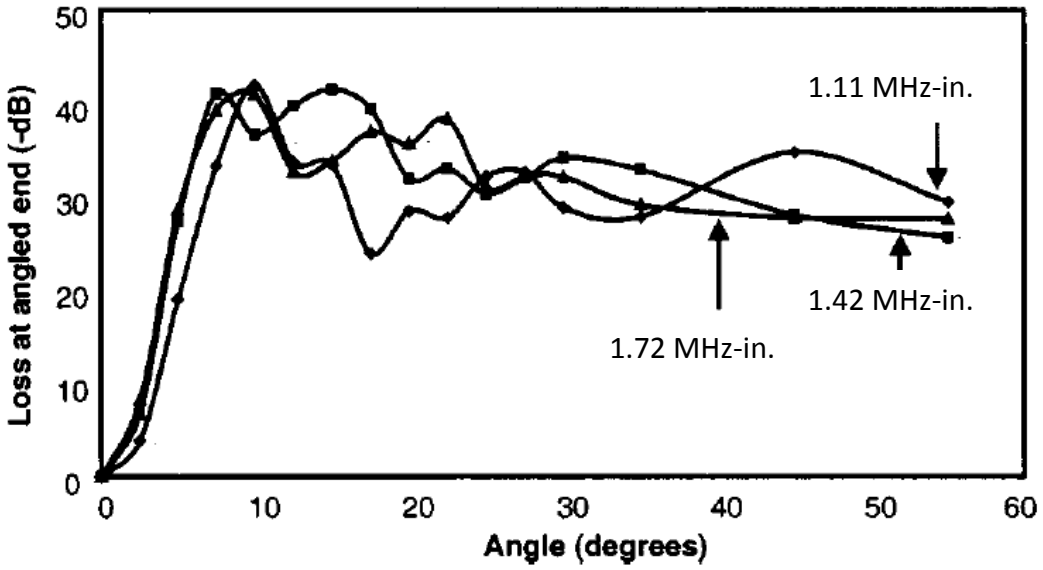

Figure 10. End angle effect on signal strength (Beard, Lowe, & Cawley, 2001)

Curvature in Steel Rods

The curvature of a rod has an effect on the ultrasonic signal. The effect of deformation in bolts was investigated in relation to the shift in overall signal centroid (Pollock, 1997). As the rod was deformed the area of direct line of sight to the end of the rod was decreased (Figure 11), thus shifting the energy into the trailing echoes (Figure 12.) The relative amplitudes of the back echo and trailing echoes were dependent upon the deformation of the rod. This shows that an ultrasonic wave echo is still detectable for deformations that eliminate a direct line of sight

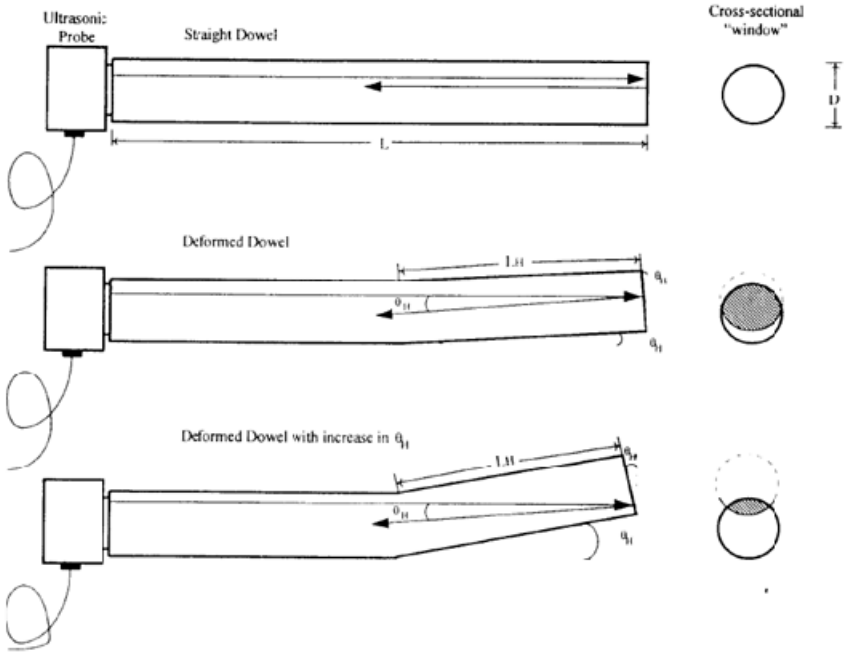

Figure 11. Deformation of the rod (Pollock, 1997)

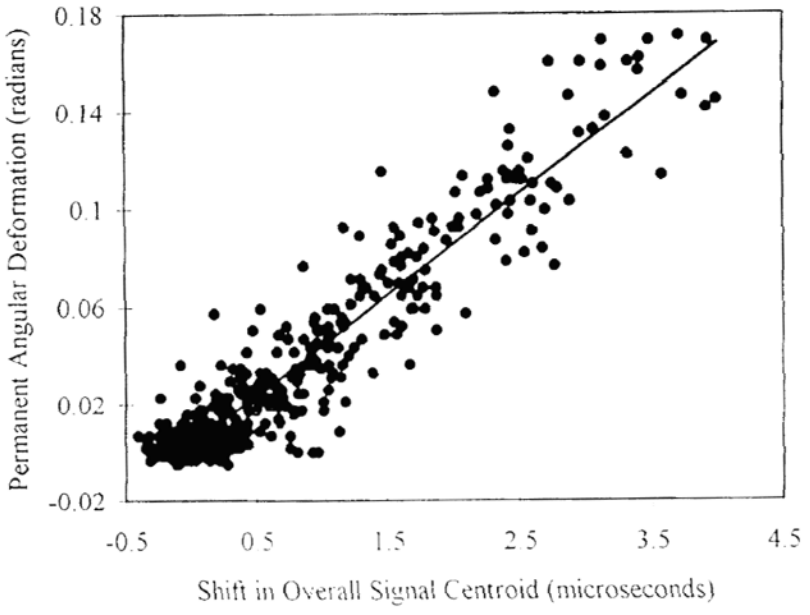

Figure 12. Shift in signal centroid due to angular deformation of rod (Pollock, 1997)

between the transducer and the reflection of interest. Further research at the University of London provided results that show a decrease in amplitude of the back echo for a rod with uniform curvature (Figure 13). A straight rod 1.2 m in length was compared with a 1.2 m rod of uniform curvature with 30 mm of center deflection. This shows that the curvature in a rod decreases the ultrasonic signal amplitude, but does not completely eliminate the signal, allowing detection of reflections in curved rods.

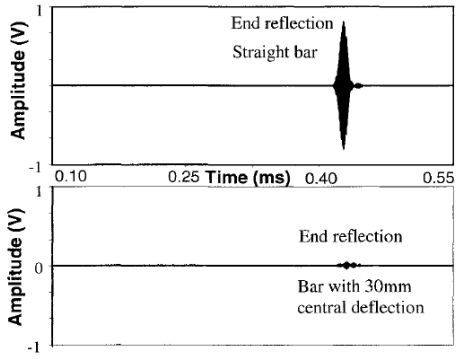

Figure 13. Time traces for a 1.2 m straight rod and a similar rod with constant curvature corresponding to 30mm of center deflection. (Beard, Lowe, & Cawley, 2001)

3 Experimental Setup and Testing

This chapter describes the ultrasonic test system that was used in this research. This particular test setup used commercial ultrasonic transducers for converting an electric pulse into a mechanical wave and then converting the reflected wave back into an electric signal. A LabVIEW program was developed for data acquisition using a desktop computer. Also, a transducer selection criterion was developed for tieback rods.

3.1 Experimental Setup

Ultrasonic testing is a common nondestructive technique. The test setup used to conduct all testing is shown in Figure 14. An ultrasonic pulse was created using a Panametrics 5058-PR Pulser Receiver in conjunction with a Parametrics M1042 piezo-electric transducer. Several transducers were available, with various diameters (0.125 in., 0.25 in. and 0.5 in.) and frequencies (2.25MHz, 5MHz, and 10 MHz). The 5MHz, 0.5 in. diameter M1042 magnetic

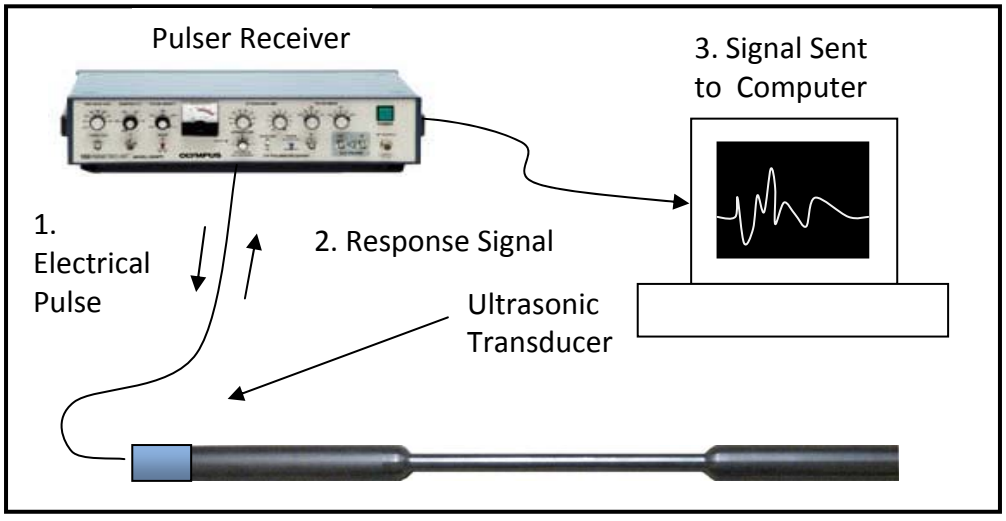

Figure 14. Ultrasonic pulse-echo test setup

transducer was used for all tests unless otherwise specified. The pulse generated by the transducer traveled through the specimen, reflecting from various surfaces, and returned to the transducer. The response signal varied dependent upon the physical geometry and material properties of the specimen. A typical ultrasonic signal is shown in Figure 7, identifying the major components of the signal including the main bang, flaw echo, back echo, and the trailing echoes. These signals were analyzed to characterize the flaws in a specimen.

3.2 Labview Program

A LabVIEW VI program was designed for the data acquisition of the research. The program operated only as data acquisition and did not involve any output into the pulser/receiver. The LabVIEW card was an NI PCI-5152 digitizer. The card read one billion samples per second (1 GS/s) per channel at 8-bit resolution. This allowed the program to effectively read at 1 GHz, which is capable of reading a 500 MHz signal without any aliasing, in order to satisfy the upper bound of the Nyquist criterion.

3.3 Transducer Characterization and Selection

The selection of the transducer is vital when designing an ultrasonic test method. Transducers are available commercially, or can be designed and fabricated for specific situations. Specially designed transducers can be fabricated to achieve a very narrow bandwidth signal, which can be useful in isolating specific frequencies during signal generation. For this research commercial transducers were used to limit the production cost for field

inspections. The main variables in commercial transducers are the diameter of the transducer and the frequency of the ultrasonic signal generated. The following is a list of transducers available for testing of the steel rods in this research (Table 1.) Using a 1.0 in. diameter rod three feet long with no flaws, the maximum amplitude of the back echo for each transducer was recorded (Figure 15.) The data shows that the 5 MHz transducers with 0.5 in. diameter provided the largest amplitude. Transducers which produce large echo amplitudes will

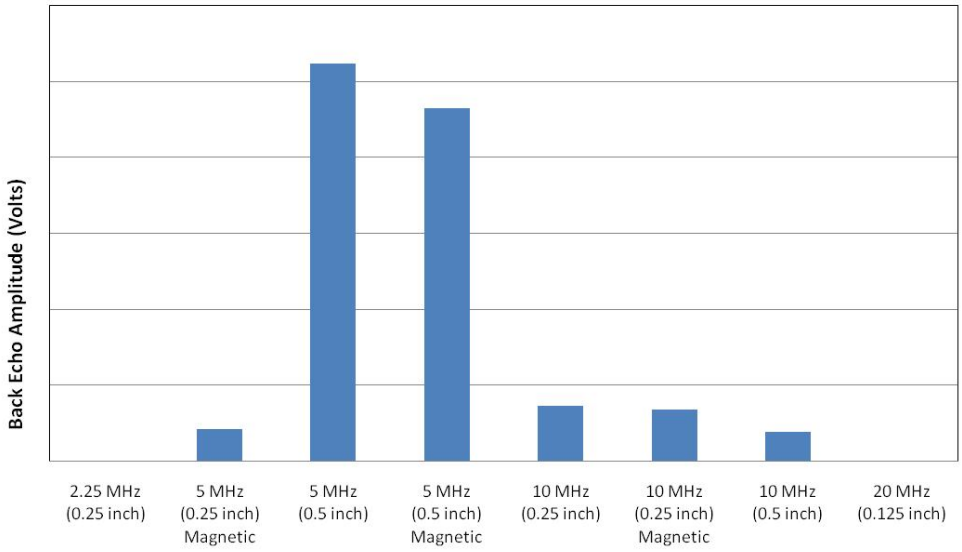

Figure 15. Transducer amplitude comparison on a rod with no simulated corrosion

increase the maximum detectable length of rod. The transducers were also tested to make sure they can detect a reduction in diameter from 1.0 in. to 0.75 in located 2 in. along a 6 in. long rod with a 1 in. diameter. The signal response was measured to find the maximum amplitude of the flaw echo and back echo (Figure 16). The 0.5 in. diameter 5 MHz transducers provided the maximum flaw echo and back echo amplitudes at a 40 dB gain setting

Table 1. Commercial transducers used in selection process

	Manufacturer (Model #)	Frequency	Diameter	Magnetic
	Xactex (CM-HR 1/4-2.25)	2.25 MHz	 0.25 in.	No
	Olympus NDT (M1057)	5 MHz	 0.25 in.	Yes
	Xactex (CM-HR 1/2-5)	5 MHz	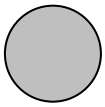 0.50 in.	No
	Olympus NDT (M1042)	5 MHz	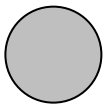 0.50 in.	Yes
	Xactex (CM-HR 1/4-10)	10 MHz	 0.25 in.	No
	Olympus NDT (M1054)	10 MHz	 0.25 in.	Yes
	Xactex (CM-HR 1/2-10)	10 MHz	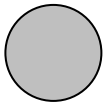 0.50 in.	No
	Xactex (CM-HR 1/8-20)	20 MHz	 0.125 in.	No

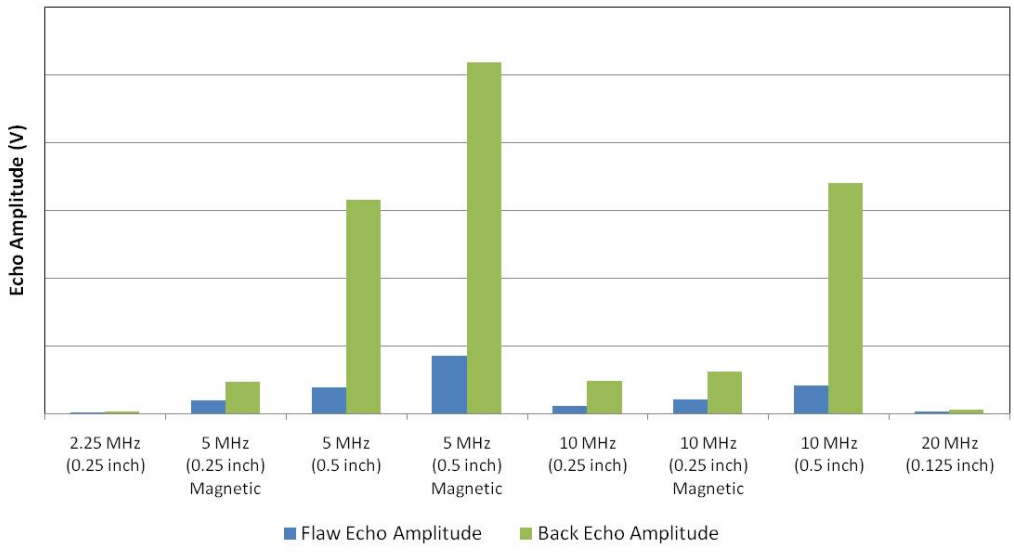

Figure 16. Flaw echo and back echo of rod with a 0.25 in. reduction in diameter

on the pulser-receiver. The 5MHz 0.5in. diameter magnetic transducer (Olympus NDT - M1042) was selected to inspect the rods. This transducer provided the largest echo amplitudes resulting in increased range of inspection for rod length, and the magnetic surface provided a consistent coupling force.

3.4 Wavelength in Steel Rod

This research investigated the use of ultrasonic waves to detect flaws in steel rods. To ensure bulk wave propagation, the wavelength of the ultrasonic pulse should be at least one order of magnitude less than the diameter of the rod (Bray & Stanley, 1989). The wavelength (λ) is calculated based upon the frequency (ω) of the transducer and the wave speed (C) in the specific medium.

$$\boldsymbol{\lambda = \frac{C}{\omega}} \qquad \textbf{Equation 26.}$$

Thus, to ensure a bulk wave in a 1.0 in. diameter rod, the wavelength must be less than 0.1 in., which corresponds with a transducer frequency greater than 2.28 MHz in a steel rod. The wavelength of the ultrasonic signal will determine the minimum flaw detectable in the specimen. A general rule states that the minimum detectable flaw dimension is approximately the wavelength of the ultrasonic pulse frequency introduced into the medium (Figure 17). In this research pulse-echo testing was evaluated as a method to detect a 0.125 in. minimum dimension.

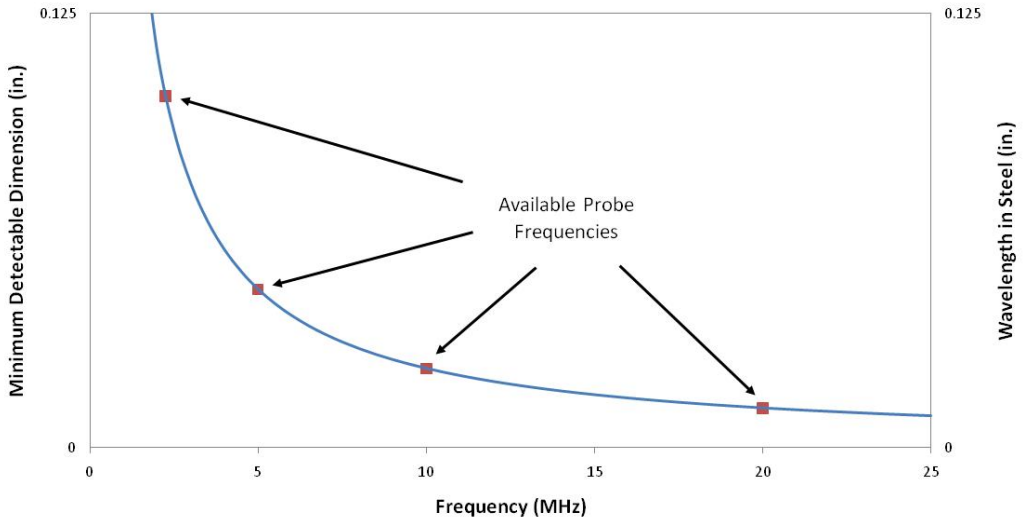

Figure 17. Minimum detectable flaw dimension in steel for multiple ultrasonic pulse frequencies

3.5 End Preparation and Transducer Coupling

The end of each rod tested was machined at a 90 degree angle relative to the longitudinal axis of the rod. A significant variation in the amplitude of the signal can occur due to coupling of the transducer to the rod. Contaminants located between the transducer and the end of the rod may result in poor coupling. Therefore, the end of each rod was cleaned, and a couplant gel

was applied before the transducer was coupled to the end of the rod. Without the gel, the transducer could not effectively couple the ultrasonic signal into the rod, resulting in an extremely poor ultrasonic wave, if any at all. A magnetic transducer was used in most tests to provide a consistent adhering force between the transducer and the end of the rod.

3.6 Steel Rods Used in Testing

Two types of steel rods were used in this research (Figure 18). 12L14 steel rods were used for fabricating and testing various geometries of simulated corrosion. Williams 75 ksi all-thread tieback rods were used to confirm detection of ultrasonic waves in actual tieback rods. The properties of the 12L14 steel and Williams grade 75 steel are shown in Table 2.

Williams tieback rod 12L14 cold drawn rod stock

Figure 18. Williams commercial tieback rod and 12L14 rod stock used in testing

12L14 Steel

The simulated corrosion geometries were machined from 1 in. diameter cold-rolled 12L14 steel. 12L14 is a lead-based steel with a smooth surface that is ideal for machining. The steel is cold drawn and fabricated according to ASTM A108 (ASTM Standard A108, 2007) or ASTM A29 (ASTM Standard A29, 2005).

Williams Grade 75 All-Thread Tieback Rods

Williams 1 in. diameter tieback rods were used to evaluate the detection of ultrasonic waves in commercial rods. The grade 75 all-thread rods were a continuously threaded rod specially designed to be used as concrete forming tie rods and anchors. All-thread tieback rods are available in lengths up to 50 feet. The rods are manufactured with a special thread designed to meet the requirements of ASTM A615 (ASTM Standard A615, 2008).

Table 2. Properties for 12L14 steel and Williams grade 75 tieback rod

Property	12L14	Williams tieback rod
Density (lbs/ft^3)	481 - 501	481 - 501
Poisson's Ratio	0.27 - 0.30	0.27 - 0.30
Elastic Modulus (ksi)	27,560 - 30,460	27,560 - 30,460
Tensile Strength (ksi)	78	100
Yield Strength (ksi)	60	75

3.7 Velocity Calculation for Steel Rods

Determining the wave speed in the steel specimens was necessary for calculating specific geometries of the steel. Ultrasonic signals were recorded for 1.0 ft. long sections of 12L14 steel and grade 75 Williams tieback rods. It was necessary to determine the wave speed using the

first and second back echo. A potential delay in the signal can occur at the main bang, because the signal is measured as the electrical impulse enters the transducer, but the back echoes are measured when the ultrasonic wave impacts the transducer. A full signal, containing two back

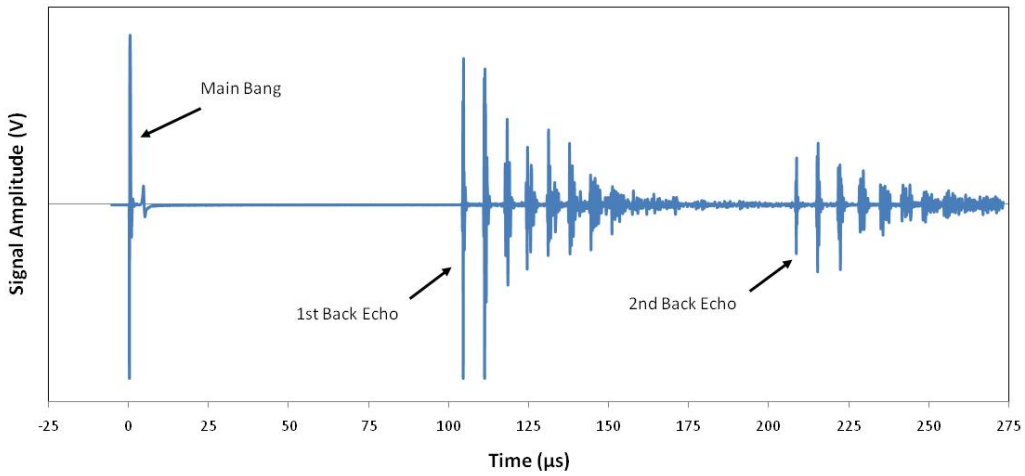

Figure 19. Full ultrasonic signal for 1.0 ft. long 1.0 in. diameter 12L14 steel rod for calculating wave speed

echoes was recorded (Figure 19). To determine the arrival time of the back echo, it was necessary to determine when the back echo signal first rises above the noise. The graphs of the first and second back echoes are shown below to determine the start time of each back echo (Figure 20.) To find the start time, it was first necessary to inspect the main bang signal. The direction that the signal amplitude first travels above or below the horizontal time axis determines the direction of the arrival of the back echoes. In the case shown, the main bang travels in the negative direction first; thus the arrival of the first and second back echoes will occur in the negative direction. Individual points were plotted in the graphs to visualize the departure of the echoes from the signal noise. The arrival times of the main bang and first and

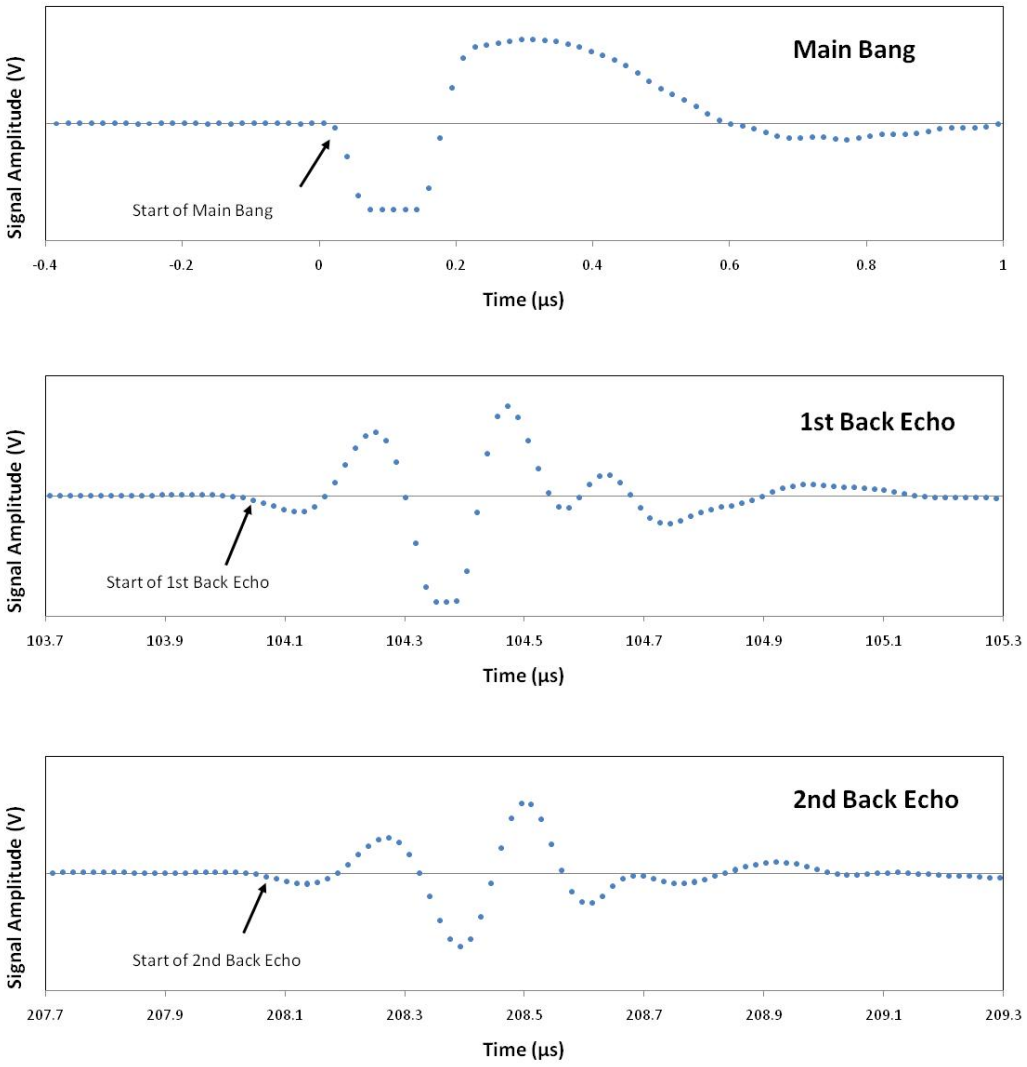

Figure 20. Main bang and first and second back echoes for 1.0 ft. long 1.0 in. diameter steel rod

second back echoes were recorded (Table 3). Then, the time between the first and second back echoes was divided by two to find the wave speed per foot of rod. Two lengths are necessary to account for the wave traveling down the rod and then returning to the transducer. The bulk longitudinal wave speeds for the steel used in the following research are shown below (Table 4.) The 12L14 Steel used for the simulated corrosion rods and the Williams tieback rods

Table 3. Arrival time of ultrasonic signal components.

Signal Component	Overall Time
Main Bang	0.00 μs
1st Back Echo	104.02 μs
2nd Back Echo	208.05 μs

Table 4. Wave speed of 12L14 steel and 75 ksi Williams steel rods

Steel Specification	Longitudinal Wave Speed (c_l)
12L14 Steel	19,220 ft/s
75 ksi Williams	19,190 ft/s

exhibited nearly identical wave speeds. The potential delay of the ultrasonic signal entering the rod was then calculated. An accurate wave speed was calculated between the first and second back echoes, this time was subtracted from the time between the main bang and first echo to calculate the time delay. The delay was calculated to be -0.01 μs. A negative delay is physically impossible, but since the time between data points is 0.018 μs, the error is due to uncertainty in the measurement. Thus, the delay between the start of the main bang and the signal entering the rod is considered negligible.

4 Detecting Physical Geometry of Simulated Corrosion

Corrosion is a primary danger that will compromise the strength of steel tieback rods through a reduction in cross section. To investigate how the physical geometry of the rod affects the ultrasonic signal, corrosion was simulated by machining reduced diameter regions into steel rods (Figure 21 and Figure 22). The simulated corrosion is characterized by a smooth surface as opposed to the irregular surface in actual corrosion. This approximation of the corrosion surface reduces the dispersion of the ultrasonic wave in the corroded region, simplifying the investigation of the fundamental principles affecting the ultrasonic signal.

Figure 21. Actual corrosion of a steel rod

Figure 22. Simulated corrosion of a steel rod

4.1 Location of Leading Edge of Simulated Corrosion

Three 12L14 steel rods, 3 ft. long and 1 in. in diameter, were machined with simulated corrosion at short, middle, and long distances from the transducer (Figure 23). The sections of simulated corrosion, 0.5 in. diameter and 2.0 in. long, were machined at 8.94 in., 16.06 in., and 23.03 in. along the lengths of the steel rods. The ultrasonic signals from these rods were used to identify the locations of simulated corrosion. The location of simulated corrosion was

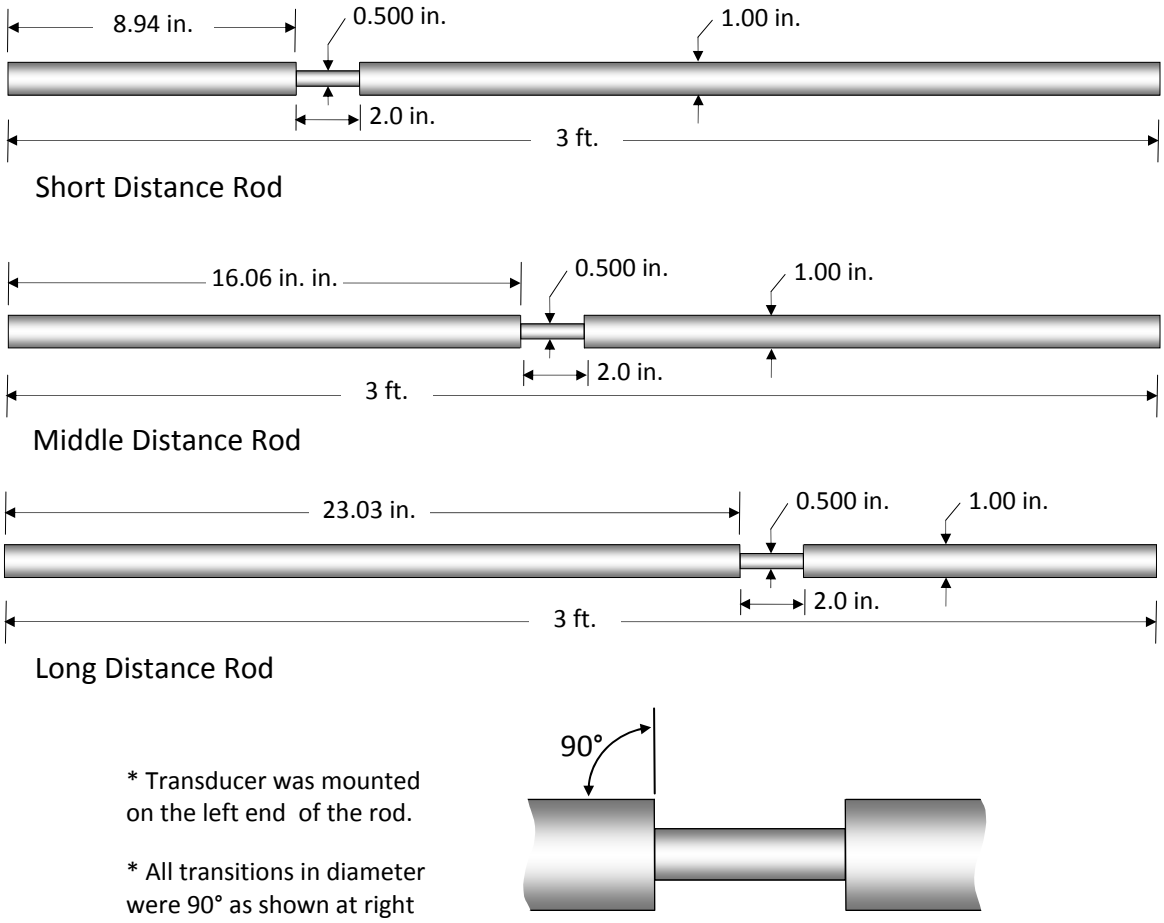

Figure 23. 3 ft. long 1.0 in. diameter rods with 2.0 in. length of 0.5 in. diameter simulated corrosion used for detection of simulated corrosion location

detectable based on the time between the main bang and the leading edge of the flaw echo (Figure 24). A distinct second flaw echo appears in the short and middle distance rods. Depending upon the location of the simulated corrosion, the second flaw echo and successive trailing echoes may arrive at the same time as the first back echo. When this overlap occurs, locating the arrival time of the back echo is difficult.

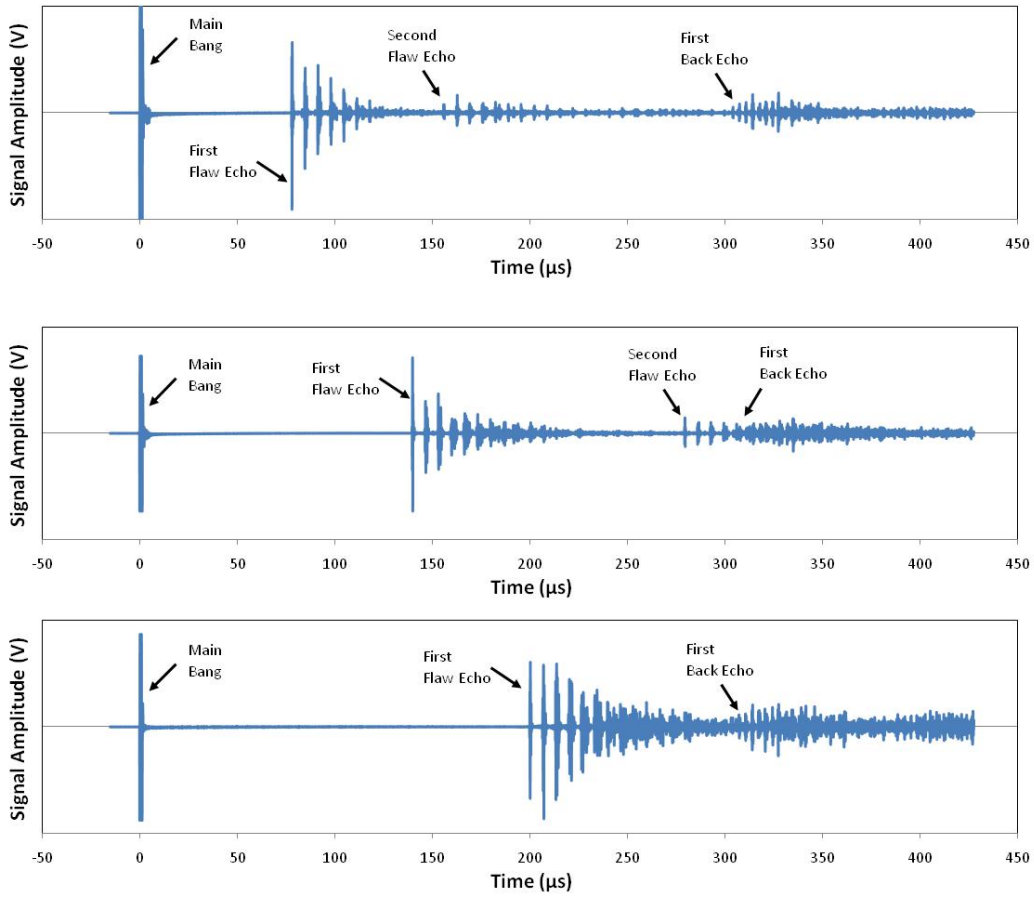

Figure 24. Ultrasonic signals for simulated corrosion located at 8.94 in., 16.06 in., and 23.03 in. from the end of the rod.

The length, L, from the transducer to the leading edge of simulated corrosion can be calculated using the following formula:

$$L = \frac{C_1 \cdot t}{2} \qquad \textbf{Equation 27}$$

where C_1 is the bulk longitudinal wave speed of the material, and t is the time between the main bang and the leading edge of the flaw echo. The time was divided by two because the ultrasonic pulse passes down the length of the rod to the flaw and then returns back to the

ultrasonic transducer. The formula for length was used to determine the location of the flaw (Table 5) for the three rods in Figure 24. A longitudinal wave speed, based on experimental data, of C_1 = 19,220 ft/s for the 12L14 steel rods was used. The results indicate that the location of simulated corrosion with a 90° transition can be accurately determined from the ultrasonic signal. Each section of simulated corrosion was located to within 0.13% of the measured location using the ultrasonic signal.

Table 5. Comparison of measured and calculated simulated corrosion locations

Measured Simulated Corrosion Location (in.)	Flaw Echo Time (μs)	Calculated Simulated Corrosion Location (in.)	% Difference
8.94	77.71	8.95	0.12%
16.06	139.62	16.08	0.13%
23.03	199.73	23.00	0.11%

4.2 Diameter Characterization

Three sets of specimens were tested to investigate the effect of the diameter of simulated corrosion on the received ultrasonic signal. The first set of rods were 3.0 ft. long with 0.5 in., 1.0 in., and 1.5 in. diameters without simulated corrosion (Figure 25). These rods were used to investigate the effect of rod diameter on the ultrasonic signal. The back echo and subsequent trailing echoes from the 0.5 in., 1.0 in., and 1.5 in. diameter rods were recorded in Figure 26. The time between trailing echoes (Δt) was measured for each of the three rods and compared with the calculated time established by Light & Joshi (Equation 25) for steel rods with C_1 =

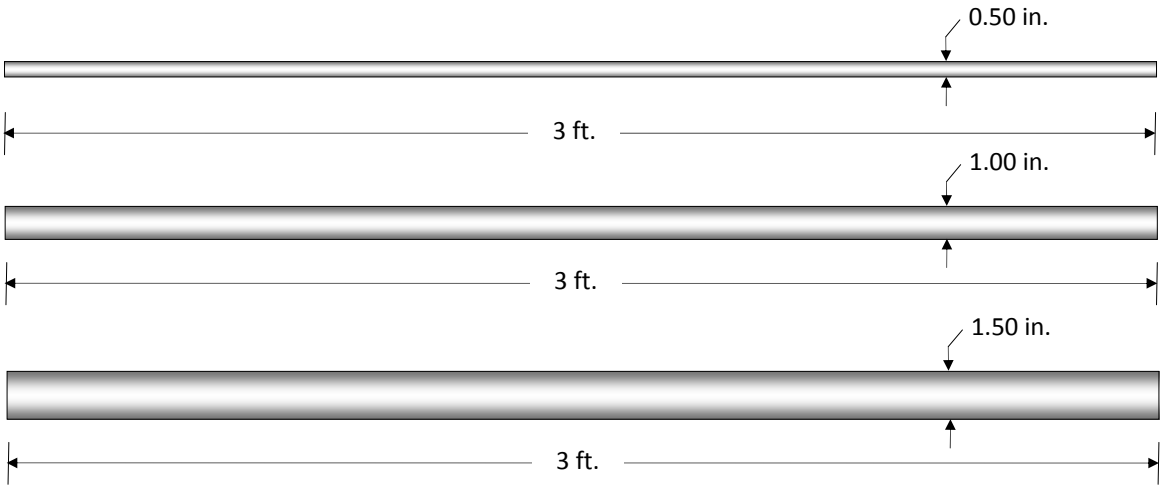

Figure 25. 3 ft. long rods with 0.5 in., 1.0 in., and 1.5 in. diameters

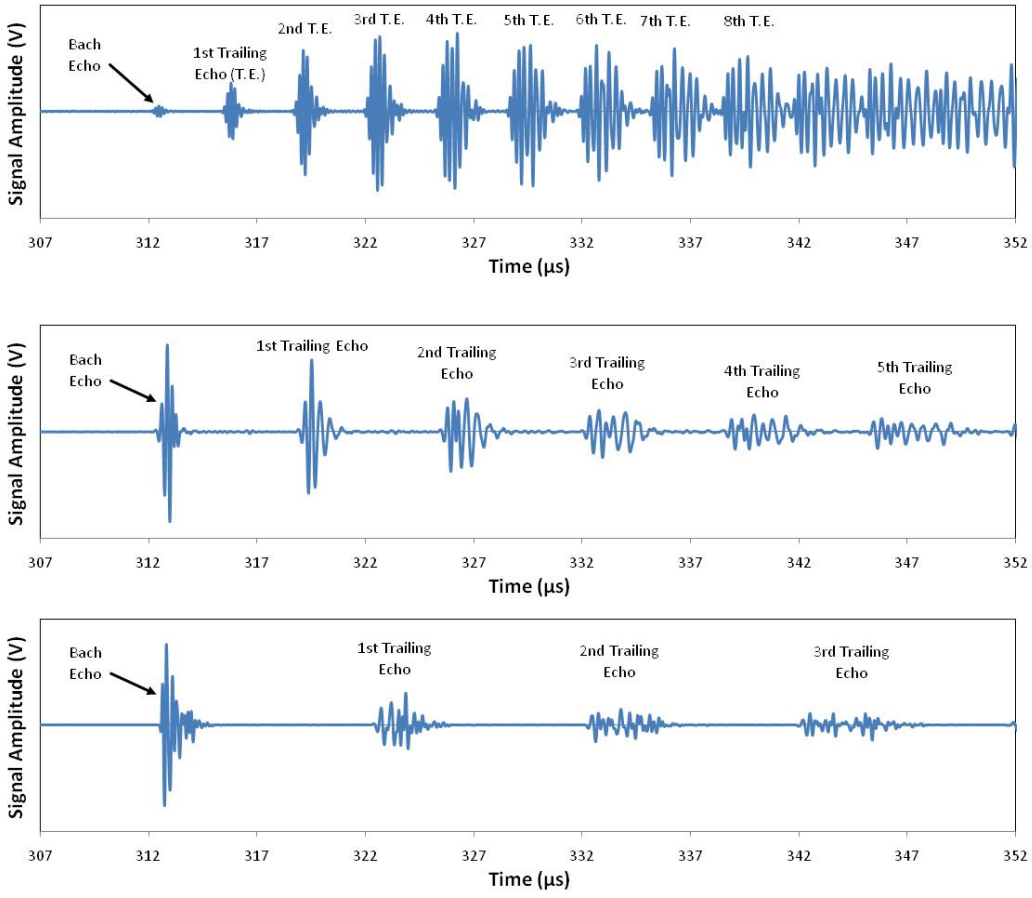

Figure 26. Trailing echoes for 0.5 in., 1.0 in., and 1.5 in. diameter rods

19,220 ft/s and C_2 = 10,597 ft/s. C_1 was measured in the lab and C_2 was a published value (Bray & Stanley, 1989). The results confirmed the accuracy of the Light & Joshi equation for multiple rod diameters (Table 6).

Table 6. Comparison of measured versus calculated time between trailing echoes using the rod diameter

Rod Diameter (in.)	Measured Time between Trailing Echoes (µs)	Calculated Time Between Trailing Echoes (µs)	% Difference
0.5	3.27	3.28	0.2%
1.0	6.61	6.56	0.9%
1.5	10.07	9.84	2.3%

The time between echoes and the diameter of each rod was plotted and compared with the equation from Light and Joshi (Figure 27). The linear trend line for the experimental data had a slope of 0.1498 in/s compared to 0.1525 in/s for the Light & Joshi equation which resulted in a 1.8% difference. These results shows a strong correlation between diameter of a rod without simulated corrosion and the time between trailing echoes in the ultrasonic signal.

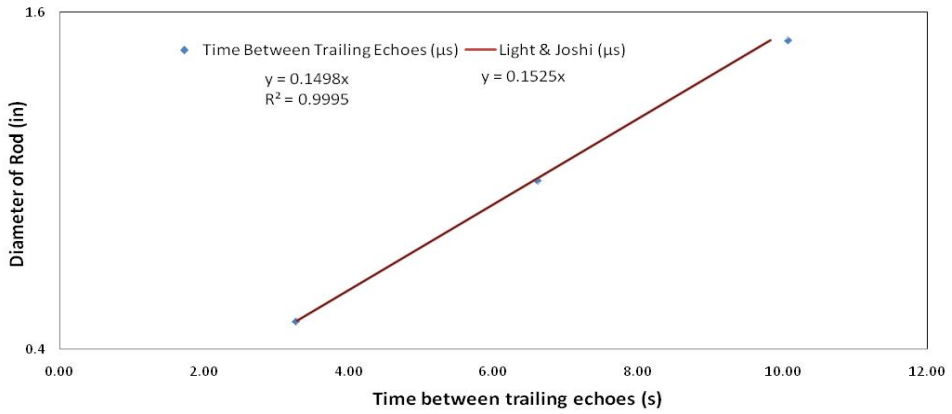

Figure 27. Correlation between rod diameter and time between trailing echoes

The second set of rods included a 3 ft. long 1.0 in. diameter rod with a 2.0 in. length of 0.5 in. diameter simulated corrosion, a 3 ft. long 0.5 in. diameter rod without simulated corrosion and a 3 ft. long 1.0 in. diameter rod without simulated corrosion (Figure 28). A 45° transition was included at each end of the simulated corrosion to address the concern that corroded regions do not typically exhibit an abrupt transition. The 45° transition also reduced the amplitude of the second flaw echo that occured coincident with the back echo in the ultrasonic signal. These rods were used to investigate the effect of 0.5 in. diameter simulated corrosion on the ultrasonic signal. The back echo and successive trailing echoes were recorded for each rod (Figure 29). The time between the trailing echoes (Δt) for each of the three rods was recorded

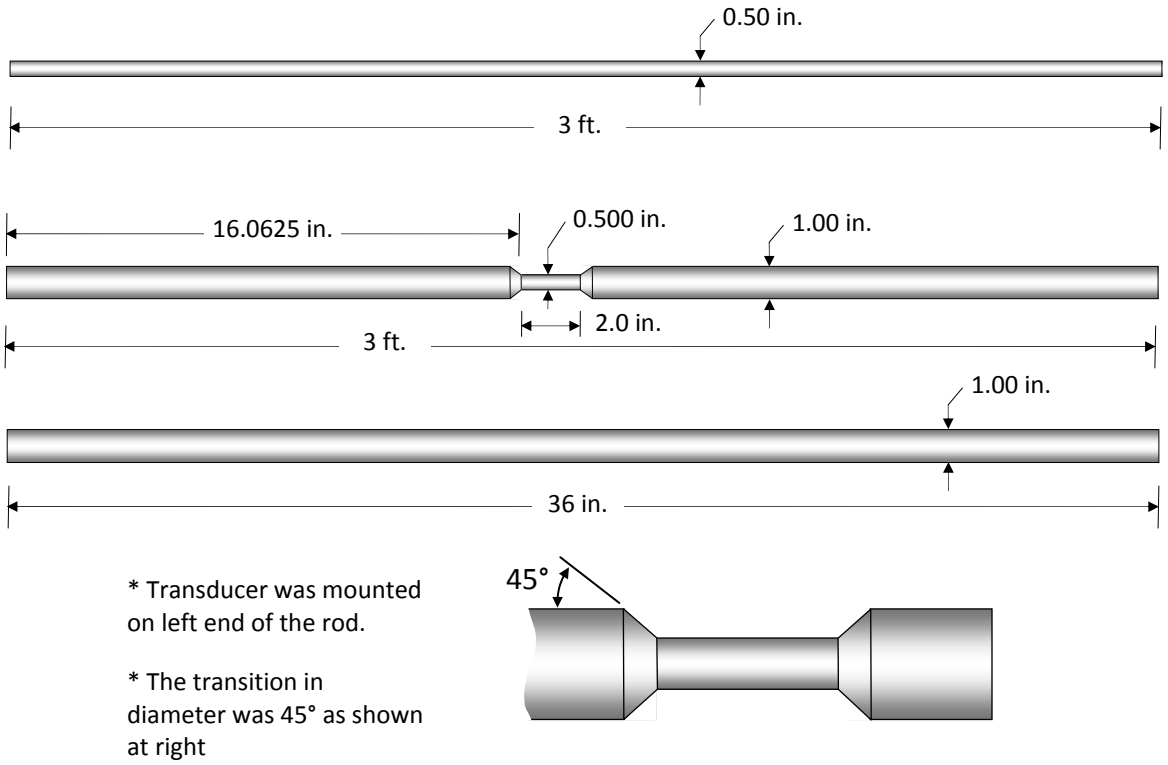

Figure 28. 1.0 in. diameter rod with 0.5 in. simulated corrosion diameter compared with 0.5 in. diameter and 1.0 in. diameter rods

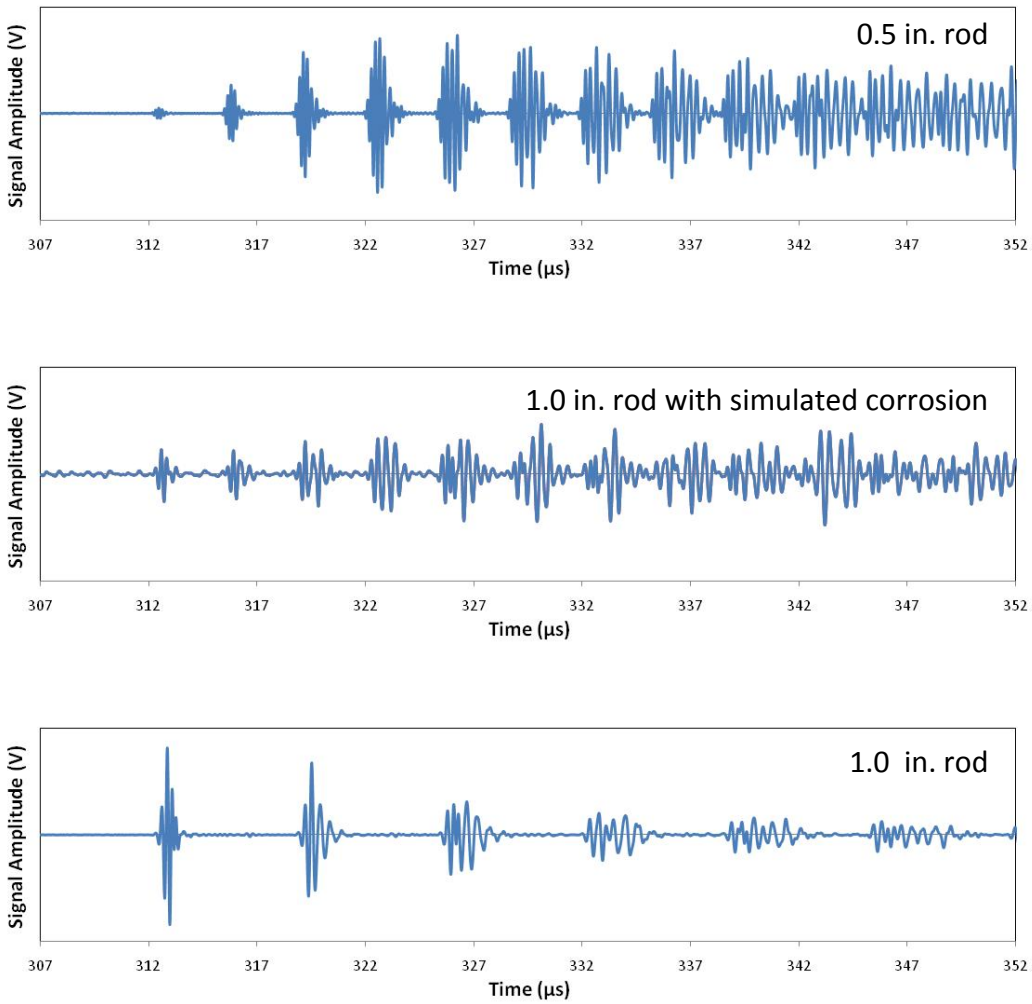

Figure 29. Comparison of ultrasonic signals for 1.0 in. diameter rod with 0.5 in. diameter simulated corrosion versus 0.5 in. and 1 in. diameter rods

in Table 7. The rod with simulated corrosion had a time between trailing echoes of 3.50 µs which was much closer to the 3.27 µs in the 0.5 in. diameter rod than the 6.61 µs in the 1.0 in diameter rod. Using Equation 25, the diameter of each rod was calculated based on the time between trailing echoes. The time between trailing echoes for the rod with simulated corrosion correlates to a 0.53 in. minimum rod diameter. This value compared with the measured 0.50

Table 7. Calculated diameter for 1.0 in. diameter rod with 0.5 in. diameter simulated corrosion, 0.5 in. diameter rod, and 1.0 in. diameter rod.

Specimen	Smallest Diameter (in.)	Measured Δt (μs)	Calculated Diameter (in)	% Difference
0.5 in. Rod	0.5	3.27	0.50	0.2%
1.0 in. Rod with 0.5 in. Simulated Corrosion Diameter	0.5	3.50	0.53	6.6%
1.0 in. Rod	1.0	6.61	1.01	0.9%

in. diameter has a 6.6% difference. These results showed that the time between trailing echoes was primarily dependent upon the minimum diameter of simulated corrosion in the rod. The third set of rods included three 12L14 steel rods, 3 ft. long and 1 in. in diameter machined with a 2.0 in. length of simulated corrosion with 0.25 in., 0.50 in. and 0.75 in. diameters (Figure 30). These rods were used to investigate trailing echo spacing for multiple diameters of simulated corrosion. The ultrasonic signal for the 0.25 in. diameter simulated corrosion did not exhibit a distinct back echo or any trailing echoes. This is because a 5 MHz frequency bulk wave is not able to propagate through a 0.25 in. diameter. A bulk wave will only propagate when the diameter of the bounded region is approximately ten times greater than the wavelength of the ultrasonic signal (Bray & Stanley, 1989). For the 5 MHz probe used to generate the ultrasonic signal, the minimum diameter is approximately 0.46 in. in steel. Thus, a bulk wave was not able to travel through the simulated corrosion region with a diameter of 0.25 in.

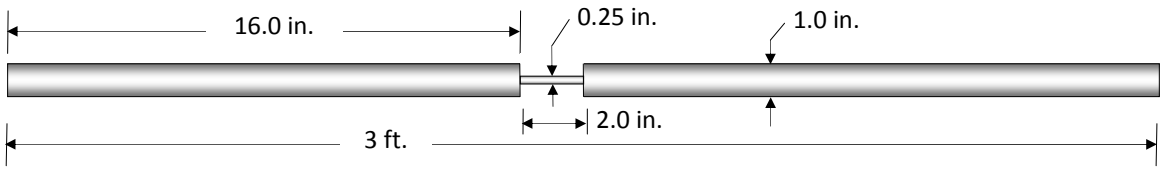

0.25 in. Simulated Corrosion

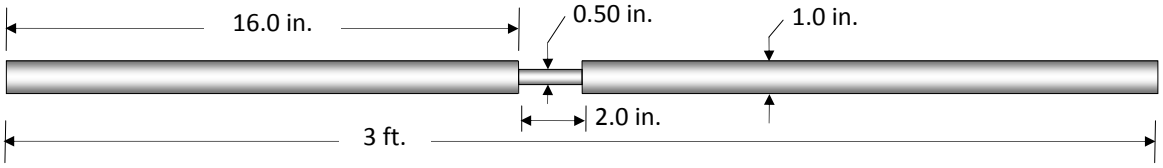

0.5 in. Simulated Corrosion

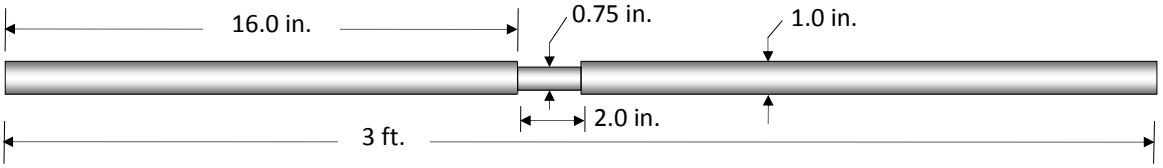

0.75 in. Simulated Corrosion

* Transducer was mounted on the left end of the rod.

* All transitions in diameter were 90° as shown at right

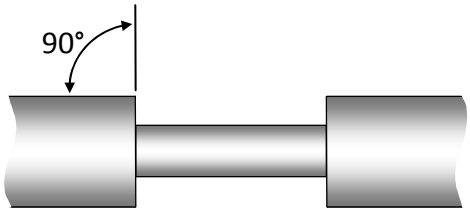

Figure 30. 3 ft. long 1.0 in. diameter rods with 2.0 in. length of 0.25 in., 0.50 in., or 0.75 in. diameter simulated corrosion

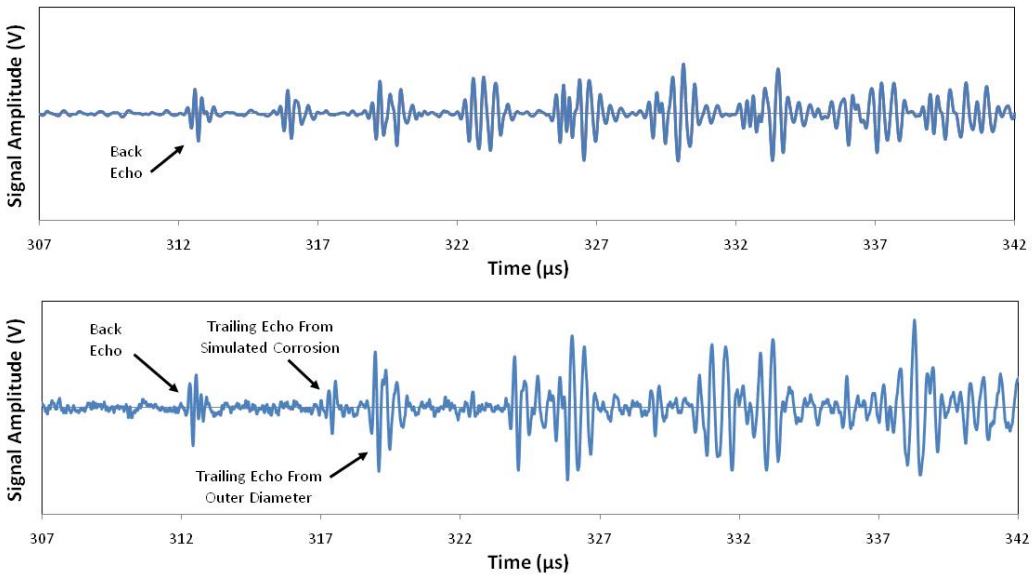

Figure 31. Ultrasonic signals for simulated corrosion diameters 0.50 in., and 0.75 in.

The back echo and subsequent trailing echoes for the 0.5 in. and 0.75 in. diameters of simulated corrosion were recorded (Figure 31). The rod with 0.75 in. simulated corrosion diameter exhibited a pattern of superimposed trailing echoes. Trailing echoes were introduced from mode conversions in the 0.75 in. diameter region and the 1.0 in. diameter region The first trailing echo represented the mode conversion in the 0.75 in. diameter region, and the second trailing echo represented the mode conversion in the 1.0 in. diameter region. The time between the back echo and the first trailing echo was measured and the corresponding simulated corrosion diameter was calculated as 0.73 in. The rod with 0.5 in. diameter simulated corrosion exhibited distinct trailing echoes. (Table 8). The rod with 0.5 in. diameter of simulated corrosion also exhibits superimposed trailing echoes. However, since the 1.0 in.

outer diameter is a multiple of the simulated corrosion diameter the superimposed trailing echoes arrive at the same time appearing as a single trailing echoes. The time between trailing

Table 8. Calculated diameter for 1.0 in. diameter rod with 0.5 in. and 0.75 in. diameter simulated corrosion

Specimen	Smallest Diameter (in.)	Measured Δt (μs)	Calculated Diameter (in)	% Difference
0.5 in. Simulated Corrosion Diameter	0.5	3.50	0.53	6.6%
0.75 in. Simulated Corrosion Diameter	0.75	4.76	0.73	3.2%

echoes was measured and the corresponding simulated corrosion diameter was calculated as 0.53 in. These results showed that 0.5 in. diameter and 0.75 in. diameter simulated corrosion can be calculated in 1.0 in. diameter rods using Equation 25. The time between trailing echoes must be measured from the back echo to the first trailing echo to detect the smallest reduced

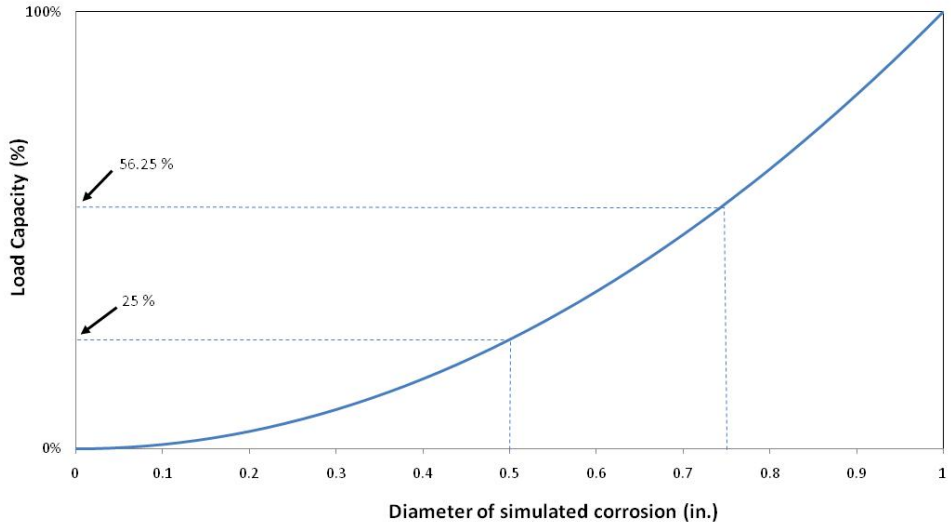

Figure 32. Percent reduction of original load capacity for simulated corrosion in a 1 in. diameter rod

diameter. The reduction in diameter of a steel rod correlates directly with a reduction of load capacity. The tensile load capacity of a steel rod is dependent upon the smallest cross-sectional area of the rod perpendicular to the longitudinal axis. The reduction can be calculated in percent of original load capacity based upon the original diameter (d_o) and the corroded diameter (d_c). The percent reduction in load capacity for a 1 in. diameter rod with reduced cross section is plotted in Figure 32. The 0.75 in. diameter simulated corrosion represents a 43.75% reduction in load capacity and the 0.5 in. diameter represents a 75% reduction in load capacity.

$$\%_{\textbf{load capacity}} = \frac{\mathbf{d_c}^2}{\mathbf{d_o}^2} \quad \text{Equation 28}$$

4.3 Length of Simulated Corrosion Characterization

In order to investigate the effect of length of simulated corrosion on the ultrasonic signal the back echo and first trailing echo were examined. The frequency content of the back echo was inspected for a shift of the peak frequency with a change in the length of simulated corrosion. Also, the ratio of maximum amplitudes of the trailing and back echoes were examined for a change with the length of simulated corrosion. All ultrasonic signals presented in this section were generated with the M1042 Olympus NDT 5 MHz transducer. The signal waveform and frequency content are shown in Figure 33.

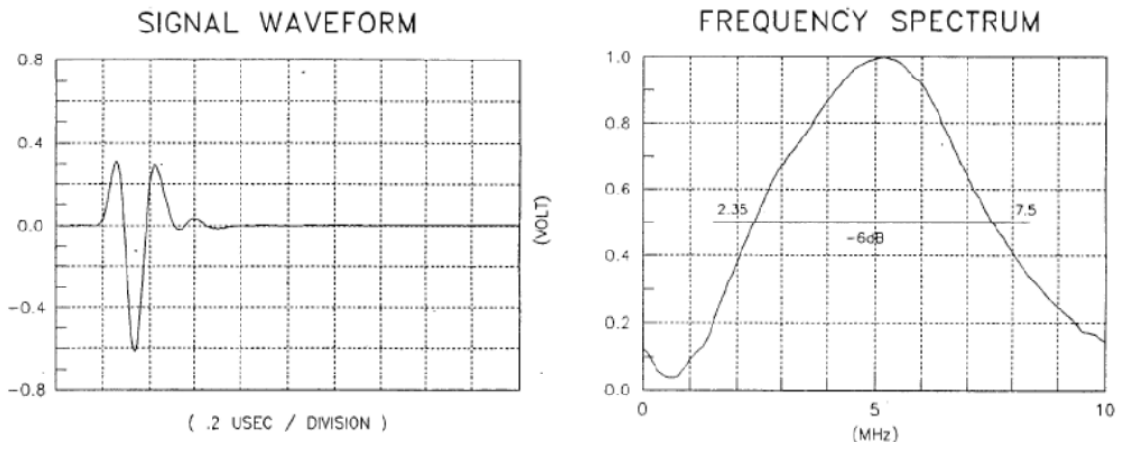

Figure 33. Signal waveform and frequency content for 5 MHz M1041 Olympus NDT transducer

4.3.1 Change in Frequency Content of Back Echo for Length of Simulated Corrosion

The frequency content of the back echo was investigated to identify any trends associated with the length of simulated corrosion. The back echoes of several rods with various length of simulated corrosion were evaluated using a Fast Fourier Transform (FFT). The FFT analysis of the back echo shows the frequency content of the time domain signal. An FFT requires the number of data points be 2^N where N is an integer. To decrease the effect of noise on the signal only the oscillations which cross the x-axis were considered in the analysis, and the remainder of the signal was replaced with zeros (Figure 34.) Before the frequency of the signal was analyzed for simulated corrosion, two tests were performed to investigate the effect of length and diameter of the rod on the frequency of the ultrasonic signal. The first test included

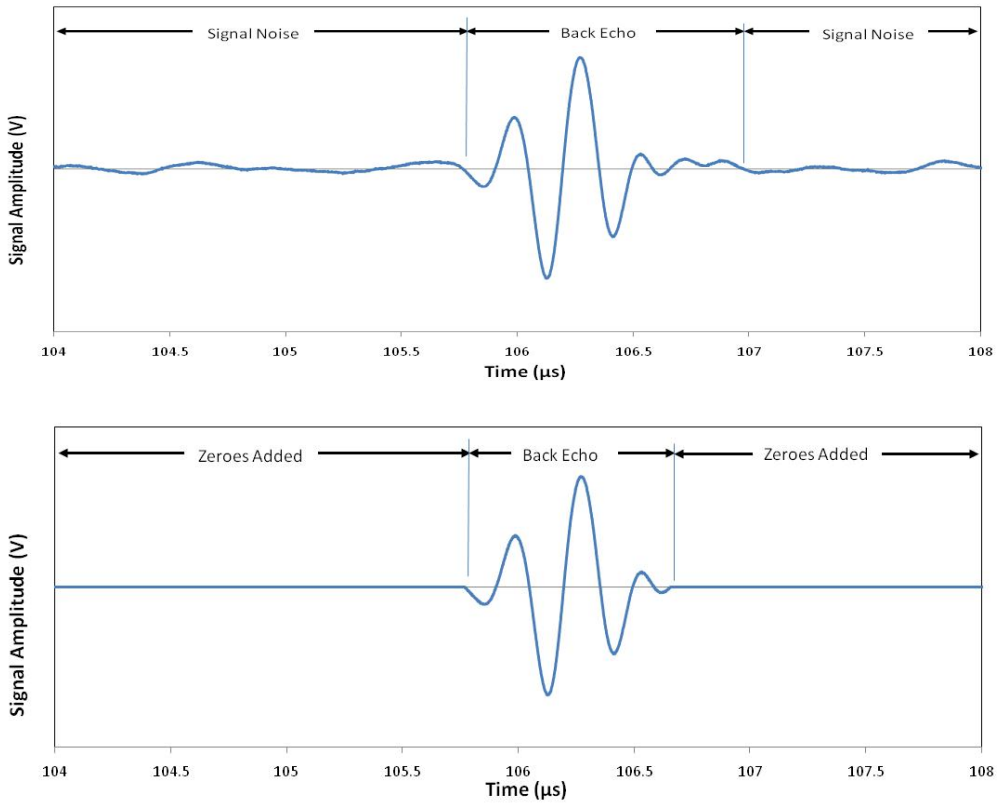

Figure 34. Back echo of 1.0 ft. long rod with a 0.5 in. simulated corrosion diameter with and without zeros

three rods 3.0 ft. in length with diameters of 0.5 in., 1.0 in., and 1.5 in. An FFT was calculated for the back echo in each rod. The peak frequencies for the 0.5 in., 1.0 in., and 1.5 in. diameter rods were 6.10 MHz, 3.91 MHz, and 4.39 MHz respectively (Figure 35). The second test included three rods 1.0 in. in diameter with lengths of 1.0 ft., 3.0 ft., and 10.0 ft. An FFT was calculated for the back echo in each rod. The results showed that the peak frequencies for the 1.0 ft., 3.0 ft., and 10.0 ft. long rods were 4.39 MHz, 3.66 MHz, and 4.64 MHz (Figure 36.) Figure 35 and Figure 36 show that the peak frequency of the back echo can vary with both rod diameter and rod length. However, a definite relationship between peak frequency, rod diameter and rod length was not established in this study.

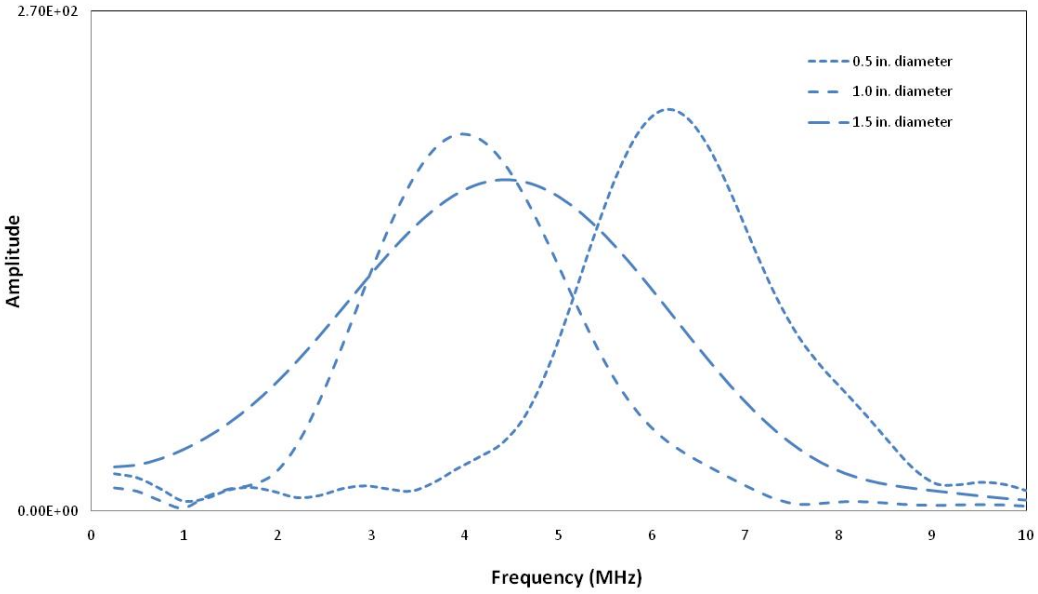

Figure 35. FFT for 3.0 ft. long rods with 0.5 in., 1.0 in., and 1.5 in. diameters

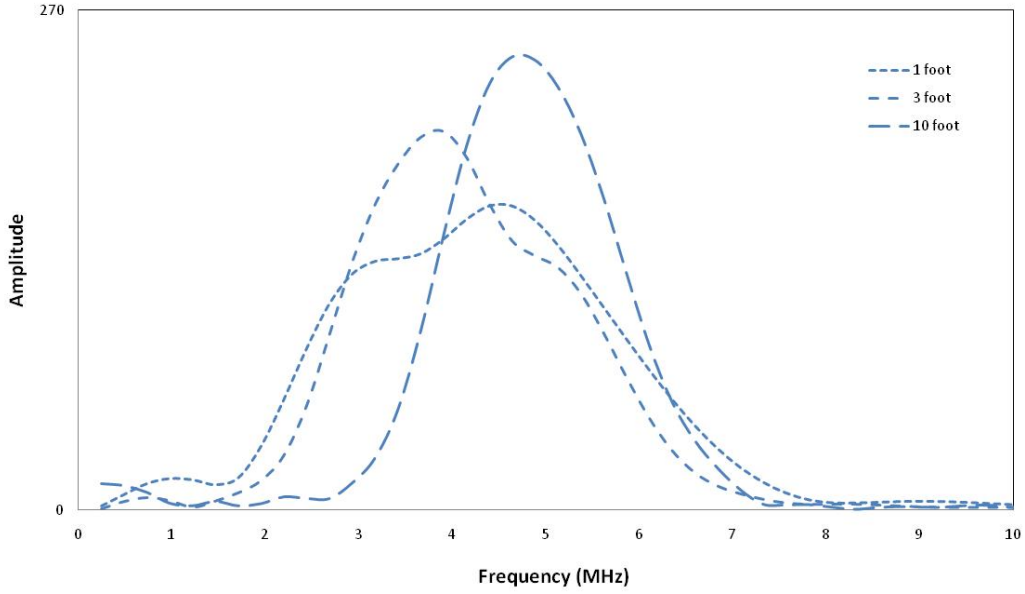

Figure 36. FFT for back echo of 1.0 in. diameter rods with 1.0 ft., 3.0 ft., and 10.0 ft. lengths

Two sets of rods 1.0 in. in diameter and 1.0 ft. and 3.0 ft. in length were tested to identify any correlation for each specific length and diameter of rods. The first set of rods included five 1.0 ft. long steel rods with 0.5 in. simulated corrosion diameter for lengths of 0.5 in., 1 in., 2 in., 4 in., and 8 in. (Figure 37). A 90° transition, from the original rod diameter to the simulated corrosion diameter, was used on each rod. The location of the simulated corrosion was 2.0 in. from the end of each rod. The FFT for the back echo was compared for each of the five rods

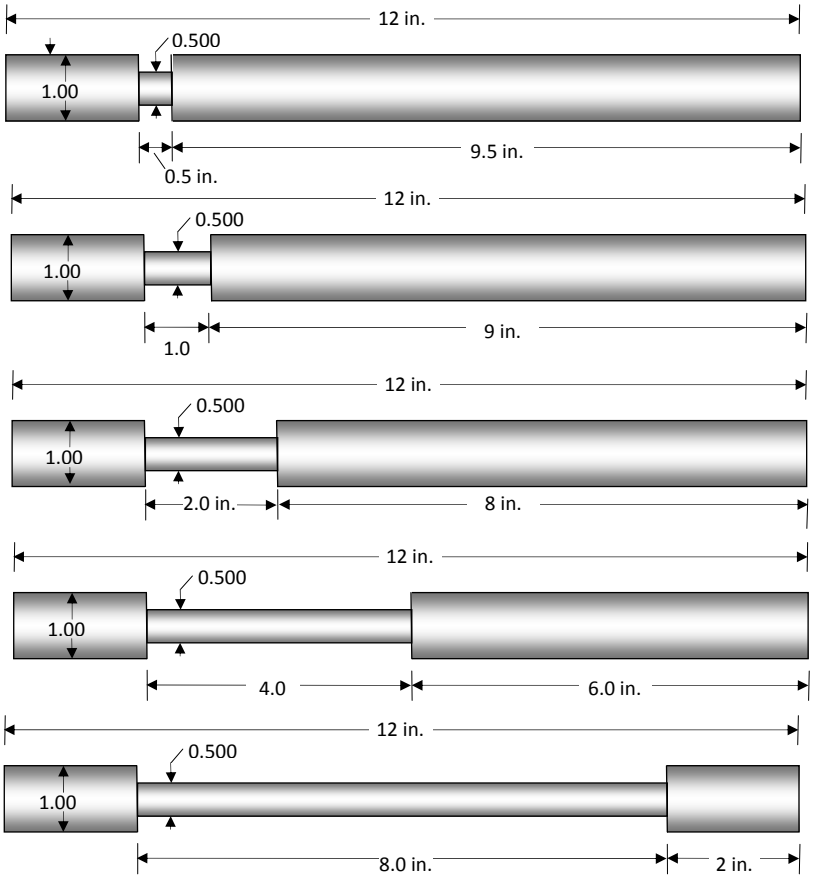

Figure 37. 1.0 in. diameter 1.0 ft. long rods with different lengths of simulated corrosion

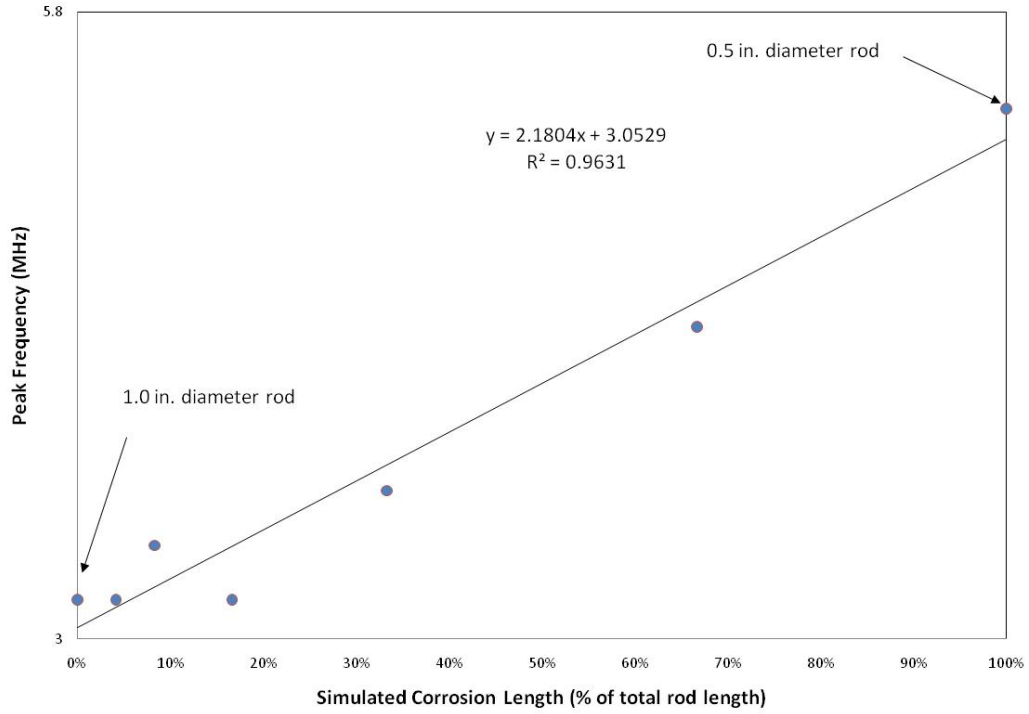

Figure 38. Frequency analysis of first back echo for multiple lengths of simulated corrosion in a 1.0 in. diameter 1.0 ft. long steel rod

(Figure 38). The peak frequency of the back echo for each rod was plotted with respect to the simulated corrosion length expressed as a percentage of total rod length. The results show an increase in peak frequency with an increase in percent length of simulated corrosion.

The second set of rods consisted of 3.0 ft. long 1.0 in. diameter rods with 2 in., 6 in., and 10 in. lengths of simulated corrosion starting at 9 in. from the transducer (Figure 39). These rods were used to investigate a relationship between the length of simulated corrosion and the peak frequency of the back echo in 3.0 ft. long rods with 1.0 in. diameters. The peak frequency of each back echo was plotted with respect to the length of simulated corrosion expressed as a

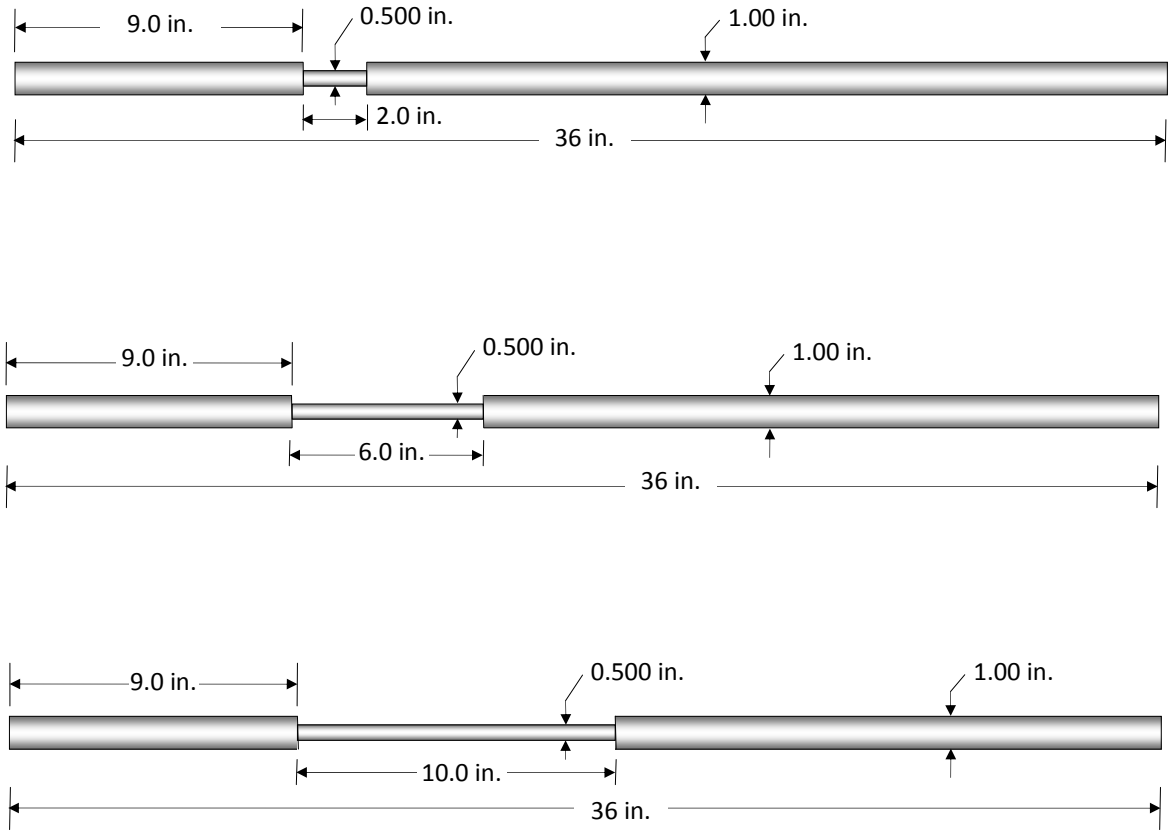

Figure 39. 3.0 ft. long 1.0 in. diameter rods with 2.0 in., 6.0 in., and 8.0 in. lengths of simulated corrosion starting at 9 in. along the rod

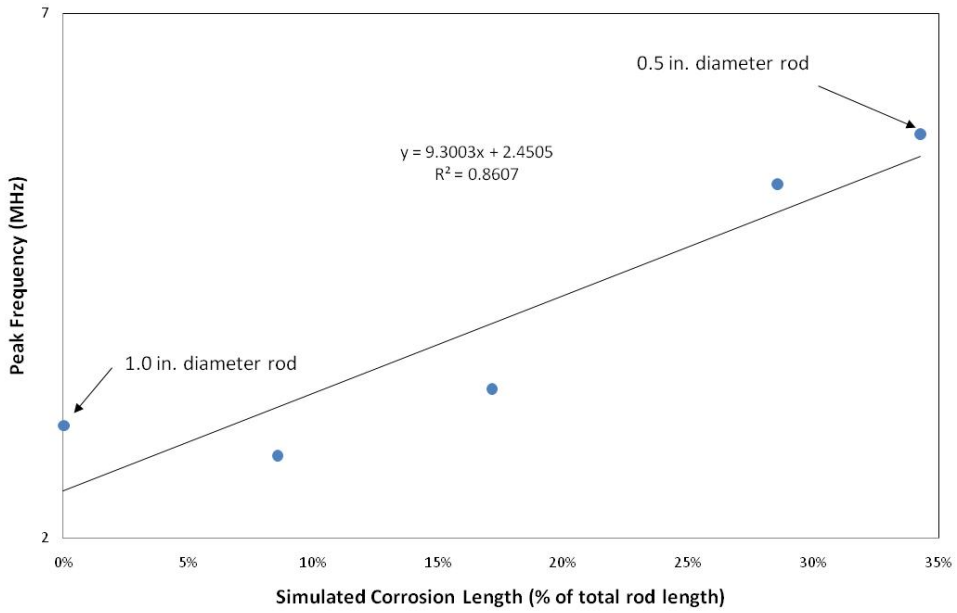

Figure 40. Peak frequency of the back echo for 3.0 ft. long rods with 2.0 in., 6.0 in., and 10.0 in. lengths of simulated corrosion.

percentage of total rod length (Figure 40). The results show an increase in peak frequency with an increase in percent simulated corrosion. The 0.5 in. and 1.0 in. diameter rods without simulated corrosion create the upper and lower bound of the frequency shift. The 1.0 in. diameter rod represents a rod without any simulated corrosion and forms the lower bound of the peak frequency. The 0.5 in. diameter rod represents a rod with full 0.5 in. diameter simulated corrosion and forms the upper bound of the peak frequency. The shift in peak frequency shows that the increase in simulated corrosion length acts as a filter for certain frequencies in the ultrasonic signal.

Overall, the results indicate that an increase in peak frequency of the back echo occurs with an increase in the length of simulated corrosion for 1.0 ft. and 3.0 ft. long rods with a 1.0 in. diameter. The 3.0 ft. long rods exhibited a stronger correlation than the 1.0 ft. long rods, but the number of data points for each rod length was limited.

4.3.2 Change in Back Echo Amplitude with Length of Simulated Corrosion

The maximum amplitudes of the back echo and the first trailing echo were investigated to identify a relationship with the length of simulated corrosion. The back echo represents an ultrasonic pulse undergoing direct reflection from the end of the rod, while the first trailing echo includes one mode conversion with shear wave propagation across the minimum diameter of the rod.

The set of 1.0 ft. (Figure 37) long rods were used for testing. The back echo and first trailing echo were recorded for each rod (Figure 41). The maximum amplitudes of the back echo and the first trailing echo were recorded in Table 9. The ratio of the amplitude of the first trailing echo to the back echo increases with the length of simulated corrosion. The amplitude ratio for each length of simulated corrosion was plotted in Figure 42. The results shown a strong correlation between the percent length of simulated corrosion and the ratio of peak trailing echo to the back echo. The increase in amplitude of the trailing echo relative to the amplitude of the back echo was due to the increased length of simulated corrosion. Assuming a point source for a transducer, Figure 43 shows a cross section of the ultrasonic wave that reflects from the simulated corrosion region for a 0.5 in. and 8 in. length of simulated corrosion.

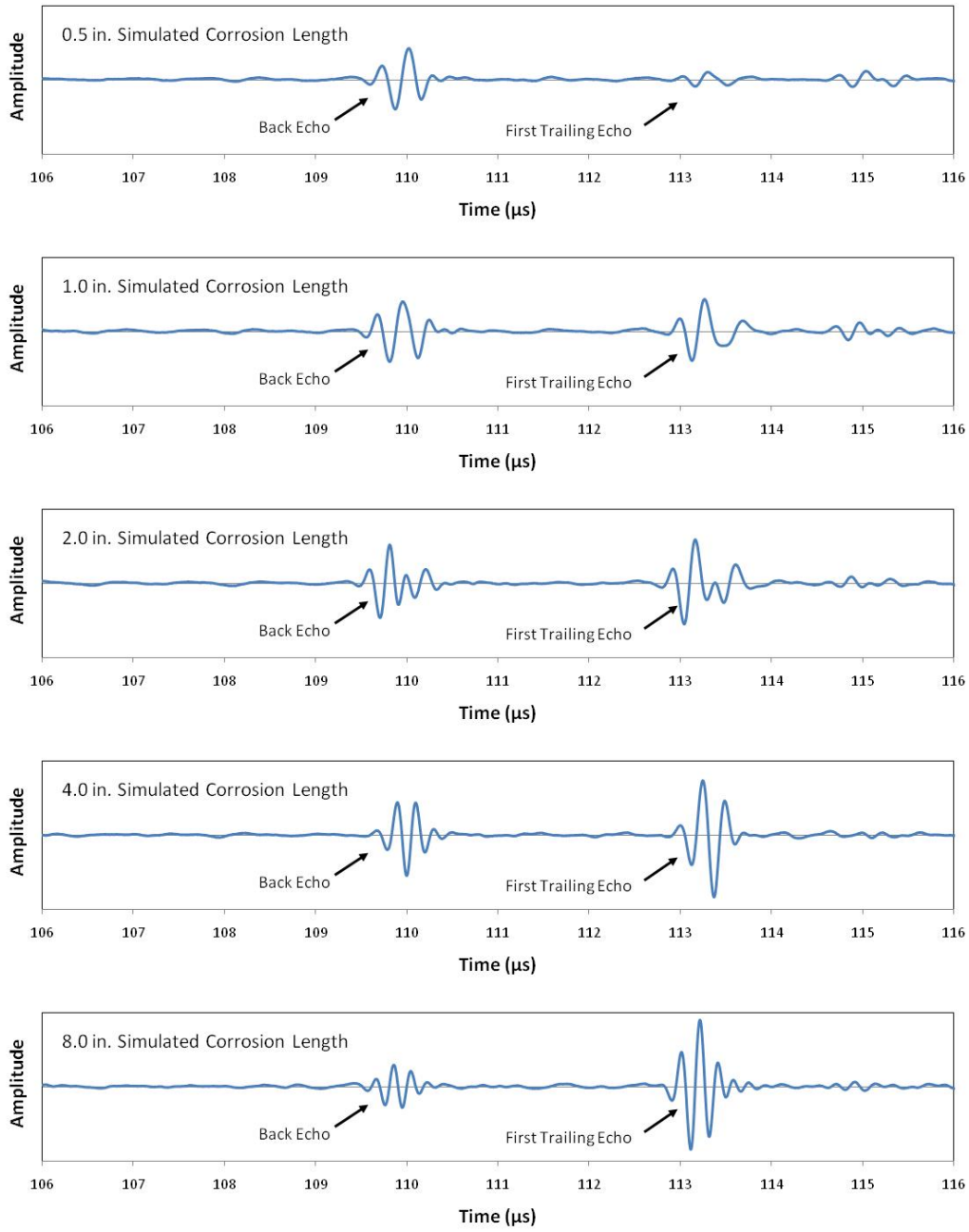

Figure 41. Back echo and first trailing echo for 1.0 ft. long rods with multiple lengths of simulated corrosion

Table 9. Maximum amplitudes of back echo and first trailing echo

	8 in. Region	4 in. Region	2 in. Region	1 in. Region	0.5 in. Region
Back Echo	0.0316	0.0443	0.0456	0.0488	0.0423
1st Trailing Echo	0.0637	0.0568	0.0517	0.0464	0.0186
Amplitude Ratio	2.011	1.280	1.135	0.951	0.439

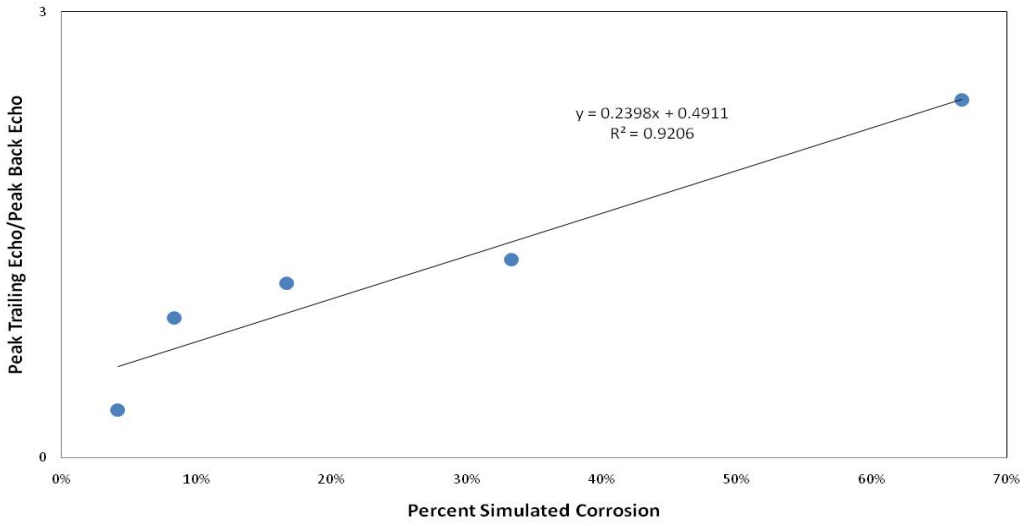

Figure 42. Ratio of trailing echo peak amplitude and back echo peak amplitude for 1.0 in. rods

The lines that border the shaded region travel through the points defined by the beginning and end of the simulated corrosion. The shaded region represents the portion of the wave that will reflect from the simulated corrosion surface. The reflections in this region include shear waves due to mode conversion. A longer length of simulated corrosion corresponds with a larger surface area for shear wave reflections, which in turn increases the amplitude of the first trailing echo relative to the amplitude of the back echo.

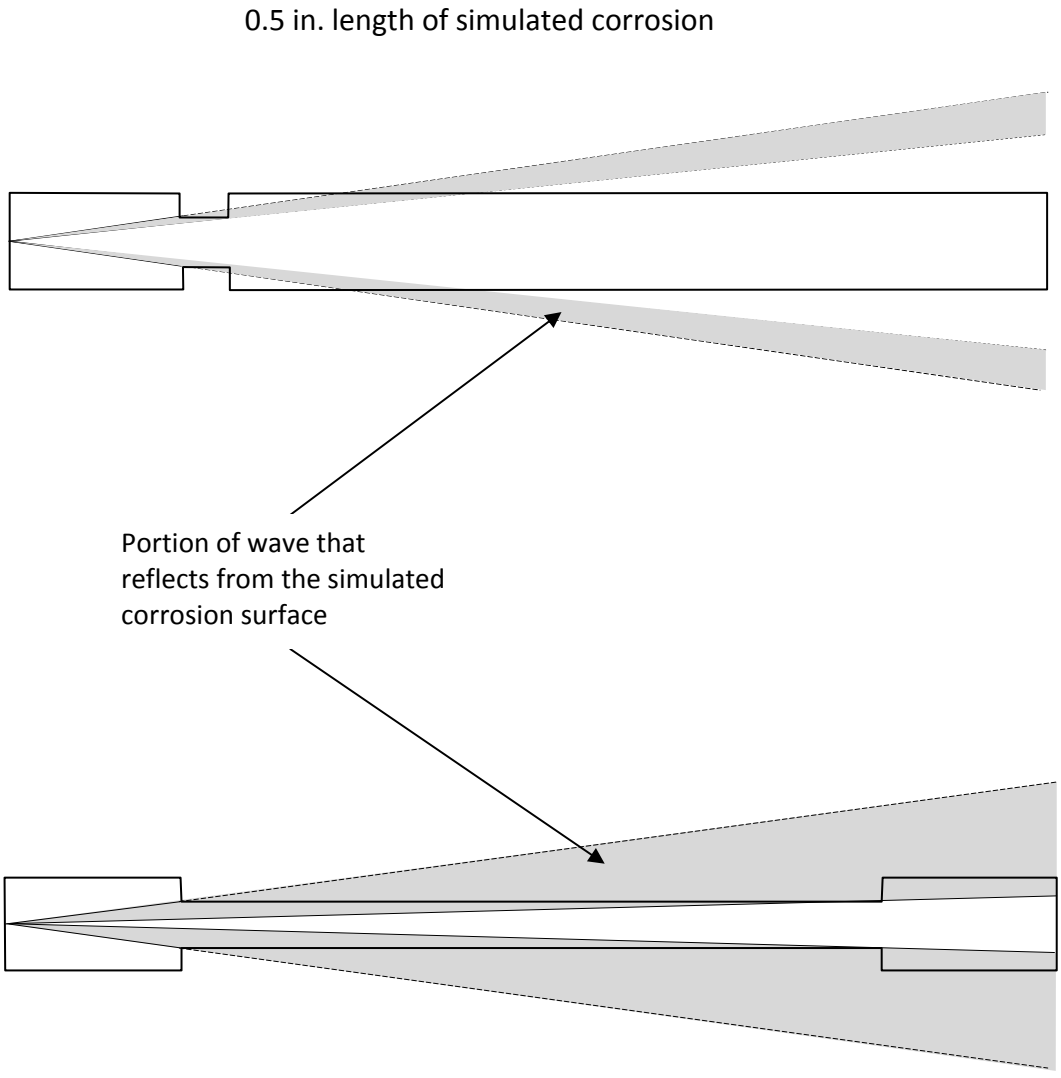

Figure 43. Comparison of reflection from the simulated corrosion surface

The amplitude of the back echo and first trailing echo were also recorded for the set of 3.0 ft. long rods (Figure 39). The ratio of the first trailing echo to the back echo was calculated and plotted (Figure 44). The ratio for the 2.0 in., 6.0 in., and 10.0 in. long simulated corrosion was 0.972, 1.113, and 2.307 respectively. Similar to the 1.0 ft. long rods, the results show that the ratio of trailing echo amplitude to back echo amplitude increases with the length of simulated corrosion.

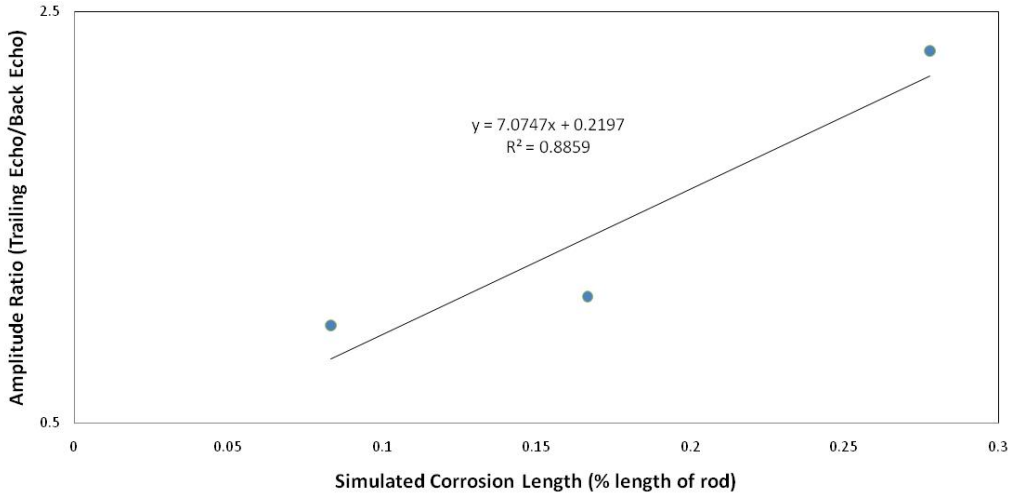

Figure 44. Ratio of trailing echo and back echo for 2.0 in., 6.0 in. and 10.0 in. long simulated corrosion in 3.0 ft. long 12L14 rods

4.4 Transition Characterization

The effect of the transition from the original rod diameter to the simulated corrosion diameter was also examined. The transition geometry of the simulated corrosion region affects the amount of energy that returns to the transducer after reflecting from the transition

surface. Six rods 1 ft. long and 1 in. in diameter, were machined with a 2 in. length of 0.5 in. diameter simulated corrosion at mid-length. A transition was machined in each rod at angles of 90°, 45°, 30°, 15°, 10°, and 5° (Figure 45). The resulting ultrasonic signal for each rod was plotted (Figure 46). Two lines were also plotted on each graph to show (1) the "front of the flaw" where the transition to simulated corrosion begins and (2) the end of the rod. Two observations were made from the ultrasonic signals. First, a decrease in transition angle caused an increase in arrival time of the flaw echo in the ultrasonic signal. This shift in time was plotted versus the transition angle (Figure 47). The results show an increasing delay in the flaw echo dependent upon the transition angle. The second observation was that the amplitude of

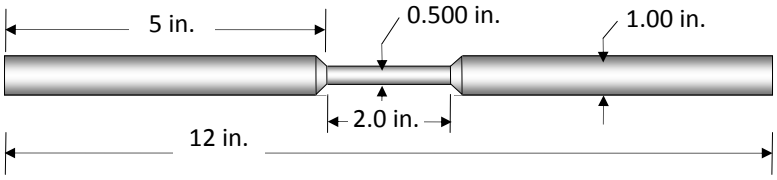

* Transducer was mounted on left end of the rod.

* The rods were machined with transitions of 90°, 45°, 30°, 15°, 10°, and 5°

Figure 45. 1.0 ft. long 1.0 in. diameter rods with multiple transition angles used for detection of simulated corrosion

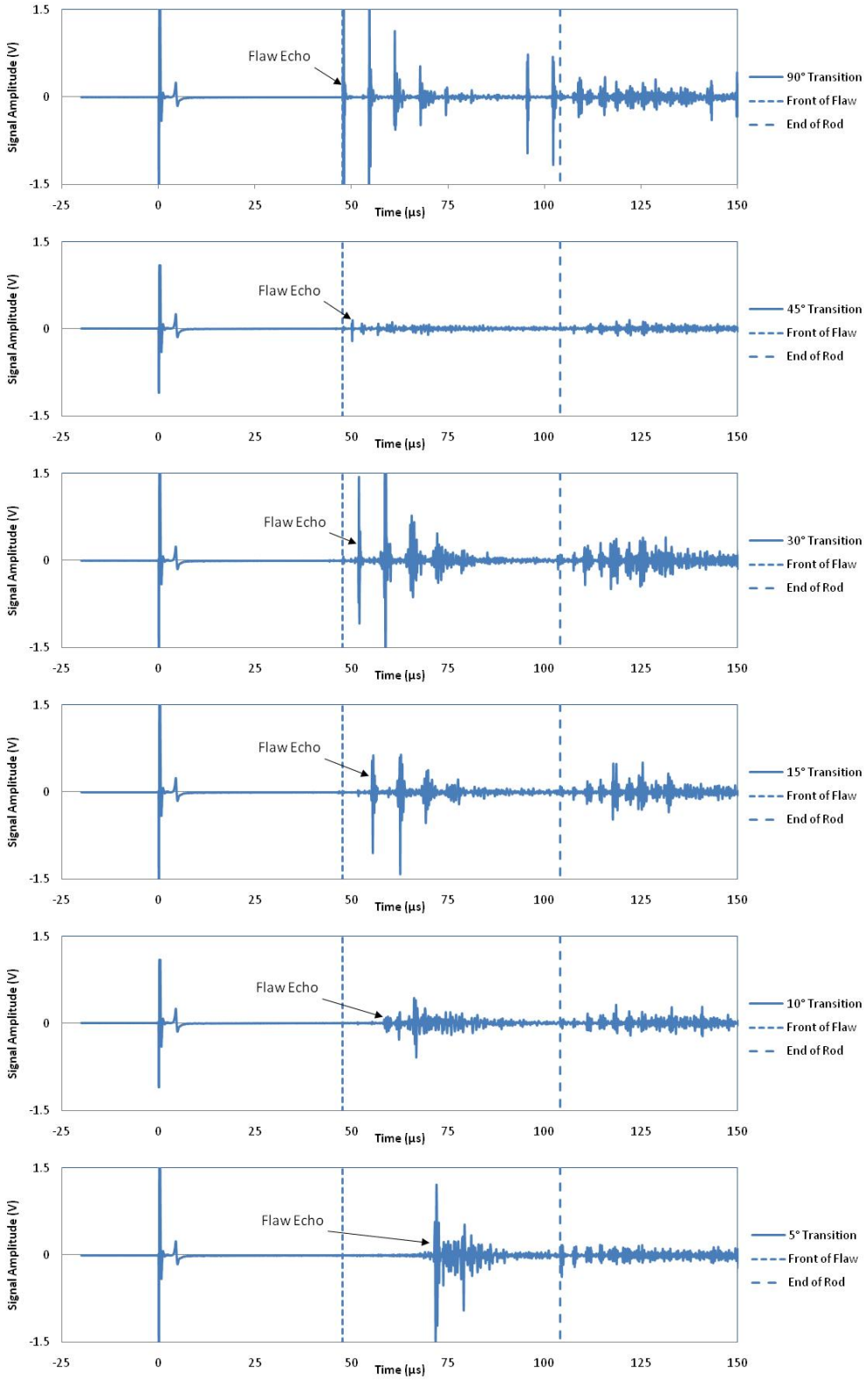

Figure 46. Ultrasonic signal for 90°, 45°, 30°, 15°, 10° and 5° transition angles

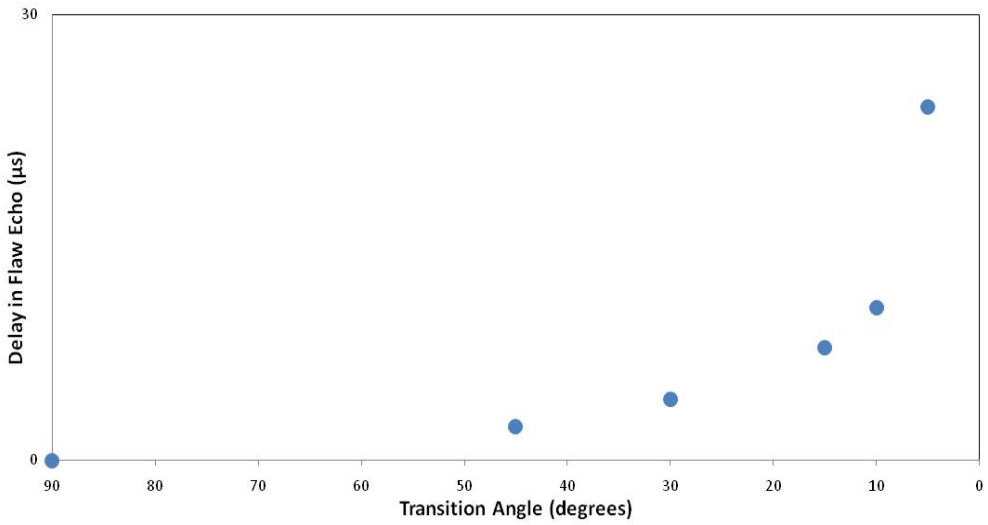

Figure 47. Delay in detectable flaw echo versus transition angle

the flaw echo does not decrease consistently with the transition angle. This phenomenon was investigated more thoroughly by machining rods with a more complete range of transition angles. To compare amplitudes between various rods, the data was normalized using notches to compare two amplitudes within a single ultrasonic signal. Multiple variables affect consistent transducer coupling. These include: force applied to the transducer (coupling force), surface condition of the rod end, amount of coupling gel, and the presence of particles between the transducer and the surface of the specimen. These variables are difficult to control consistently. To maintain a consistent comparison, a notch was added to each rod to create a repeatable baseline echo in every ultrasonic signal. The signal echo associated with the reflection from this notch was compared to the amplitudes of any echoes of interest in order to normalize the data. Three notch locations were evaluated to select an appropriate baseline notch location. Each notch was cut into a 1 in. diameter, 6 in. long rod. The notch was

made 0.125 in. deep around the circumference of the rod and was 0.25 in. wide (Figure 48). The notches were cut at three different distances from the leading edge of the rod: 0.5 in., 1.0 in., and 1.5 in. The rods were tested with the 5 MHz magnetic transducer, and the ultrasonic signal was recorded (Figure 49). The notch located 1 in. away from the ultrasonic transducer was selected because it provided an echo that could be measured in the same order of magnitude as the flaw echoes found in Figure 46, and did not add extra noise to the ultrasonic signal. In contrast, the notch located 2 in. from the transducer provided increased noise following the back echo, while the notch located 0.5 in. from the transducer provided a pulse with a negligible amplitude.

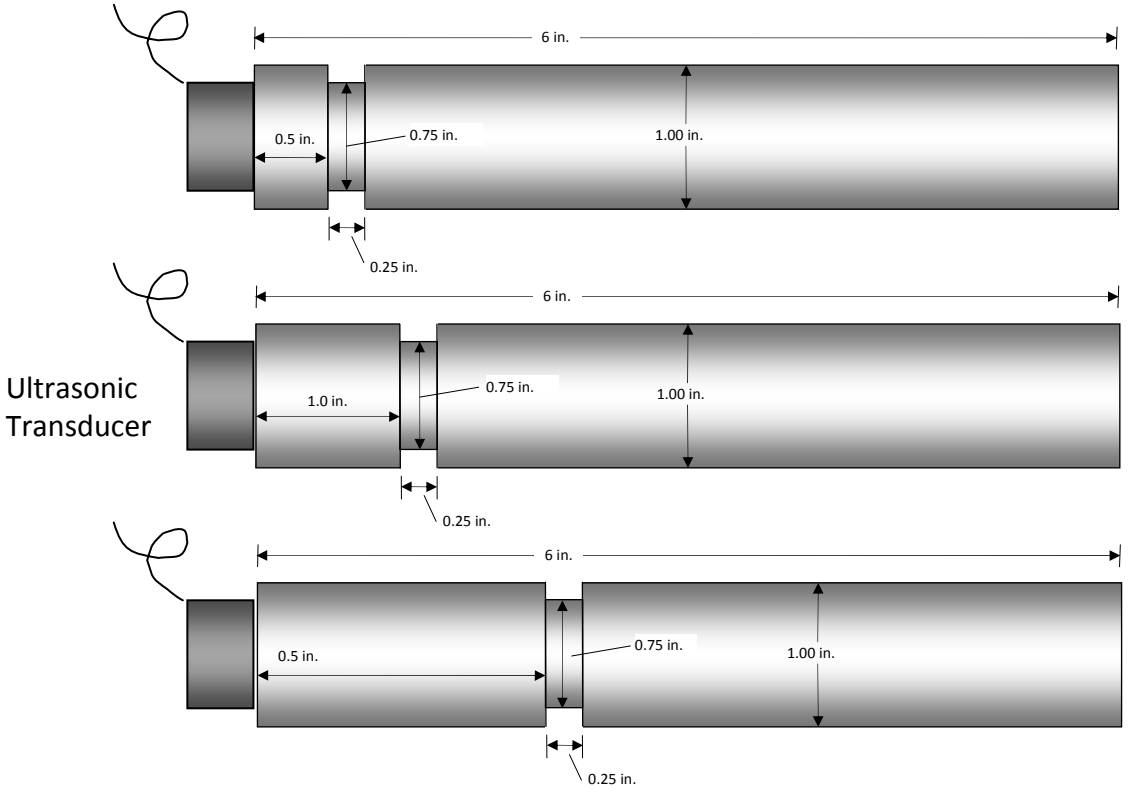

Figure 48. 6.0 in. long 1.0 in. diameter rods with 0.125 in. deep 0.25 in. wide notches located 0.5 in., 1.0 in., and 2.0 in. from the end of the rod

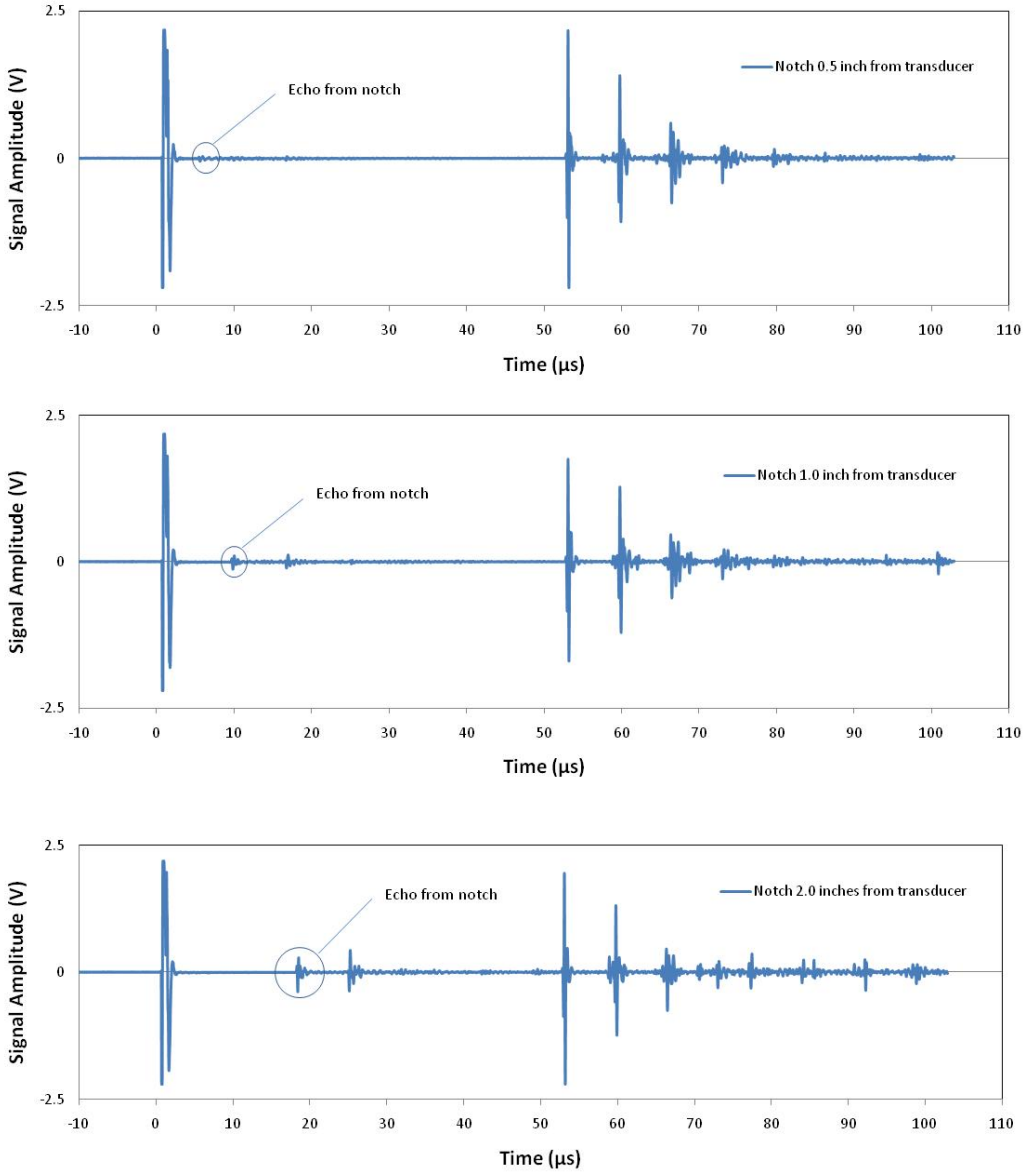

Figure 49. Notch echo comparison for notches located 0.5 in., 1.0 in., and 2.0 in. from the end of the rod

4.4.1 Linear Transitions with Notches

Twenty-two 1.0 ft. long 1.0 in. diameter rods with 5° increments of transition angles were machined (Figure 50). A notch 0.125 in. deep around the circumference and 0.25 in. wide was machined at 1 in. from the end of the rod. The amplitude of the flaw echo was divided by the

amplitude of the echo from the notch to normalize the data. The maximum amplitude of the flaw echo from the simulated corrosion for each rod was normalized and plotted (Figure 51). The maximum amplitude of the flaw echo was divided by the maximum amplitude of the notch

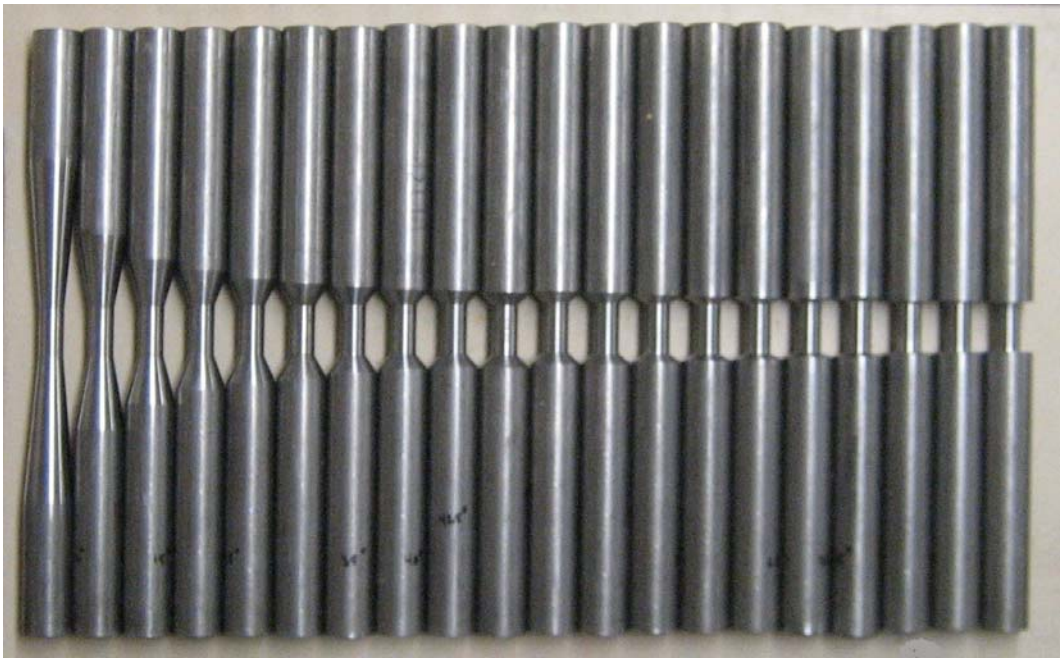

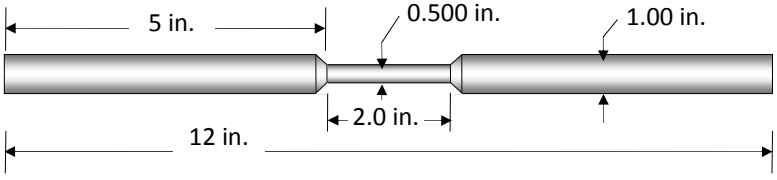

* The rods were machined with transition angles of 90°, 85°, 80°, 75°, 70°, 65°, 60°, 55°, 50°, 47.5°, 45°, 42.5°, 40°, 35°, 32.5°, 30°, 27.5°, 25°, 20°, 15°, 10°, 5°

Figure 50. 1.0 ft. long 1.0 in. diameter rods with multiple transition angles

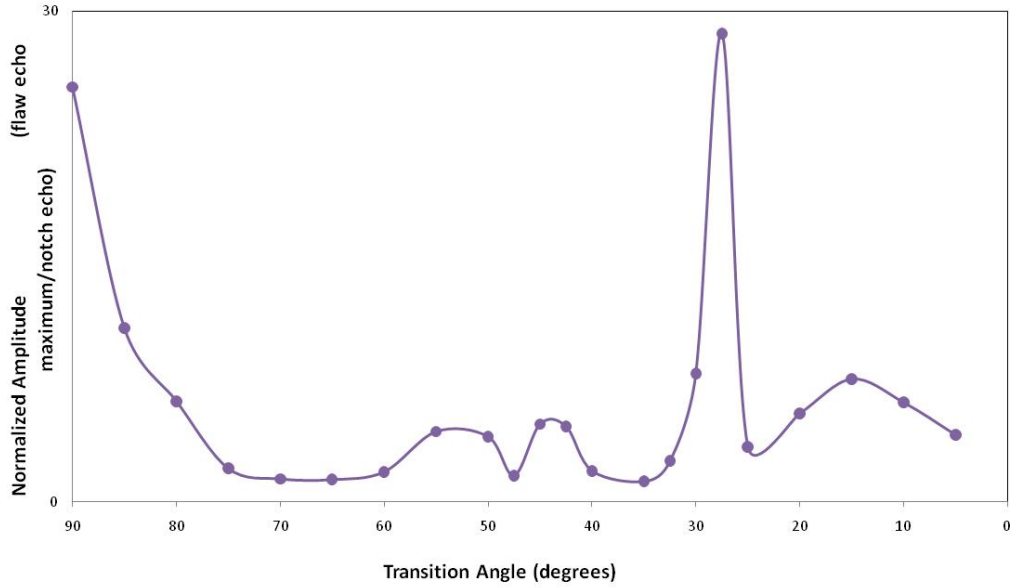

Figure 51. Normalized maximum amplitude of flaw echo versus transition angle

echo. The normalized amplitude decreased sharply from a transition angle of 90° to 75°. However, instead of continuing to decline, the normalized amplitude leveled off and then showed several small peaks along with a significant peak at a transition angle of 30° and a smaller peak at a transition angle of approximately 43°. The peaks were investigated using the ray method, assuming a point source at the end of the rod. Two possible scenarios were considered.

The first scenario considered was the direct longitudinal wave reflection from the transition surface. According to Snell's law (Figure 3), a longitudinal wave reflects at the angle of incidence of the longitudinal wave arrival at the surface, because the wave speeds are the same (Figure 52). Table 10 documents the angle of travel of the reflected longitudinal wave with

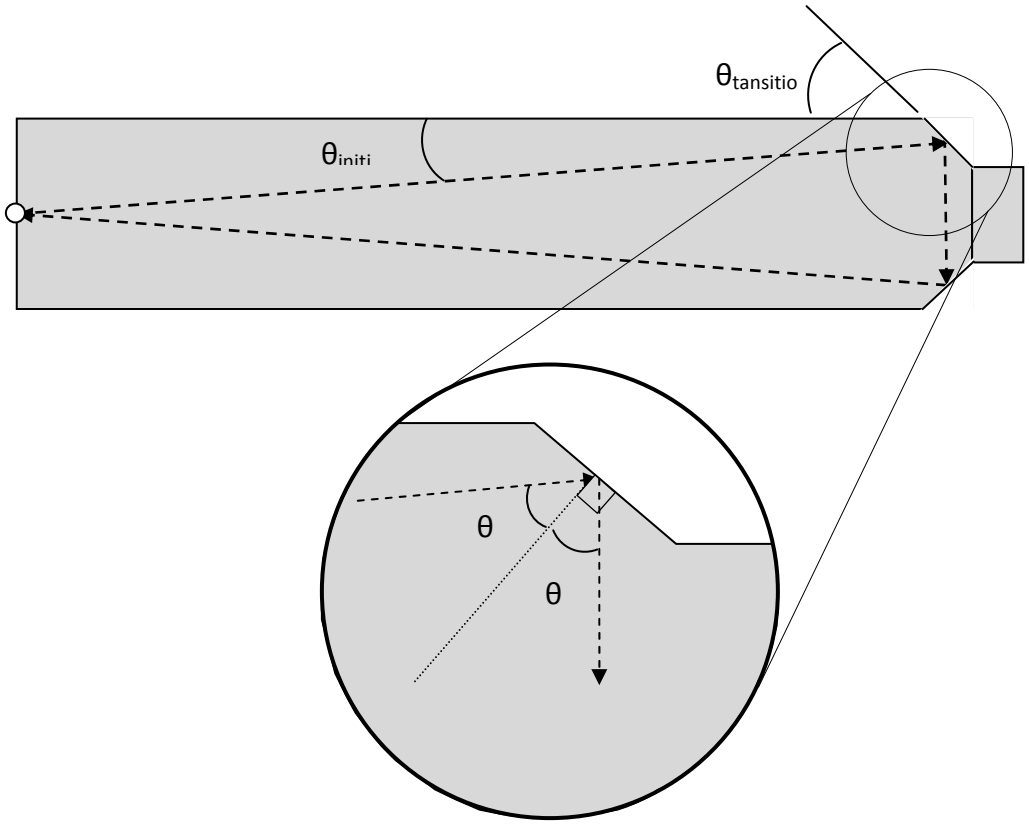

Figure 52. Longitudinal wave reflection from transition surface

respect to the axis of the rod. When the longitudinal wave reflects from the transition surface at a 90° angle to the longitudinal axis of the bar, the wave will reflect from the opposite transition surface one more time and return to the point source, due to symmetry. This 90° reflection occurs at a 42.5° transition angle. This represents the small peak at approximately 43° in Figure 51. The value was approximate because the transducer was approximated as a point source.

Table 10. Angle of longitudinal wave reflection from transition surface

Transition Angle $\theta_{transition}$	Initial Wave Angle $\theta_{initial}$	Incident Angle θ_1	Reflected Wave Relative to Rod Axis θ_{axis}
5	4.76	80.24	165.24
10	4.76	75.24	155.24
15	4.75	70.25	145.25
20	4.73	65.27	135.27
25	4.71	60.29	125.29
30	4.69	55.31	115.31
35	4.67	50.33	105.33
40	4.64	45.36	95.36
42.5	4.62	42.87	90.00
45	4.61	40.39	85.39
50	4.58	35.42	75.42
55	4.55	30.45	65.45
60	4.51	25.49	55.49
65	4.48	20.52	45.52
70	4.44	15.56	35.56
75	4.40	10.60	25.60
80	4.36	5.64	15.64
85	4.33	0.67	5.67
90	4.29	-4.29	-4.29

The second scenario considered was the direct shear wave mode conversion from the transition surface. The initial longitudinal wave mode converts at the transition surface producing a shear wave reflection. According to Snell's law, the shear wave reflects at an incident angle that is dependent upon the arrival incident angle and the speeds of the longitudinal wave (C_1) and shear wave (C_2) (Figure 53). Table 11 documents the angle of travel of the reflected shear wave with respect to the axis of the rod. When the shear wave reflects from the transition surface

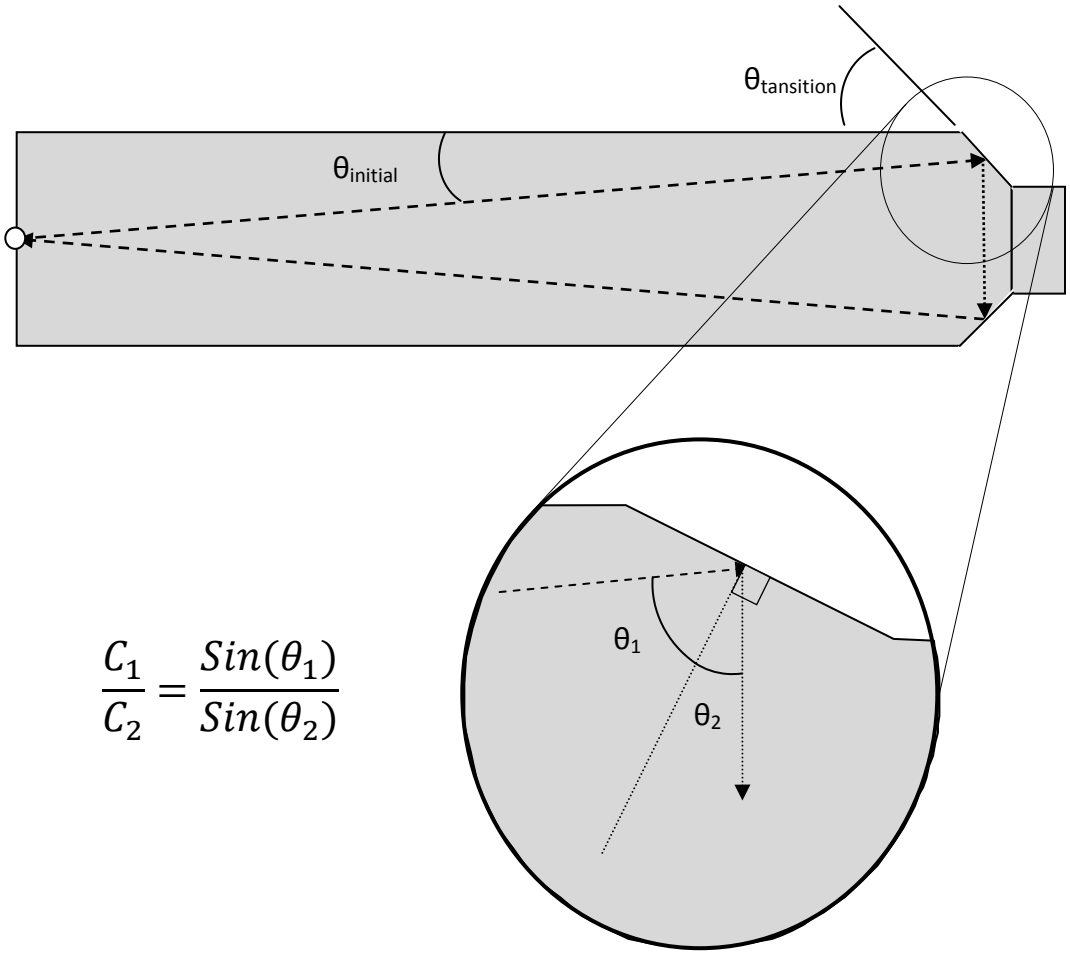

$$\frac{C_1}{C_2} = \frac{Sin(\theta_1)}{Sin(\theta_2)}$$

Figure 53. Shear wave reflection from transition surface

at a 90° angle to the longitudinal axis of the rod, the wave reflects from the opposite transition surface one more time and return to the point source, due to symmetry. This 90° reflection occurs at a 27.8° transition angle. This represents the large peak at approximately 28° in Figure 51. The value was approximate because the transducer was approximated as a point source.

Table 11. Angle of shear wave reflection from transition surface

Transition Angle $\theta_{transition}$	Initial Wave Angle $\theta_{initial}$	Incident Long. Angle θ_1	Incident Shear Angle θ_2	Reflected Wave Relative to Rod Axis θ_{axis}
5	4.76	80.24	32.95	117.95
10	4.76	75.24	32.26	112.26
15	4.75	70.25	31.30	106.30
20	4.73	65.27	30.09	100.09
25	4.71	60.29	28.64	93.64
27.8	4.70	57.50	27.71	90.00
30	4.69	55.31	26.99	86.99
35	4.67	50.33	25.14	80.14
40	4.64	45.36	23.12	73.12
45	4.61	40.39	20.95	65.95
50	4.58	35.42	18.66	58.66
55	4.55	30.45	16.24	51.24
60	4.51	25.49	13.74	43.74
65	4.48	20.52	11.16	36.16
70	4.44	15.56	8.51	28.51
75	4.40	10.60	5.83	20.83
80	4.36	5.64	3.11	13.11
85	4.33	0.67	0.37	5.37
90	4.29	-4.29	-2.37	-2.37

Overall, the results provide evidence to support two conclusions. First, except for the 27.5° transition angle, the flaw echo experienced a significant decrease in amplitude below 80° but was still detectable. The flaw echo was detectable for gradual transitions as low as 5°. Second, transitions cause a delay in the ultrasonic signal between the main bang and the flaw echo. The more gradual the transition, the longer the delay. The largest delay was 23.8 μs for the 5° transition which corresponds to a 5.5 in. in steel rods. Thus, the location of simulated corrosion must be adjusted based upon the transition angle of the simulated corrosion.

5 Williams Commercial Tieback Rod Testing

The rods tested to evaluate the physical geometry of simulated corrosion were machined from 12L14 smooth rod stock. Commercially available tieback rods are typically fabricated with an all-thread surface. Williams commercial tieback rods were selected for testing to evaluate differences in the ultrasonic signal due to the threaded surface.

5.1 Types of Tieback Rods Used in Geotechnical Applications

Various styles of tieback rods have been used in construction of sheet pile systems. The two most common styles are shown below (Figure 54). The upset thread style was common in previous construction. Upset threads are rolled into the steel rod, rather than cut, to ensure the minor diameter of the threads is greater than the outer diameter of the rod. These tieback rods were typically fabricated from smooth A36 steel rod. The majority of current geotechnical practices use all-thread tieback rods. These tieback rods are fabricated from a high grade steel with threads formed along the entire length of the rod.

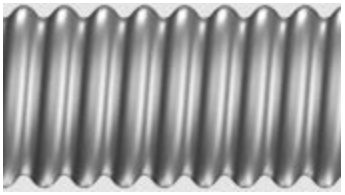

Rods used in old construction (Upset Threads)	Rods used in new construction (All-Thread)

Figure 54. Upset thread and all-thread rods

The ultrasonic signals for 12L14 smooth rod stock and Williams all-thread rods were compared. The rods tested were 10 feet long with a 1.0 in. major diameter. The full ultrasonic signal for each type of rod, including multiple back echoes, is provided in Figure 55. A distinct difference

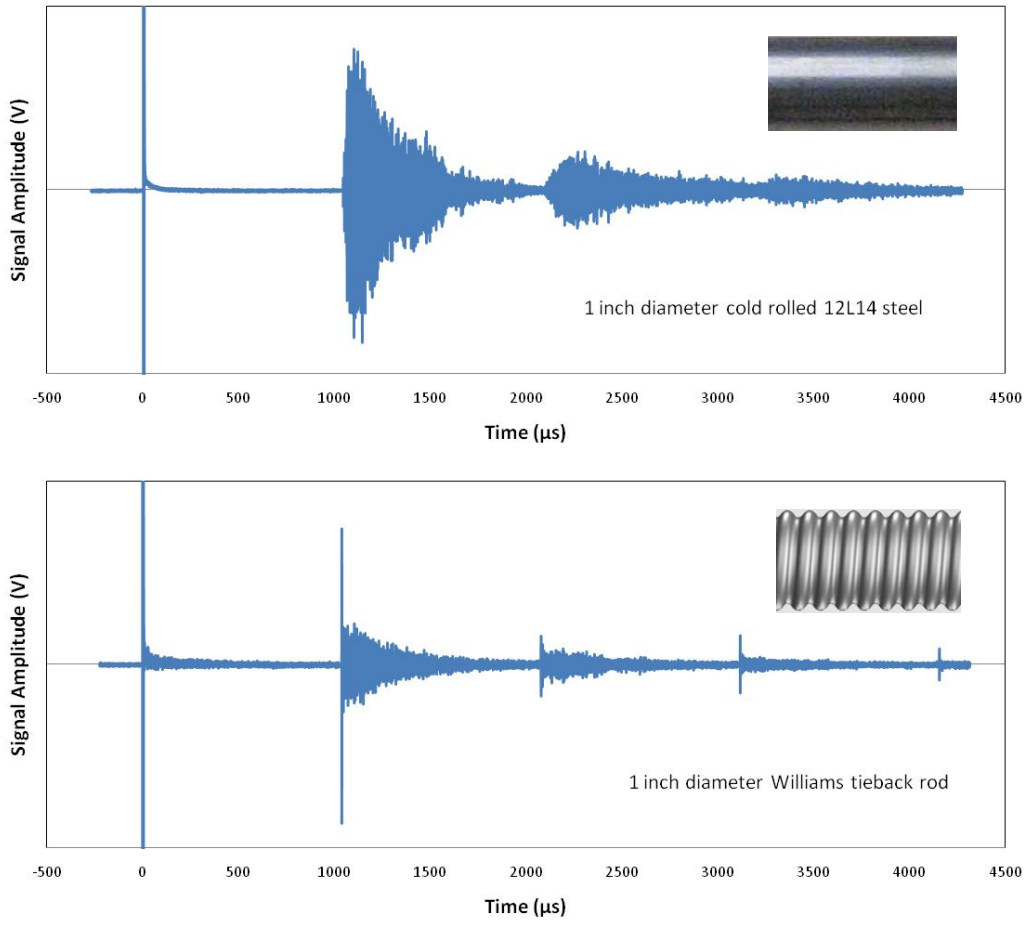

Figure 55. Comparison of 10 ft. long Williams threaded rod and 12L14 smooth steel rod

is evident in the portion of the signal following each back echo for the two rods. Figure 56 provides a closer look at the back echo and subsequent trailing echoes of each rod. The ultrasonic signal for the 12L14 steel rod shows several distinct trailing echoes after the back echo. The Williams tieback rod shows a distinct back echo with only one distinguishable trailing

echo. The time between the back echo and the trailing echo was difficult to measure in the Williams threaded rod due to increased noise in the ultrasonic signal. Threads in the Williams rod cause dispersion of the ultrasonic wave due to spurious reflections from the threaded surfaces. Since trailing echoes involve at least one reflection from the surface of the rod, detecting trailing echoes from a threaded surface proves to be difficult. This implies that calculating the exact outer diameter of a threaded rod may not be possible using the time between trailing echoes (Δt). An approximation of the diameter may be calculated using the Δt between the peaks, instead of the leading edge, of back echo and the first trailing echo.

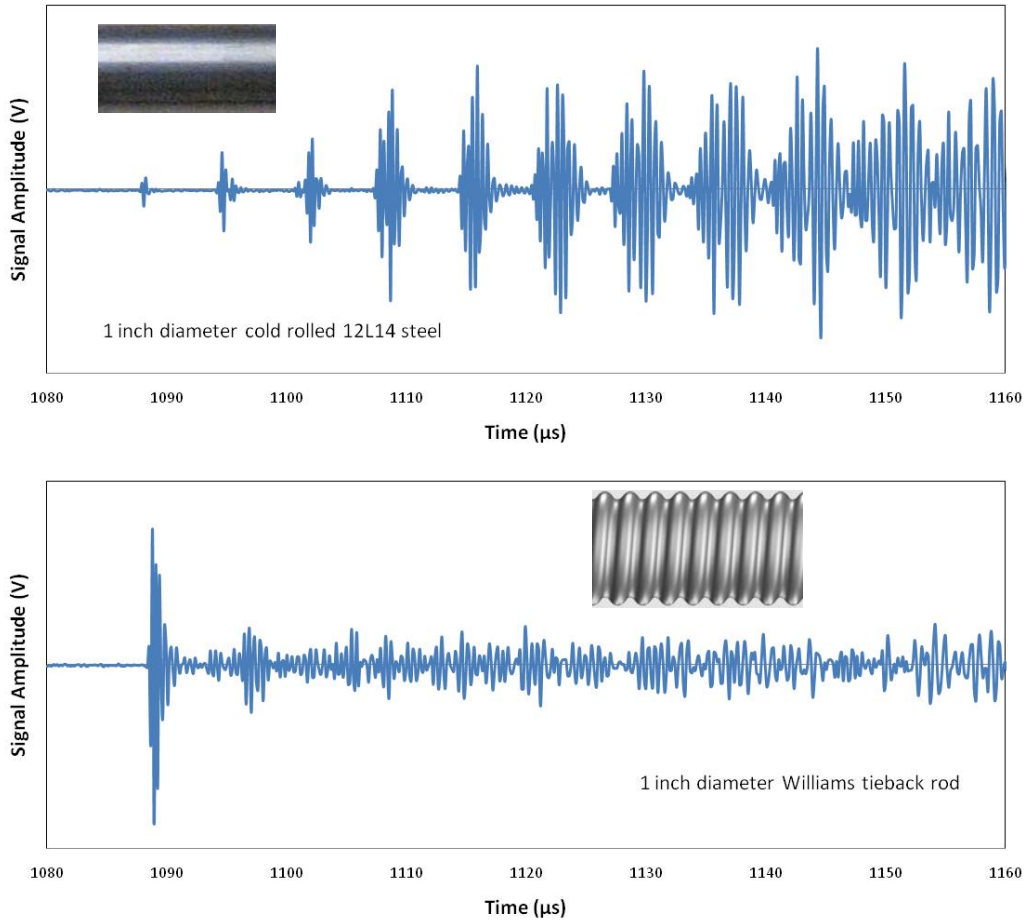

Figure 56. Trailing echo comparison for 12L14 smooth rod and Williams threaded rod

5.2 Projected Length of Rod to be Inspected

The maximum specimen length available for the study was 10 ft. long. Thus, a process was established to determine the maximum detectable rod length using the pulse-echo method with the available commercial ultrasonic transducers. Three rods, 1.0 ft., 3.0 ft., and 6.0 ft. in length, were cut from the same Williams 1.0 in. diameter tieback rod. Each rod was tested with the pulse-echo method using the Olympus NDT M1042 5 MHz magnetic transducer coupled to the end of the rod. The attenuation of the ultrasonic signal was determined by

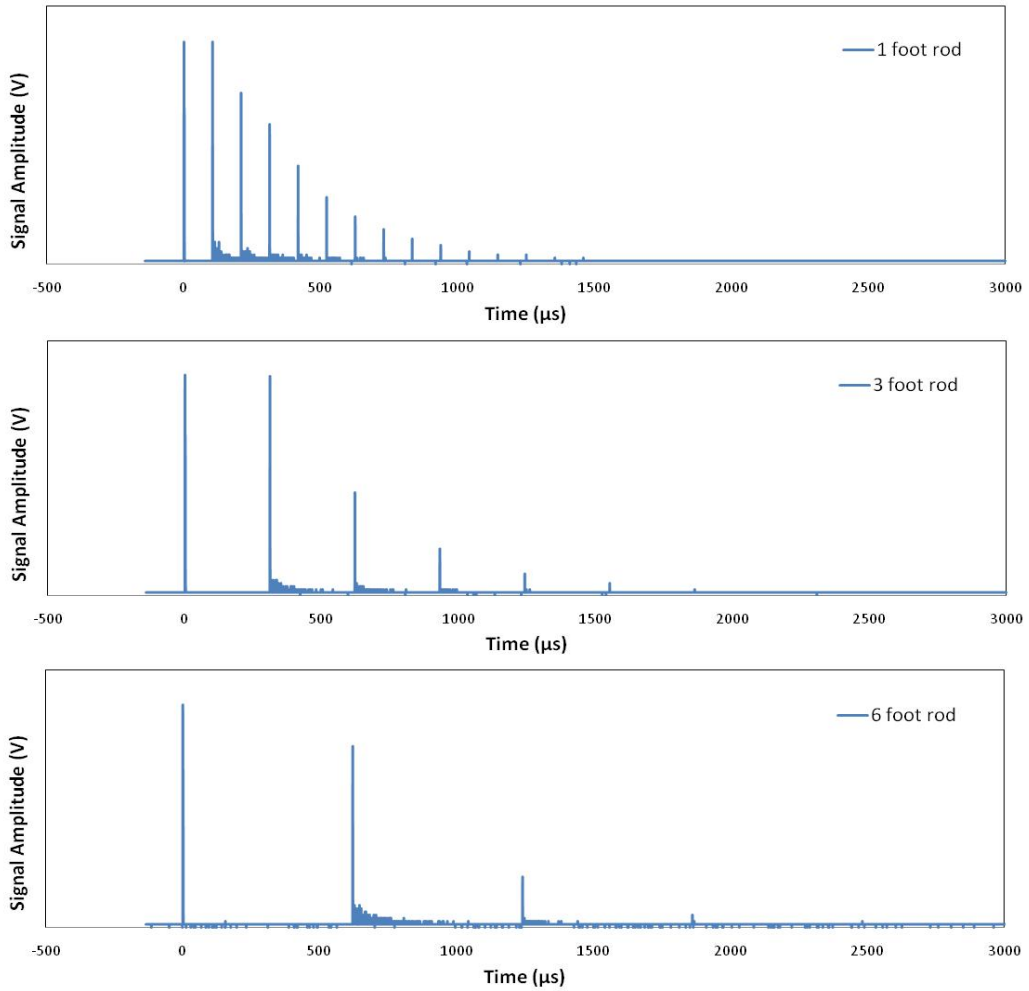

Figure 57. Rectified time domain signals for 1 ft., 3 ft. and 6 ft. long Williams rods

evaluating the peak values of successive back echoes in each rod. A rectified A-scan, which acquires the absolute value of the ultrasonic signal amplitude, including all detectable back echoes, was recorded (Figure 57). The attenuation of the wave amplitude along the rod was defined by Equation 29 (Kolsky, 1963)

$$a = a_o e^{\alpha x} \quad \textbf{Equation 29}$$

where a_o is the initial amplitude, α is the coefficient of attenuation, and x is the distance along the rod. The units of the coefficient of attenuation are Nepers (Np) per length, where a Neper is a dimensionless quantity. The peak amplitude of each back echo was plotted with respect to the distance traveled (Figure 58.) The best fit trend line was calculated and displayed with the

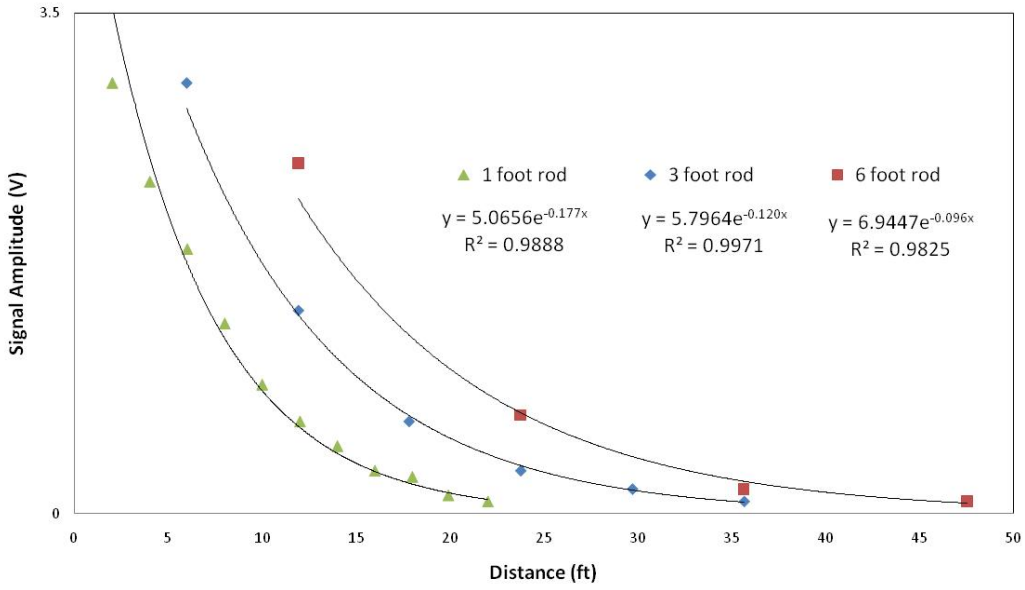

Figure 58. Signal attenuation for 1.0 ft., 3.0 ft., and 6.0 ft. long Williams rods.

equation and R^2 value. The attenuation coefficients (α) for the 1 ft., 3 ft., and 6 ft. rods were 0.177 Np/ft., 0.120 Np/ft., and 0.096 Np/ft. respectively. The differences in magnitude of α were due to scattering which occurred each time the ultrasonic wave reflected from an end of the rod. When the ultrasonic wave traveled an equivalent 12 feet along the 1 ft. long rod, the wave reflected from an end surface 11 times. For the 3 ft. and 6 ft. long rods, the same 12 ft. equivalent length included 3 and 1 end reflections respectively. The results show a decrease in attenuation coefficient with a decrease in the number of end surface reflections. Longer rods have fewer reflections resulting in a smaller attenuation coefficient.

Figure 55 shows that a 10 ft. long 1.0 in. diameter Williams tieback rod exhibits 4 distinct back echoes in the ultrasonic signal. This shows that the pulse echo method using a 5 MHz probe could be used to detect a back echo in a 1.0 in. diameter 40 ft. long Williams tieback rod. This was a conservative estimate since an actual 40 ft. rod would not include the attenuation from the multiple end reflections in the 10 ft. rod.

5.3 Signal Attenuation for Williams Rods in Soil

The effect of ultrasonic signal attenuation in soil was important for testing Williams commercial tieback rods. The amount of energy transmitted into the surrounding medium during ultrasonic inspection of a tieback rod is dependent upon the properties of that medium. Williams tieback rods with various surrounding media were tested to investigate the effect on signal attenuation. Three sections of 3 ft. long Williams tieback rods were placed in plywood boxes with approximately 5.5 in. of cover in each direction. An ultrasonic transducer was coupled to

one end of the tieback rod which protruded through the end of the box (Figure 59). Each box was filled with one of three soils: sand, loose soil, and compacted soil.

Figure 59. Boxes constructed for signal attenuation tests in soils

5.3.1 Soil Characterization

Two soils, sand and Palouse soil, were used in the tests. The sand was collected from a quarry run by Atlas Concrete company in Lewiston, Idaho. The Palouse soil was collected from topsoil in the Palouse region of Washington State. The soils were characterized according to the protocol developed by the Army Corps of Engineers for earth retentions systems, including grain size distribution and Atterberg limit tests (US Army Corps of Engineers, 1994).

A grain size distribution test was performed according to ASTM D422 (ASTM Standard D422, 2007). The results were plotted for each soil in Figure 60 and the coefficient of uniformity (C_u) and coefficient of curvature (C_c) were calculated for each soil. The results were recorded in Table 12.

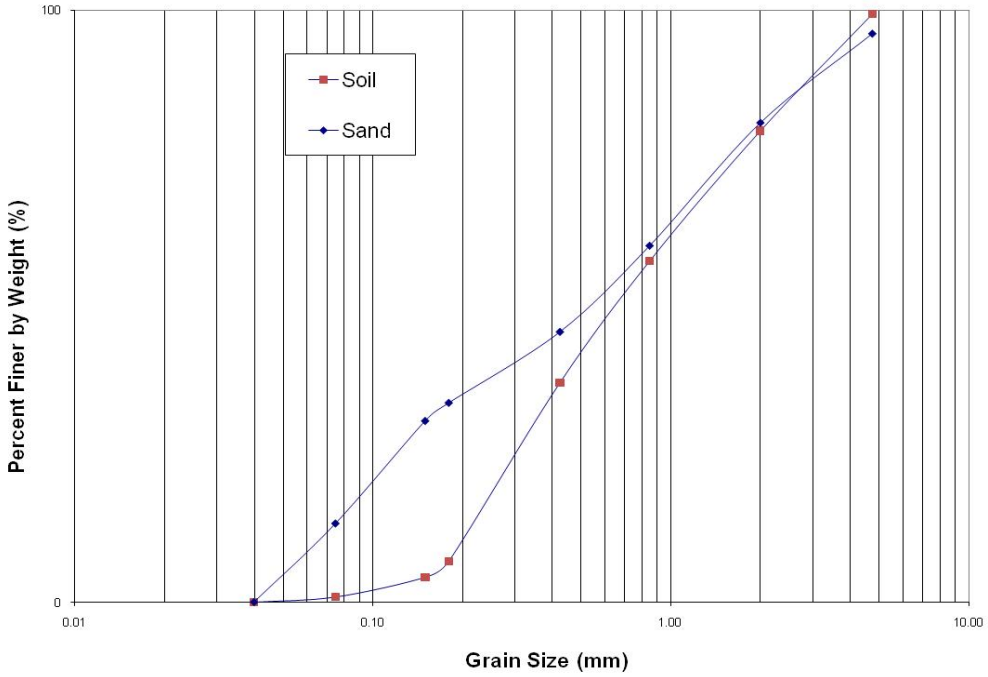

Figure 60. Grain size distribution for sand and soil samples

Table 12. Soil characterization

Type	Coefficient of Uniformity (C_u)	Coefficient of Curvature (C_c)
Sand	4.65	0.66
Palouse Soil	13.08	0.41

Atterberg limits tests were performed according to ASTM D4318 (ASTM Standard D4318, 2005). The Atterberg limits are a scaling system used to characterize the relationship between the water content of a soil and its physical behavior. The liquid limit (LL), plastic limit (PL), plasticity index (PI), and the flow index for the Palouse soil were determined. Figure 61 shows the

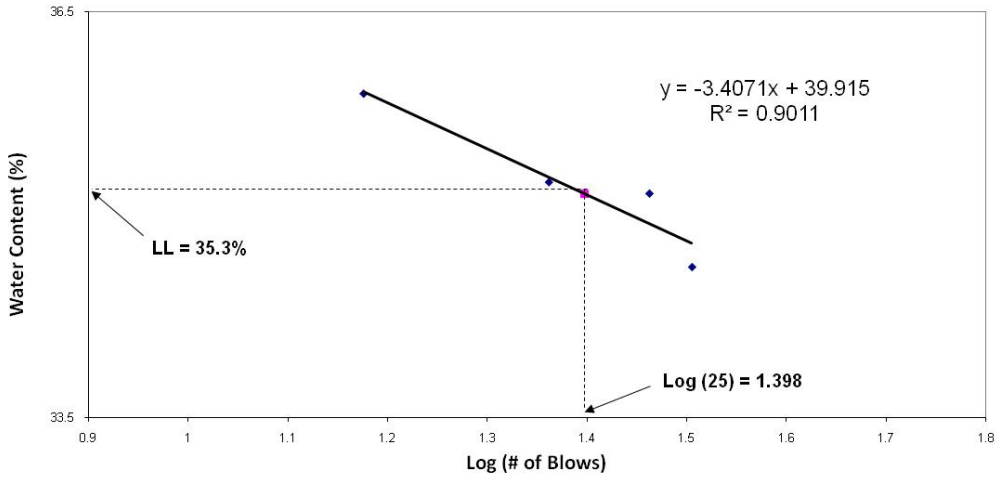

Figure 61. Atterberg limit test of Palouse soil

experimental data used to determine the liquid limit (LL). The plastic limit (PL) was measured experimentally and the plasticity index (PI) and the flow index were calculated using LL and PL. The results were provided in Table 13.

Table 13. Results of Atterberg limit test for Palouse soil

PL	23.4
LL	35.3
PI	11.9
Flow Index	-1.33

Using the soil properties measured, the USCS soil classification was determined for sand and Palouse soil. The sand used was a poorly graded sand (SP) and the Palouse soil was a silty sand (SM).

5.3.2 Soil Preparation

The sand and loose soil were placed in the boxes completely surrounding the Williams tieback rods. For the sand and loose soil no compaction was used. For the compacted soil a 25 lb.

tamper with a 5 in. by 7 in. base plate was used to compact the soil. The soil was compacted in 3 in. layers. Approximately 5 in. of soil was placed in the box without the tieback rod and compacted with approximately 15 blows per square foot. After the second layer was compacted, the Williams tieback rod was positioned in the box. Two more layers of soil were compacted on top of the tieback rod using the same compaction technique.

Each soil was tested with two water contents. The first test was performed using the original water content as it arrived on site, establishing the "baseline" water content. After tests were performed with the "baseline" water content, water was added at a steady rate of 0.2 gallons per minute for 1 hour to saturate the soil. The soil was allowed to drain for 24 hours before the second set of tests was performed. This was considered the "wet" condition. Table 14 records the calculated water content for each soil condition according to ASTM D2216 (ASTM Standard D2216, 2005).

Table 14. Water content for each soil test

	Sand	Loose Soil	Compacted Soil
Baseline	5.28%	12.18%	12.18%
Wet	7.74%	28.21%	25.90%

5.3.3 Signal Attenuation for Tieback Rods in Soil

Attenuation tests of 3.0 ft. sections of threaded Williams tieback rods were performed for the "baseline" and "wet" condition for each soil. Control tests without any surrounding soil were also performed on each of the three rods. The ultrasonic signal was recorded to determine the maximum number of detectable back echoes. The maximum amplitude of each detectable

back echo was plotted, and an exponential decay trend line with R^2 value was added (Figure 62). The exponent value represents the coefficient of attenuation for the signal with respect to

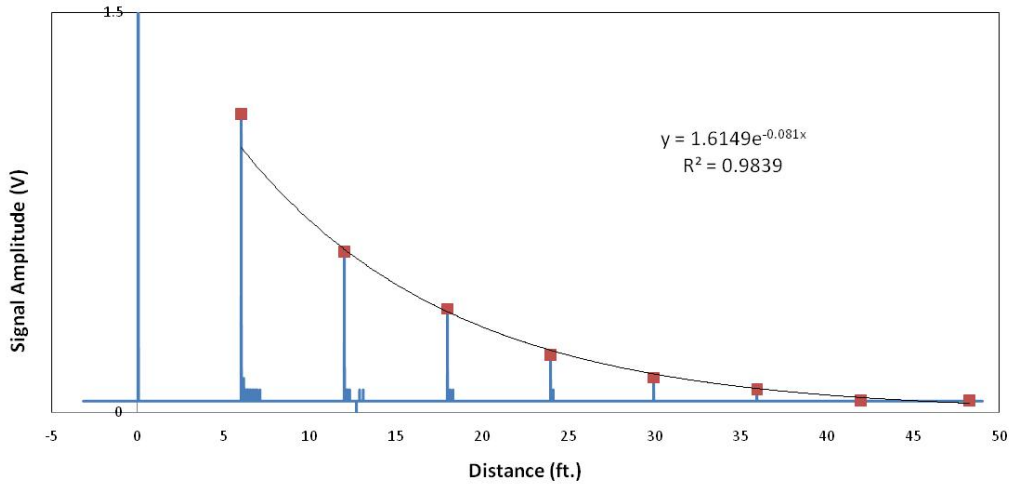

Figure 62. Exponential decay of back echo peaks in 3.0 ft. long Williams rod

distance traveled. In order to evaluate repeatability, 10 signals were recorded for each soil, and the transducer was removed and reapplied after each measurement. The coefficient of attenuation for each condition was averaged, and recorded in Table 15. The results show that there was no major change in attenuation due to the surrounding medium. The control rods for sand, loose soil, and compact soil had an average coefficient of attenuation of 0.0803 Np/ft., 0.0705 Np/ft., and 0.0883 Np/ft. respectively. The discrepancy between each of the control rods was due to variations in the surface at the end of each rod. An increase in surface roughness increases scattering during wave reflection. For sand, the coefficients of attenuation were 0.0803 Np/ft., 0.0793 Np/ft., and 0.0817 Np/ft. for the control, "baseline", and "wet" samples. There was no significant increase in attenuation from the control to the "baseline" or "wet" condition. The "baseline" condition even had a coefficient lower than the control. For

Table 15. Attenuation coefficients of the ultrasonic signal for Williams tieback rods in soils

Sand			Loose Soil			Compacted Soil		
Control	Baseline	Wet	Control	Baseline	Wet	Control	Baseline	Wet
0.081	0.075	0.078	0.072	0.069	0.065	0.095	0.076	0.083
0.074	0.084	0.08	0.068	0.069	0.074	0.094	0.076	0.082
0.084	0.083	0.087	0.066	0.073	0.073	0.083	0.079	0.071
0.079	0.082	0.085	0.065	0.072	0.07	0.083	0.076	0.07
0.079	0.08	0.079	0.064	0.076	0.075	0.093	0.095	0.089
0.083	0.08	0.078	0.077	0.075	0.067	0.081	0.09	0.089
0.08	0.083	0.081	0.073	0.075	0.061	0.088	0.08	0.083
0.079	0.073	0.081	0.073	0.073	0.073	0.089	0.081	0.083
0.083	0.079	0.086	0.075	0.086	0.076	0.093	0.075	0.09
0.081	0.067	0.082	0.072	0.086	0.067	0.084	0.075	0.091
Average	Average	Average	Average	Average	Average	Average	Average	Average
0.0803	0.0793	0.0817	0.0705	0.0754	0.0701	0.0883	0.0803	0.0831
Std. Dev.	Std. Dev.	Std. Dev.	Std. Dev.	Std. Dev.	Std. Dev.	Std. Dev.	Std. Dev.	Std. Dev.
0.0029	0.004	0.0033	0.0045	0.0061	0.0049	0.0053	0.0069	0.0074
CoV	CoV	CoV	CoV	CoV	CoV	CoV	CoV	CoV
0.0361	0.0504	0.0404	0.0638	0.0809	0.0699	0.0600	0.0859	0.0890
	z-Test	z-Test		z-Test	z-Test		z-Test	z-Test
	0.640	-1.008		-2.044	0.190		2.908	1.807

the loose soil the coefficients of attenuations were 0.0705 Np/ft., 0.0754 Np/ft., and 0.0701 Np/ft. for the control, "baseline", and "wet" samples. Again, there was no significant increase in attenuation from the control to the "baseline" or "wet" condition. For the compact soil the coefficients of attenuation were 0.0883 Np/ft., 0.0803 Np/ft., and 0.0831 Np/ft. for the control, "baseline", and "wet" samples. In this case the attenuation coefficients for the "baseline" and the "wet" condition were slightly less than the coefficient of attenuation for the control. The z-Test for each "baseline" and "wet" test compared with the control showed that all tests, except the "baseline" for the compacted soil, were within a 99% confidence interval ($-2.58 \leq z \leq 2.58$). Normalized data is also shown in Table 16 which is calculated by dividing each of the "baseline"

and "wet" condition tests by the average control value for each rod. For example, the average "baseline" value for sand of 0.979 shows that the attenuation coefficient was 97.9% of the average control value. These results show that the attenuation coefficient for the "baseline" and "wet" condition of the ultrasonic signal for sand, loose Palouse soil, and compact Palouse soil was within plus or minus 9.1% for percent water contents up to 7.74%, 28.21%, and 29.50% respectively for Williams tieback rods.

Table 16. Normalized attenuation coefficients of the ultrasonic signal for Williams tieback rods in soils

Sand		**Loose Soil**		**Compacted Soil**	
Baseline	Wet	Baseline	Wet	Baseline	Wet
0.934	0.971	0.979	0.922	0.861	0.940
1.046	0.996	0.979	1.050	0.861	0.929
1.034	1.083	1.035	1.035	0.895	0.804
1.021	1.059	1.021	0.993	0.861	0.793
0.996	0.984	1.078	1.064	1.076	1.008
0.996	0.971	1.064	0.950	1.019	1.008
1.034	1.009	1.064	0.865	0.906	0.940
0.909	1.009	1.035	1.035	0.917	0.940
0.984	1.071	1.220	1.078	0.849	1.019
0.834	1.021	1.220	0.950	0.849	1.031
Average	Average	Average	Average	Average	Average
0.979	1.017	1.070	0.994	0.909	0.941
Std. Dev.	Std. Dev.	Std. Dev.	Std. Dev.	Std. Dev.	Std. Dev.
0.067	0.041	0.086	0.070	0.078	0.084
CoV	CoV	CoV	CoV	CoV	CoV
0.069	0.040	0.080	0.070	0.085	0.090

The percent of the incident wave that is transmitted to the surrounding media during a reflection is dependent upon the impedance of the two materials in contact (Krautkramer & Krautkramer, 1990). If the two materials have the same impedance and are in perfect contact,

then all the energy will transfer through the boundary. The transmittance percent for two dissimilar impedances is given by

$$\boldsymbol{D = \frac{2Z_2}{Z_2+Z_1}} \qquad \textbf{Equation 30}$$

where Z_1 is the impedance of the steel (Z = 46.0 MRayls) and Z_2 is the impedance of the surrounding media, for the materials in this study. Figure 63 shows the transmittance of a steel rod embedded in several surrounding media including water (Z = 1.48 MRayls) and concrete (Z = 8.0 MRayls). For a tieback rod in soil, part of the surrounding media is air (Z = 0.000429 MRayls), which drastically decreases the transmittance of the incident wave to the surrounding media. Considering that a portion of the surrounding media is air and the first back echo only has one reflection, the transmittance is negligible. Thus, the inspectable lengths of tieback rods will not vary when the rods are embedded in soils.

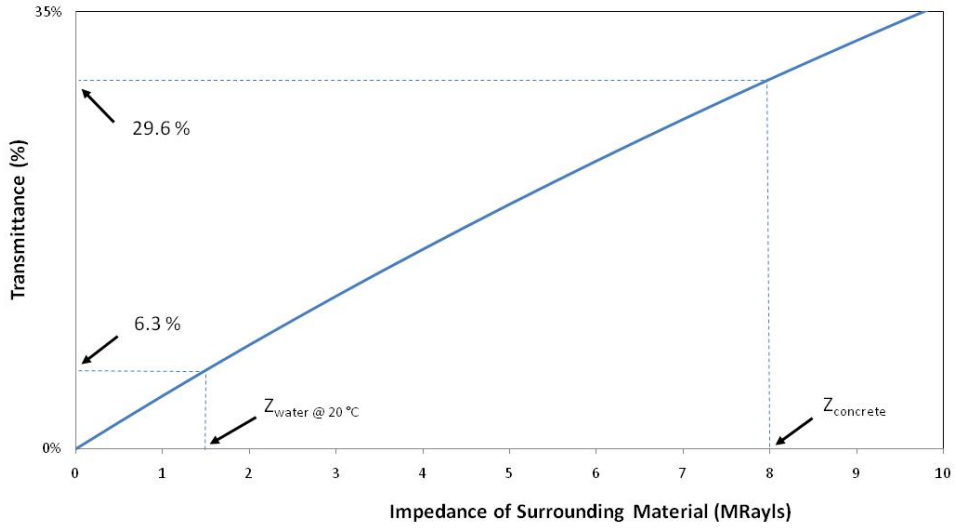

Figure 63. Transmittance for steel with water and concrete surrounding media

5.4 Actual Tieback Rods with Flaws

Simulated corrosion was machined in 3 ft. Williams tieback rod sections to determine if specific geometries could be detected in commercial tieback rods. These included location of simulated corrosion, diameter of simulated corrosion, length of simulated corrosion, and the transition of simulated corrosion.

5.4.1 Location of Simulated Corrosion

Three Williams steel rods, 3 ft. long and 1 in. in diameter, were machined with simulated corrosion at various locations to validate the pulse-echo method for location the leading edge of simulated corrosion in a Williams tieback rod. Simulated corrosion with a 0.5 in. diameter

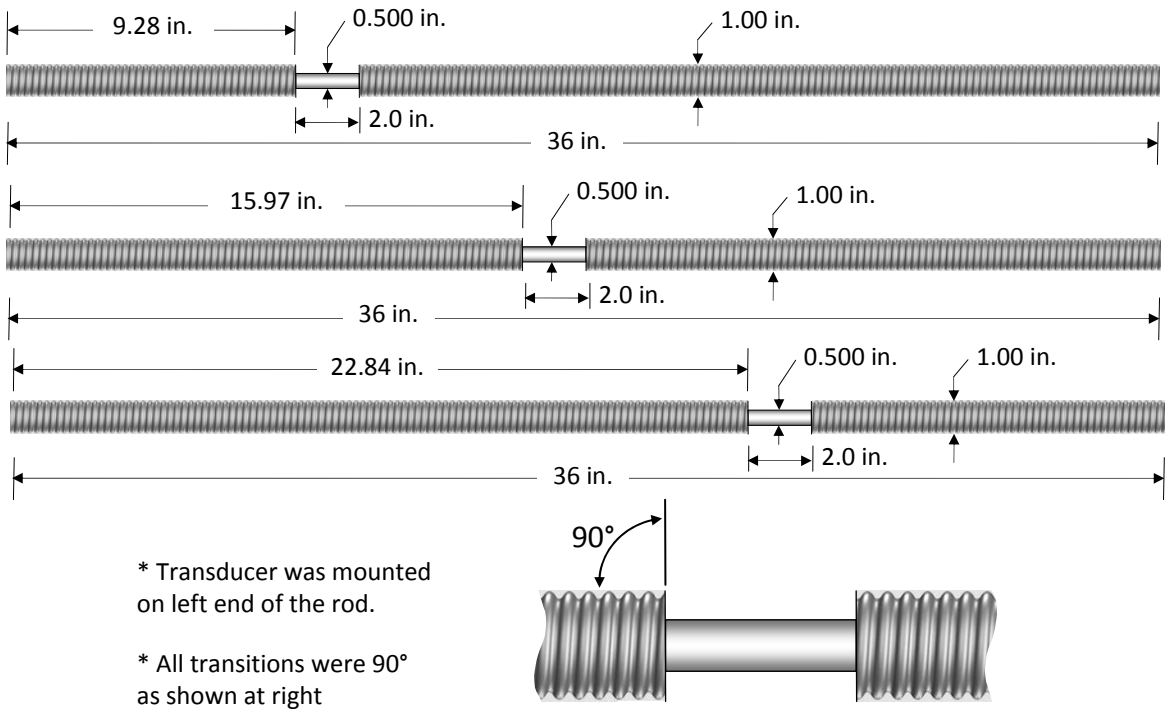

Figure 64. 3.0 ft. long 1.0 in. diameter Williams tieback rods with 2.0 in. length of 0.5 in. simulated corrosion diameter at 9.28 in., 15.97 in., and 22.84 in. along the rod

and 2.0 in. length was machined at 9.28 in., 15.97 in., and 22.84 in. along the length of the steel rods (Figure 64). The location of simulated corrosion was easily detectable based on the time between the main bang and the leading edge of the flaw echo. The following signals (Figure 65) show a flaw echo appearing in the ultrasonic signal that correlates directly with the location of the flaw. The formula for length (Equation 27) was used to determine the location of the flaw (Table 17) for each of the three rods in Figure 65. The three rods showed a maximum percent difference of 1.59% between measured and calculated flaw location. The

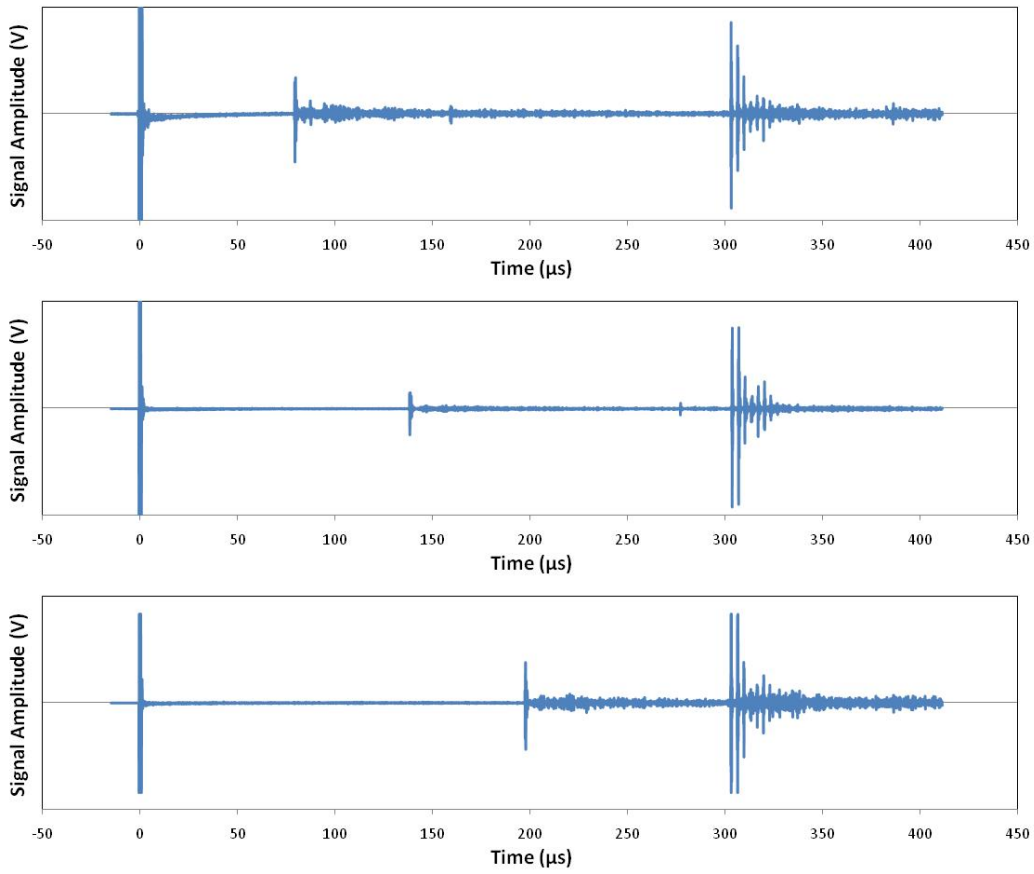

Figure 65. Ultrasonic signals from 3.0 ft. long 1.0 in. diameter Williams tieback rods with 2.0 in. length of 0.5 in. diameter simulated corrosion at 9.28 in., 15.97 in., and 22.84 in. along the rod.

results show that the ability to locate the flaw position was not affected by the threads of the Williams rods.

Table 17. Comparison of measured and calculated location of simulated corrosion

Measured Flaw Location (in.)	Flaw Time (μs)	Calculated Flaw Location (in)	% Difference
9.28	79.3	9.13	1.59%
15.97	138.3	15.93	0.27%
22.84	197.4	22.73	0.47%

5.4.2 Diameter of Simulated Corrosion

To verify the detection of simulated corrosion diameter on Williams tieback rods, two 3 ft. long rods were machined with 0.5 in. diameter and 0.75 in. diameter simulated corrosion regions

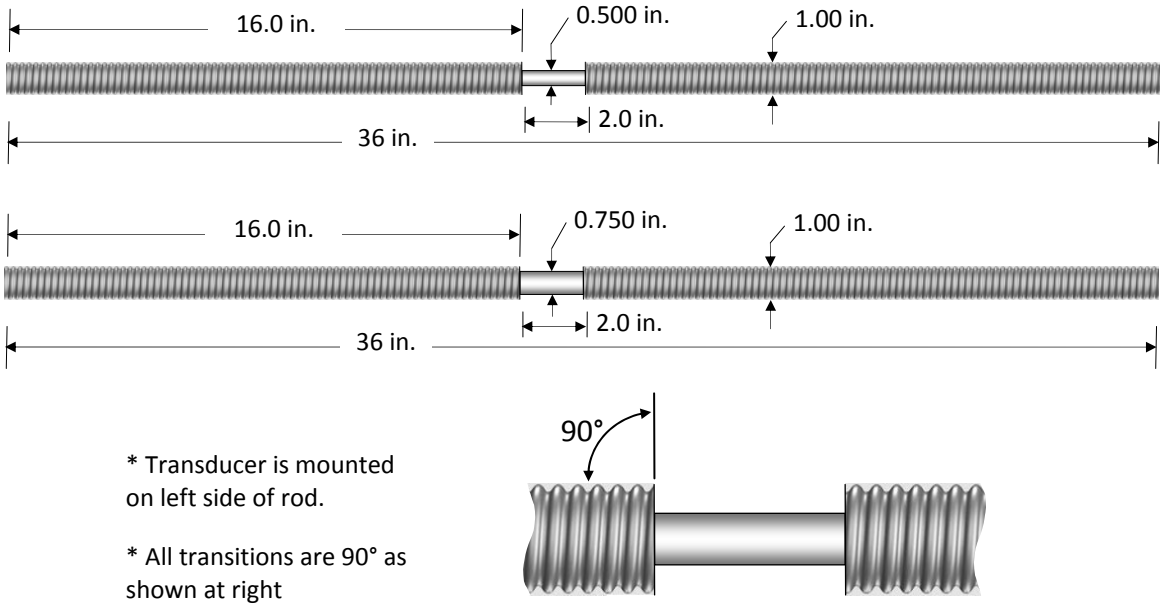

Figure 66. 3.0 ft. long 1.0 in. diameter Williams rods with 2.0 in. lengths of 0.5 in. and 0.75 in. diameter simulated corrosion

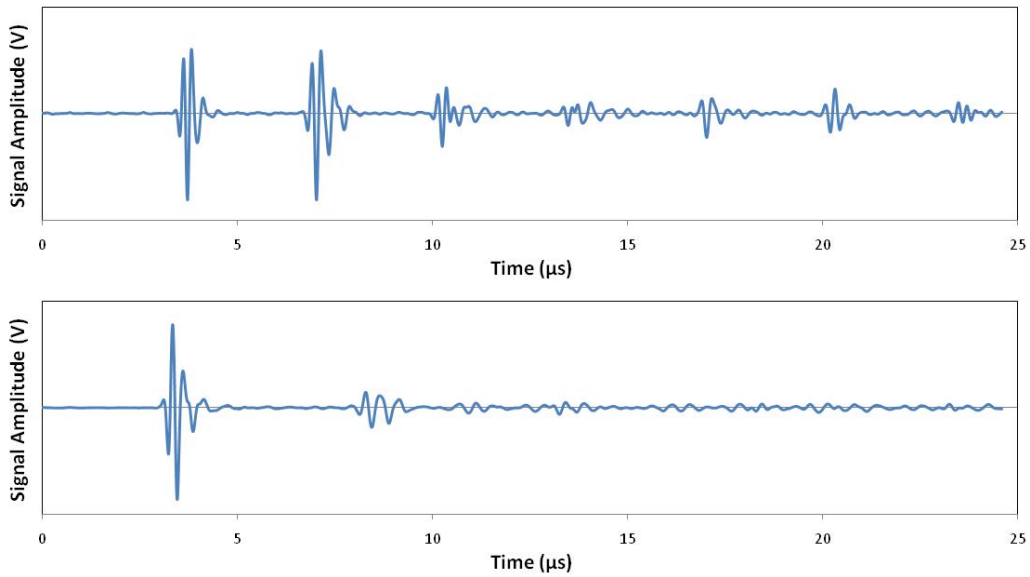

Figure 67. Comparison of Williams rods with 0.5 in. and 0.75in. diameter of simulated corrosion

(Figure 66). The first back echo with each distinguishable trailing echoes was provided in Figure 67. The time between the trailing echoes was measured (Table 18.) Using Equation 25 the diameter was calculated from the spacing of the trailing echoes. The 0.5 in. simulated corrosion diameter rod had a calculated diameter of 0.51 in. resulting in a 1.9% difference. The 0.75 in. simulated corrosion diameter rod had a calculated diameter of 0.73 resulting in a 2.6% difference. This provides a very strong correlation between the minimum diameter (or simulated corrosion diameter) and the time between trailing echoes for the Williams rod.

Table 18. Time between trailing echoes for 0.5 in. and 0.75 in. simulated corrosion diameter

Rod	Smallest Diameter (in.)	Measured Time (µs)	Calculated Diameter (in.)	% Difference
0.5 in. Simulated Corrosion	0.50	3.34	0.51	1.9%
0.75 in. Simulated Corrosion	0.75	4.79	0.73	2.6%

5.4.3 Length of Simulated Corrosion

Two rods were machined with 2 in. and 8 in. lengths of simulated corrosion to investigate the length of simulated corrosion in Williams rods. The 0.5 in. simulated corrosion diameter was machined in 3 ft. lengths of 1 in. diameter Williams rods starting at 9.0 in. from the end

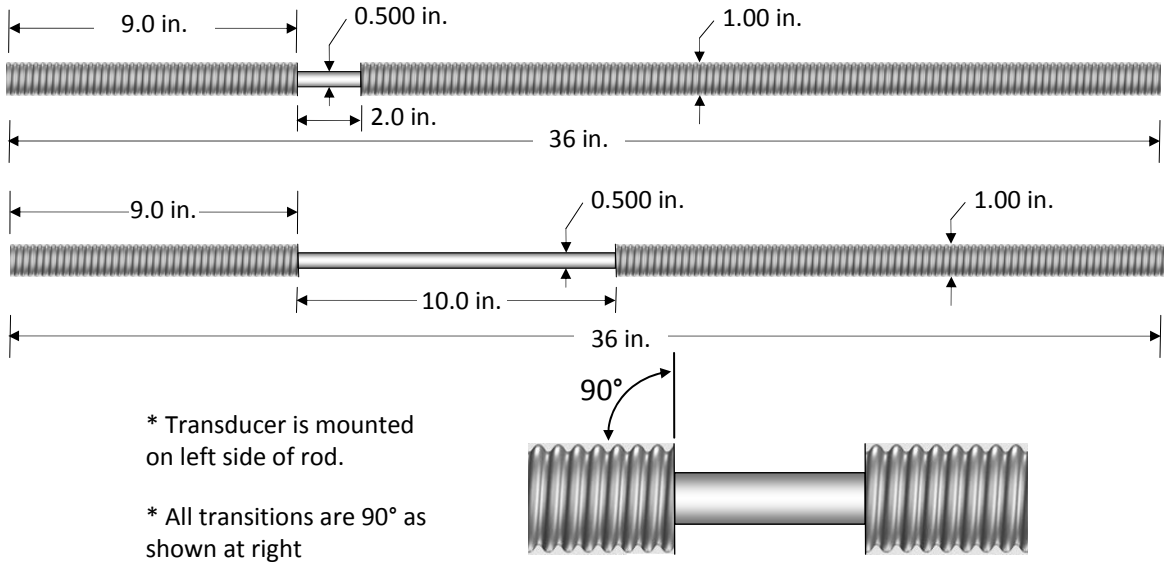

Figure 68. 3.0 ft. long 1.0 in. diameter Williams tieback rods with 2.0 in. and 10.0 in. lengths of 0.5 in. diameter simulated corrosion

(Figure 68). An FFT was taken of the back echo for each rod. The results (Figure 69) show that the peak frequency for the 2in. and 10 in. length of simulated corrosion lies between the 0.5 in. diameter and 1.0 in. diameter 3.0 ft. long rod of 12L14 steel. This shows that the threaded rod does not affect the frequency content of the back echo. The amplitude of the back echo and first trailing echo were also recorded for each rod. The ratio of the first trailing echo to the back echo was calculated and plotted with the data for the 12L14 rods with simulated corrosion (Figure 70). The ratio for the 2.0 in. and 10.0 in. long simulated corrosion was 1.147 and 2.050,

respectively. This was comparable to the 0.972 and 2.307 values for the 12L14 rod with 2.0 in. and 10.0 in. simulated corrosion respectively.

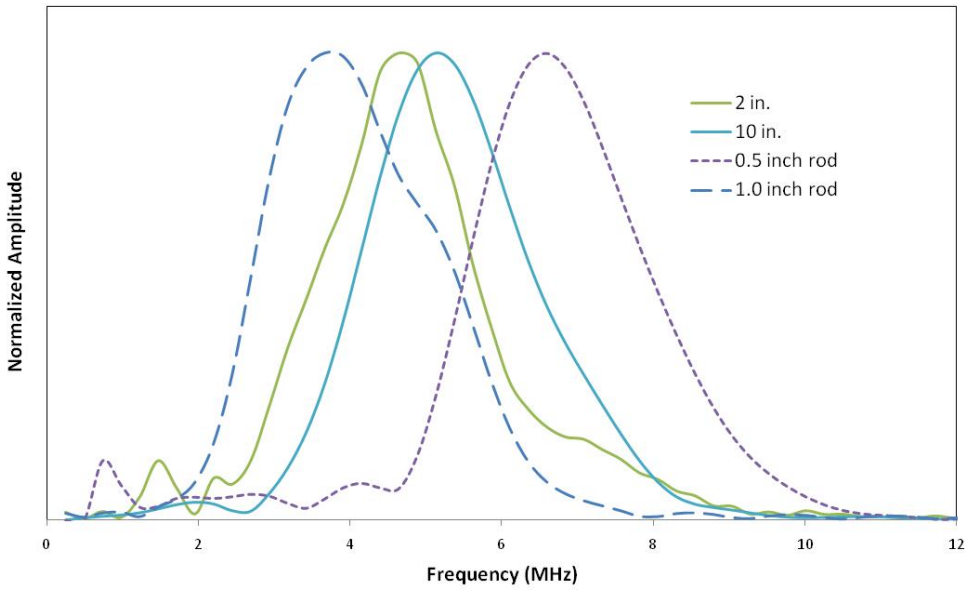

Figure 69. Frequency of ultrasonic signal of Williams rods with 2.0 in and 8.0 in. lengths of simulated corrosion.

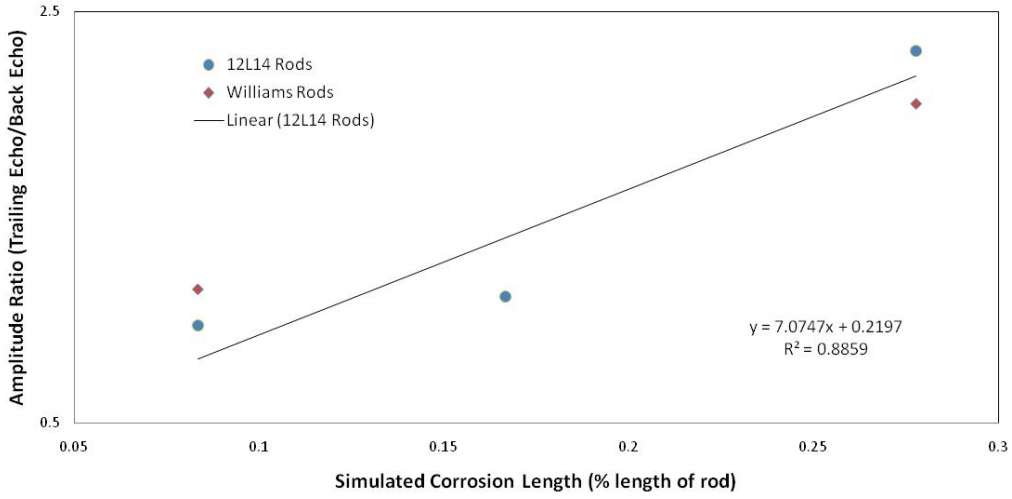

Figure 70. Ratio of trailing echo and back echo for 2.0 in. and 10.0 in. long simulated corrosion in 3.0 ft. long Williams rods

5.4.4 Transition of Simulated Corrosion

Finally, a 3 ft. long Williams rod was machined with a 0.5 in. simulated corrosion diameter and a 45° transition angle (Figure 71). This rod was used to investigate the ability to detect the location, diameter, and length of simulated corrosion for a rod with a 45° transition angle in a Williams rod. The full ultrasonic signal from the pulse-echo test was recorded for the Williams rod with a 45° transition (Figure 72). The signal shows a distinct flaw and back echo. The flaw and back echo were each followed by four distinct trailing echoes.

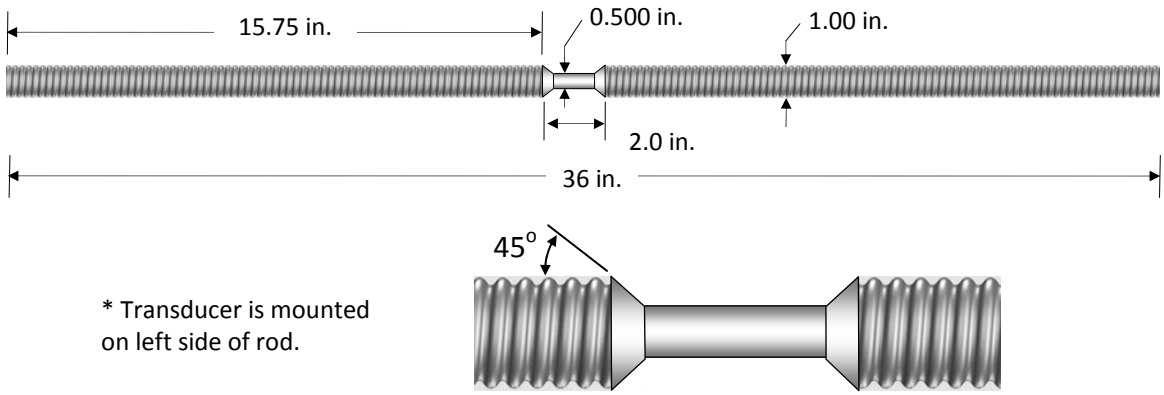

Figure 71. Rod used for simulated corrosion detection with a 45° transition angle

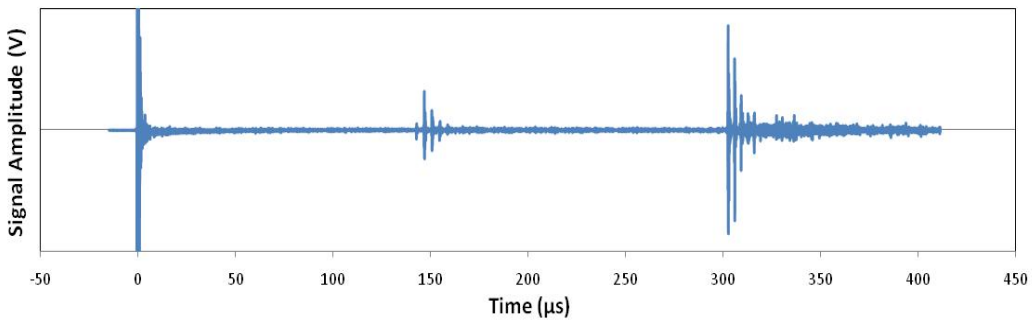

Figure 72. Full ultrasonic signal for 2 in. length of 0.5 in. diameter simulated corrosion with 45° transition angle for Williams tieback rod

The arrival time of the flaw echo was 138.7 µs. Using the longitudinal wave speed of the 75 ksi steel, the flaw location was calculated to be 15.97 in, which has a 1.41% difference from the measured 15.75 in. to the beginning of the transition of the flaw (Table 19). This shows that the method used in the previous chapter for locating the position of simulated corrosion can be used in Williams rods with a 45° transition angle.

Table 19. Calculated simulated corrosion location for Williams rod with 45° transition angle

Measured Flaw Location (in.)	Flaw Time (µs)	Calculated Flaw Location (in)	% Difference
15.75	138.7	15.97	1.41%

The back echo and subsequent trailing echoes were recorded for the Williams rod with a 45° transition angle. The back echo and four trailing echoes were visible (Figure 73.) The arrival time of the first back echo and two trailing echoes were used to calculate the time between echoes. This time between trailing echoes was used to calculate the diameter of the simulated

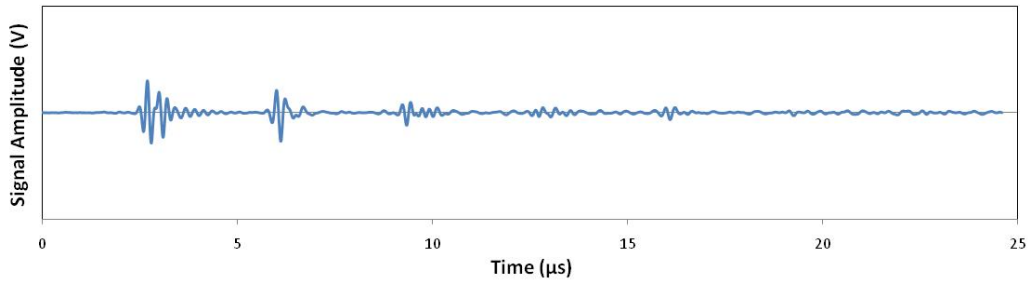

Figure 73. First back echo and successive trailing echoes for 2 in. simulated corrosion with 45° transition

corrosion according to Equation 25 (Table 20). The calculated diameter was 0.502 in. which had a 0.4% difference from the measured value of 0.500 in. This shows that the method for detecting the diameter of simulated corrosion can be used for Williams rods with a 45° transition angle.

Table 20. Comparison of measured and calculated diameter of simulated corrosion for Williams rod with 45° transition angle

Rod	Smallest Diameter (in.)	Measured Time (μs)	Calculated Diameter (in.)	% Difference
0.5 in. simulated corrosion	0.500	3.27	0.502	0.4%

The FFT of the first back echo was recorded for the Williams rod with a 2 in. length of simulated corrosion and a 45° transition angle. The result was plotted with the FFT signals from a 0.5 in. diameter and 1.0 in. diameter 3.0 ft. long rods of 12L14 steel. The results show that the

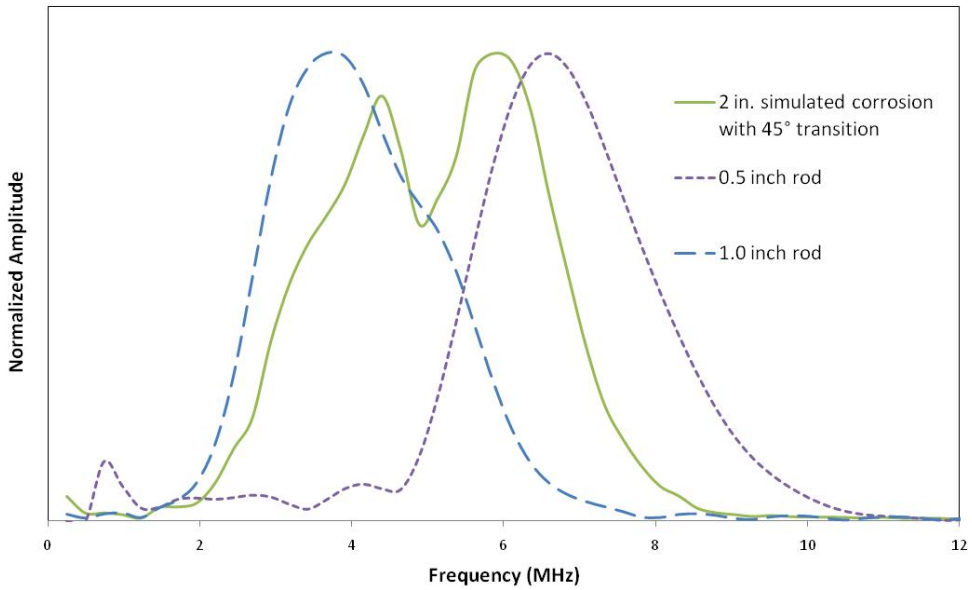

Figure 74. Frequency of back echo of 2 in. long 0.5 in. diameter simulated corrosion with 45° transition in Williams rod

frequency domain for the Williams rod with a 45° transition lies between the frequency domain for the 0.5 in. and 1.0 in. rod. The frequency domain of the ultrasonic signal for the Williams rod with simulated corrosion has two major peaks as compared to the single peaks for the rods without any corrosion.

The amplitude of the back echo and first trailing echo were also recorded. The ratio of the first trailing echo to the back echo was calculated and plotted with the data for the 12L14 rods with simulated corrosion (Figure 75). The ratio for the 2.0 in. long simulated corrosion with a 45° transition was 0.865. There was an 11% difference from the 0.972 value for the 12L14 rod.

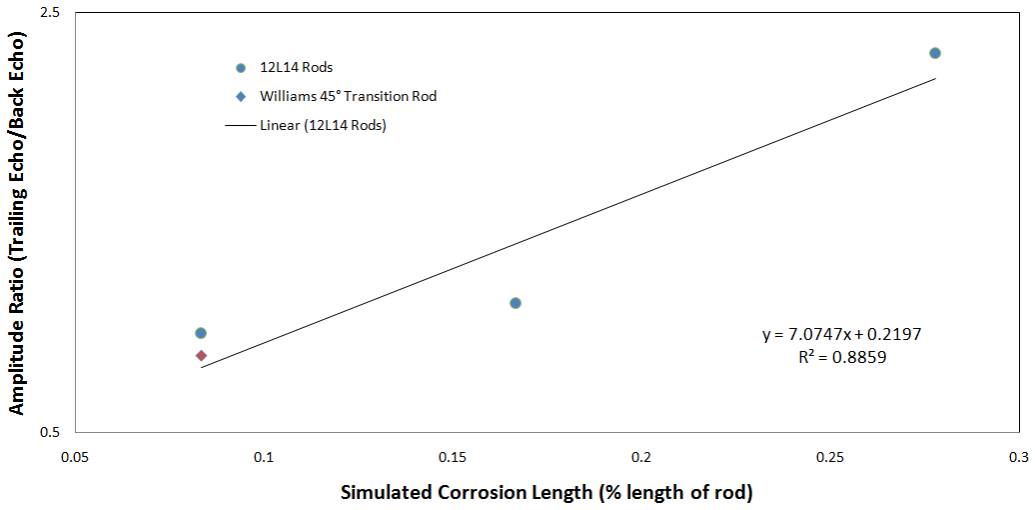

Figure 75. Ratio of trailing echo and back echo for 2.0 in. simulated corrosion length with 45° transition in 3.0 ft. long Williams rods

6 Inspection Procedures

This chapter outlines the recommended procedures for inspecting steel tieback rods for corrosion in the field. The tests performed in the previous sections involved simulated corrosion of steel tieback rods. Inspection of rods in the field would involve rods with actual corrosion. Actual corrosion incorporates a rough surface in the corroded region as opposed to the smooth surfaces of simulated corrosion. The following guidelines consider these differences in developing inspection procedures for field testing.

6.1 Inspection of Simulated Corrosion

The research performed at Washington State University identified methods to determine the location and diameter of simulated corrosion on 1.0 in. diameter 12L14 steel rods and 1.0 in. diameter Williams steel all-thread tieback rods. Figure 76 depicts the full ultrasonic signal for a

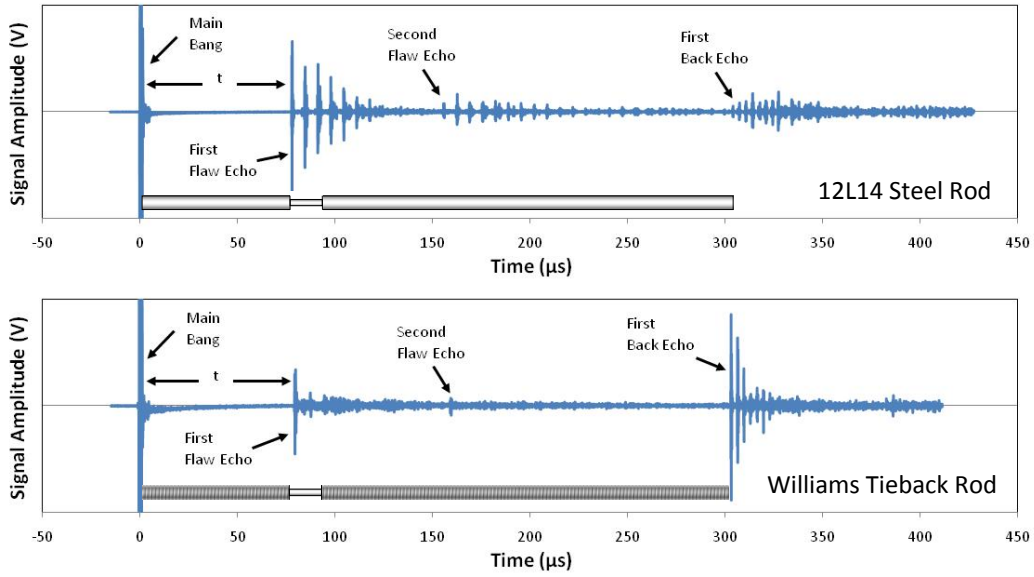

Figure 76 Ultrasonic pulse-echo signal for 12L14 smooth steel rod and Williams steel all-thread tieback rod both with simulated corrosion

3.0 ft. long 1.0 inch diameter 12L14 smooth surface rod and a Williams commercial tieback rod both with a 2.0 in. long section of 0.5 in. diameter simulated corrosion starting 9.0 in. from the left end. Older construction practices included smooth A36 steel rods with upset threads at either end, and current practices use Williams, DWYIDAG, SAS or Con-Tec all-thread rods. The location of the simulated corrosion can be identified from the ultrasonic signal. If the length is known, any echo that appears before the back echo is evidence of corrosion, cracking, or some other flaw. The location of a flaw is calculated based on the time between the "main bang" and the "flaw echo". The length, L, from the transducer to the leading edge of simulated corrosion can be calculated using Equation 30 where C_1 is the bulk longitudinal wave speed of the

$$L = \frac{C_1 \cdot t}{2} \qquad \textbf{Equation 31}$$

material and t is the time between the main bang and the leading edge of the flaw echo. The typical value for the longitudinal wave speed in steel is C_1 = 19,190 ft/s. The time, t, is

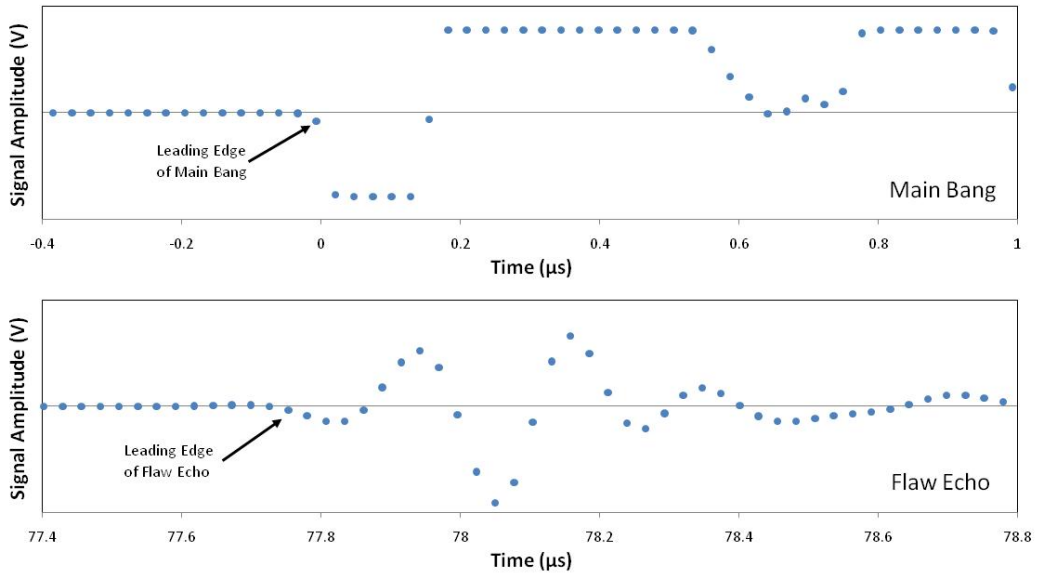

Figure 77. Location of the leading edge for the main bang and flaw echo

measured from the leading edge of the main bang to the leading edge of the flaw echo. The leading edge for each echo is defined as the first point that appears outside the bounds of the signal noise. Figure 77 plots each point of the ultrasonic signal in the range of the main bang and the flaw echo to identify the leading edge. For rods with a transition from the original diameter to the flaw diameter, the measured time may include a delay from the actual flaw location. The maximum delay for a 5° transition angle in a 1.0 in. diameter rod with 0.5 in. diameter simulated corrosion was 23.8 µs, which corresponds to an error of 0.44 in. for determining the location of the flaw.

Figure 78 depicts the back echo and trailing echoes for a 3.0 ft. long 1.0 inch diameter 12L14 smooth surface rod and a Williams commercial tieback rod, both with a 2.0 in. long section of 0.5 in. diameter simulated corrosion starting 17.0 in. from the left end of the rod. The time between the trailing echoes following the first back echo can be directly related to the diameter

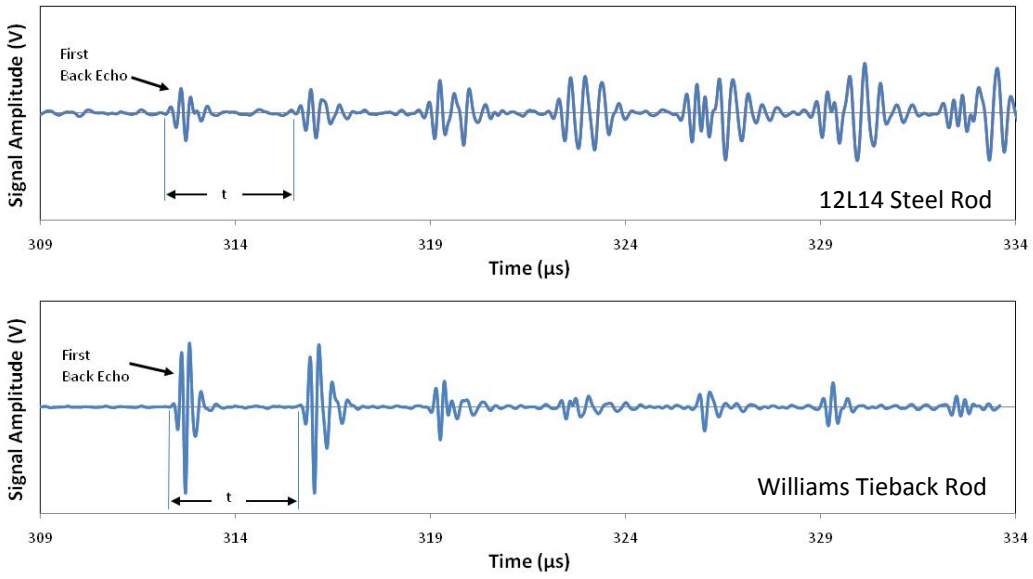

Figure 78. First back echo and subsequent trailing echoes for inspection of simulated corrosion diameter inspection in 1.0 in. diameter 12L14 steel rod and 1.0 in. diameter Williams rod

of simulated corrosion. Equation 31 correlates the diameter of the rod (d) to the time between echoes (Δt), based upon the speed of longitudinal wave propagation (C_1) and the speed of transverse wave propagation (C_2). The time between trailing echoes is measured in the same

$$\boldsymbol{d = \frac{\Delta t\, C_1 C_2}{\sqrt{C_1^2 - C_2^2}}} \quad \textbf{Equation 32}$$

manner as the time between the main bang and the flaw echo. The individual points of each echo are plotted to identify the leading edge which is the first point to raise above or below the noise of the signal. Typical values for the longitudinal and shear wave speed in steel are C_1 = 19,190 ft/s and C_2 = 10,597 ft/s. The diameter of simulated corrosion can be used in conjunction with the original diameter to determine the reduction in load capacity. Equation 32 depicts the percent load capacity for a rod with simulated corrosion.

$$\%_{\textbf{load capacity}} = \frac{\mathbf{d_c}^2}{\mathbf{d_o}^2} \quad \text{Equation 33}$$

The load capacity is dependent upon the diameter of the corroded region, d_c, and the original rod diameter, d_o. The ability to identify the location and diameter of corrosion provides an inspector with the ability to approximate the structural integrity of a tieback rod.

The selection of the ultrasonic transducer is critical when inspecting a tieback rod. The main variables to consider in commercial transducers are the diameter of the transducer and the frequency of the ultrasonic signal generated. The transducer diameter should be as large as possible without exceeding the diameter of the rod. An increase in the diameter of the

transducer results in an increase in the energy generated in the ultrasonic wave which in turn increases the range of inspection. The transducer wavelength is dependent upon the diameter of the tieback rod and the smallest expected flaw dimension. To ensure bulk wave propagation the transducer wavelength should be at least one order of magnitude less than the diameter of the rod. The wavelength of the ultrasonic signal will determine the minimum flaw detectable in the specimen. The minimum detectable flaw dimension is approximately the wavelength of the ultrasonic pulse frequency introduced into the medium (Figure 17). These two criteria will determine the transducer frequency selection.

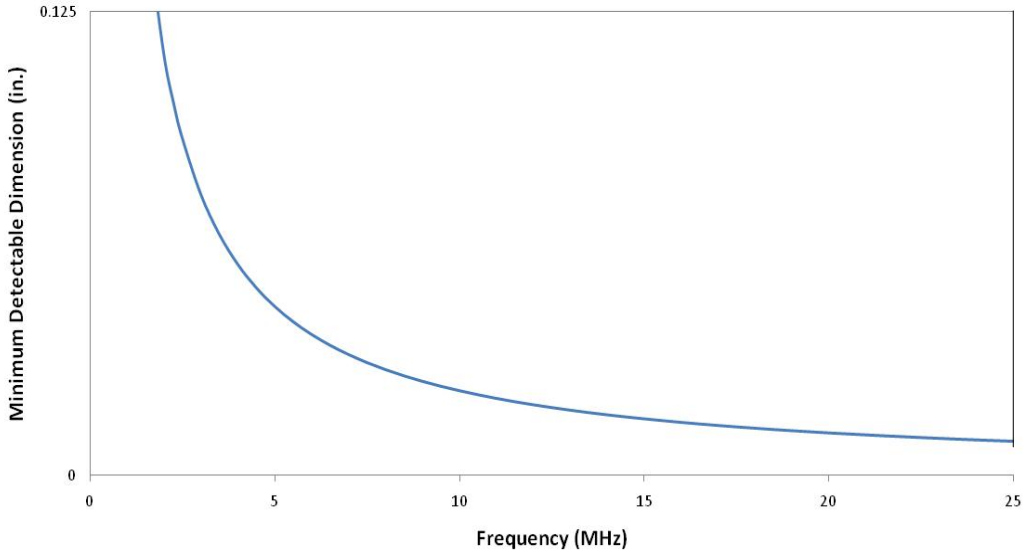

Figure 79. Minimum detectable flaw dimension in steel

6.2 End preparation and Transducer Coupling

A significant variation in the amplitude of the signal can occur due to the condition of the rod end. If the surface is not planar, the wave will experience dispersion from a reflection from the

end of the rod. Another source of amplitude loss can occur in the coupling of the transducer to the rod. It is imperative to have a smooth planar surface to attach the transducer. Thus, it may be necessary to cut a new surface at the end of the rod. Also, contaminants located between the transducer and the end of the rod may result in poor transfer of energy to the rod. Therefore, the end of each rod must be cleaned, and a couplant gel applied before the transducer is coupled to the end of the rod. Without the gel, the transducer will not effectively couple the ultrasonic signal into the rod, resulting in an extremely poor ultrasonic wave, if any at all. A magnetic transducer is also recommended to provide a consistent adhering force between the transducer and the end of the rod.

6.3 Commercial Tieback Rod Testing

The following guidelines are presented to assist in developing an inspection procedure for tieback rods in the field. Transitioning from testing smooth 12L14 samples to in-situ testing of commercial tieback rods introduces several potential limitations. First, turnbuckles are often used when a design calls for rods longer than 50 ft. An ultrasonic signal is not able to propagate through the turnbuckle, thus only the first section of rod is inspectable. Second, actual corrosion will not have a smooth surface, or a single diameter. The irregular surface of actual corrosion will increase scattering of the ultrasonic wave during reflection. Third, curvature in the tieback rod may eliminate the detection of the back echo. If a direct line of sight through the rod from the front to the back of the rod is eliminated then detection of a direct back echo is not possible. These factors may limit the effectiveness of ultrasonic inspection in some scenarios. The following charts provide guidelines for the use of the ultrasonic pulse-echo

method for inspecting tieback rods. The guidelines are divided into two sections. The first section covers inspections of new construction. These guidelines assume that initial ultrasonic pulse-echo measurements will be performed after the placement of the rods and prior to the facade construction, which covers the ends of the tieback rods. The second section covers inspection of existing construction. This section is divided into two sections. The first sub-section includes tieback rod lengths that are recorded in the design plans. The second section is for inspection of tieback rods with unknown length.

6.3.1 New Construction

This section introduces inspection guidelines for tieback rods in new construction. Performing several measurements during the construction can significantly increase the ability to monitor corrosion in steel tieback rods. An ultrasonic pulse-echo measurement performed after the placement of the rods, and prior to the façade construction generates a "control signal" to compare with subsequent measurements during the life of the rod. The control signal should include two separate inspections. First, a full signal showing all detectable back echoes, and second the first back echo with all detectable trailing echoes. The full signal can be used to calculate the actual longitudinal wave speed of each rod, using the time between the main bang and the first back echo. A published value for the shear wave speed, C_2 = 10,597 ft/s will be used. The following is a series of steps to aid in future inspections:

Step #1: Calculate the longitudinal wave speed from the "control signal"

Determine the time between the main bang and the first back echo from the control signal. Using the rod length and Equation 30 calculate the longitudinal wave speed.

Step #2: Perform a pulse-echo inspection on the tieback rod

Record three different sections of the ultrasonic signal. First, record the full signal, extending to the first back with all detectable trailing echoes. Second, record the back echo with all detectable trailing echoes. Third, record any flaw echo and all detectable trailing echoes that appear before the back echo.

Step #3: Compare the "control signal" with the full ultrasonic signal from the inspection

Note any differences between the "control signal" and the inspection signal recorded in Step #1. Any echo that appears before the back echo represents a flaw in the rod. Also, any variation in the amplitude of the back echo or subsequent trailing echoes can represent the growth of a flaw, or bending of the tieback rod.

Step #4: Verify the length of the tieback rod

Measure the time between the main bang and the back echo. Use this measurement to calculate the length of the rod, using the longitudinal wave speed from Step #1 with Equation 30. Compare the calculated rod length with the original rod length to ensure that there are no complete breaks in the rod.

Step #5: Verify the outer diameter of the tieback rod

If a flaw echo does not exist, calculate the time between trailing echoes after the back echo. If a flaw echo exists, calculate the time between trailing echoes after the flaw echo. Using the appropriate time between trailing echoes, the longitudinal wave speed from Step #1, a shear wave speed of 10,597 ft/s and Equation 31 to calculate the diameter of the rod. The original diameter of the rod should be visible from the exposed end of the tieback rod. The calculated diameter and the original diameter should be approximately the same. Measuring the time between trailing echoes may be difficult for threaded rods, because the threads cause dispersion of the ultrasonic wave when it mode converts and reflects from the outer diameter to create the trailing echoes.

Step #6: Calculate the location of the flaw (if a flaw echo exists)

Measure the time between the main bang and the first flaw echo. Use this measurement to calculate the distance to the flaw, using the longitudinal wave speed from Step #1 with Equation 30. Repeat this step for each distinct flaw echo. Be careful not to mistake a second flaw echo as an additional. An echo that appears at twice the distance of the first flaw is most likely a second flaw echo and not an additional flaw.

Step #7 Determine the minimum diameter of the tieback rod (if a flaw exists)

Measure the time between the back echo and the first trailing echo. Use this measurement to calculate the minimum diameter of the rod, using the longitudinal wave speed calculated in Step #1, and a shear wave speed of 10,597 ft/s with Equation 30.

6.3.2 Existing Construction

Interpretation of inspection of existing construction is more difficult than new construction. Since there is not a control signal generated during the construction process, these guidelines must be divided into two sub-categories. The first approach assumes that the original plans are available which identify the original rod length. The second approach is for inspection of rods of unknown length.

6.3.2.1 Original rod length is known

Rods with a known length provide dimensions to identify the back echo in the ultrasonic signal. The following is series of steps to aid in inspection of tieback rods of known length:

Step #1: Calculate the time between the main bang and the back echo

Using the length of the rod and a longitudinal wave speed of C_1 = 19,190 ft/s calculate the expected time between the main bang and the back echo using Equation 30.

Step #2: Perform a pulse-echo inspection on the tieback rod

Record three different sections of the ultrasonic signal. First, record the full signal, extending to the first back with all detectable trailing echoes. Use the expected time from the main bang to the trailing echo from Step #1 to approximate the time window necessary to capture the entire signal. Second, record the back echo with all detectable trailing echoes. Third, record any flaw echo that appears before the back echo and all detectable trailing echoes.

Step #3: Verify the length of the tieback rod

Measure the time between the main bang and the back echo in the ultrasonic signal. Use this measurement to calculate the length of the rod, using a longitudinal wave speed of C_1 = 19,190 ft/s with Equation 30. Compare the calculated rod length with the original rod length to ensure that there are no complete breaks in the rod.

Step #4: Verify the outer diameter of the tieback rod

If a flaw echo does not exist, calculate the time between trailing echoes after the back echo. If a flaw echo exists, calculate the time between trailing echoes after the flaw echo. Using the appropriate time between trailing echoes and Equation 31, calculate the diameter of the rod.

Measuring the time between trailing echoes may be difficult for threaded rods, because the threads cause dispersion of the ultrasonic wave when it reflects and mode converts from the outer diameter to create the trailing echoes.

Step #5: Calculate the location of the flaw (if a flaw echo exists)

Measure the time between the main bang and the first flaw echo. Use this measurement to calculate the distance to the flaw, using a longitudinal wave speed of C_1 = 19,190 ft/s with Equation 30. Repeat this step for each distinct flaw echo. Be careful not to mistake a second flaw echo as second flaw. An echo that appears at twice the distance of the first flaw is most likely a second flaw echo and not a second flaw.

Step #6 Determine the minimum diameter of the tieback rod (if a flaw exists)

Measure the time between the back echo and the first trailing echo. Use this measurement to calculate the minimum diameter of the rod, using the longitudinal wave speed of C_1 = 19,190 ft/s, and a shear wave speed of C_2 = 10,597 ft/s with Equation 30.

6.3.2.2 Unknown length of rod

A rod with unknown length requires a close inspection of the trailing echoes to identify possible flaws in the rod. The following is series of steps to aid in inspection of tieback rods of unknown length:

Step #1: Perform a pulse-echo inspection on the tieback rod

Record three different sections of the ultrasonic signal. First, record the full signal, including all detectable echoes. Second, record the furthest echo with all detectable trailing echoes. Third, record any other echo that appears in the signal with all detectable trailing echoes.

Step #2: Determine if no detectable flaws are present

Measure the time between trailing echoes for each echo recorded. Using the time between trailing echoes, a longitudinal wave speed of C_1 = 19,190 ft/s, a shear wave speed of 10,597 ft/s and Equation 31 calculate a diameter for each set of trailing echoes. If the corresponding diameter for the first two sets of trailing echoes is approximately equal to the original diameter of the rod, then the echoes represent the first and second back echoes. Since no flaw echoes

appear between the main bang and the first back echo, there are no detectable flaws in the rod.

Step #3: Identify the minimum diameter in the tieback rod

If any of the diameters calculated in Step #2 are less than the original diameter, then there is a flaw present in the rod. The minimum diameter calculated may not be the actual minimum diameter of the rod, because the signal may have reflected from a crack in the rod, or the flaw that represents a smaller diameter in the rod. Without knowing the length of the rod, determining the absolute minimum diameter is impossible.

Step #4: Calculate the partial length of rod inspected for minimum diameter

The partial length inspected for simulated corrosion can be calculated using the second to last echo detected. The second to last echo represents the last reduced diameter that the ultrasonic wave traveled through before returning to the transducer. Record the time between the main bang and the second to last echo. Use this measurement to calculate the inspected length of rod using a longitudinal wave speed of C_1 = 19,190 ft/s with Equation 30.

7 Summary and Conclusions

This dissertation concentrated on the detection of simulated corrosion in steel tieback rods. Ultrasonic signals were used to determine the physical geometry of 0.25 in., 0.50 in., and 0.75 in. diameter simulated corrosion in 1.0 in. diameter steel rods. Research was also performed to investigate the use of ultrasonic waves in Williams commercial tieback rods. Guidelines were developed for inspecting tieback rods with actual corrosion in field applications.

The location, diameter, length, and transition of concentric simulated corrosion were investigated for straight steel rods. For a 90° transition angle, the location of simulated corrosion was detectable based upon the time between the main bang and the flaw echo in the ultrasonic signal and the longitudinal wave speed of the steel. A decrease in the transition angle results in a delay in the arrival time of the flaw echo. The largest delay was 23.8 μs for the 5° transition which represents a potential error of 5.5 in. when estimating the location.

The minimum diameter of concentric simulated corrosion in a straight rod was detectable based upon the distance between the back echo and the first trailing echo, and the longitudinal and shear wave speeds of the steel in accordance with previous research by Light & Joshi (Light & Joshi, 1987). The time between the back echo and first trailing echo is exclusively dependent upon the minimum diameter of the rod, and is not dependent upon the transition angle of the simulated corrosion.

The length of concentric simulated corrosion in a straight rod was detectable based on two different techniques. First, an increase in the peak frequency of the back echo correlated with

an increase in the length of simulated corrosion. Second, the ratio of the amplitude of the first trailing echo and the back echo correlated with an increase in the length of simulated corrosion.

The investigation of the transition of the simulated corrosion concluded that the flaw echo is detectable for abrupt transitions of 90° down to as small as 5°. The flaw echo experienced a decrease in amplitude below a 80° transition angle but was still detectable. Two peaks were evident at transition angles of 27.5° and 45°. These peaks correlate to a shear and longitudinal wave reflection directly across the rod from the transition surface.

Williams all-thread tieback rods were investigated including projected detectable rod length, signal attenuation due to surrounding media, and simulated corrosion in tieback rods. The signals in tieback rods showed a distinct back echo, with low signal amplitude following, due to the dispersion of the wave from the threads. Since the back echo did not reflect from the threads, the amplitude was not affected. The signal attenuation tests revealed that there was no significant amplitude loss in the back echo for sand, loose soil, or compact soil. A projected detectable rod length was found to be 40 feet with the pulse-echo method. Finally, simulated corrosion in Williams tieback rods showed that location and diameter of simulated corrosion were detectable in threaded rods with a 90° and a 45° transition angle.

The work presented in this dissertation forms original research that contributes to the following fields:

1. Safety of structures within the field of Civil Engineering
2. Adding to the current literature of NDT testing

These contributions include:

1. Effect of transitions on the ultrasonic signal
2. Effect of length of corrosion on the ultrasonic signal
3. Effect of soil on tieback rod signal attenuation
4. Detection of simulated corrosion in Williams tieback rods

Based on the research presented, the following recommendations were made for future research.

1. Investigate the minimum detectable cross-section loss in 1.0 in. diameter tieback rods. For example, machine rods with 0.8125 in., 0.875 in, 0.9375 in. diameter of simulated corrosion and identify the smallest simulated corrosion that exhibits a flaw echo.
2. Investigate the detectability of simulated corrosion in larger diameter tieback rods. For example, machine simulated corrosion in 2.0 in. and 3.0 in. diameter Williams rods, and identify the detectable geometries.
3. Investigate the detectability of additional geometric characteristics of simulated corrosion on the ultrasonic signal for the pulse-echo method. For example:
    - machine simulated corrosion with a variation in diameter in the corroded region, instead of uniform reduced diameter.
    - machine non-concentric loss of cross-section in steel rods.
4. Investigate the detection of ultrasonic signals in rods with curvature to mimic rods that have bent during settlement. Bend multiple commercial tieback rods to various radii and monitor the ultrasonic signal.

5. Investigate the effect of various thread characteristics on the ultrasonic signal using commercial tieback rods from a variety of manufacturers. Include all-thread rods from DWYIDAG, SAS and Con-Tec.
6. Investigate in situ testing to establish “control signals” for tieback rods in new or existing construction, followed by periodic monitoring to assess changes in the ultrasonic signal that occur due to field conditions over time.
7. Investigate multiple simulated corrosion regions in the same rod. For example, machine rods with multiple lengths of 0.5 in. diameter simulated corrosion in the same rod, or multiple lengths of 0.5 in. and 0.75 in. diameters.
8. Investigate the detectability of actual corrosion in steel rods on the ultrasonic signal. Use accelerated-corrosion in salt spray chambers to induce corrosion.

References Cited:

ASTM Standard A108. (2007). *Standard Specification for Steel Bar, Carbon and Alloy, Cold-Finished , DOI: 10.1520/A0108-07* . West Conshohocken, PA: ASTM International.

ASTM Standard A29. (2005). *Standard Specification for Steel Bars, Carbon and Alloy, Hot-Wrought, General Requirements for , DOI: 10.1520/A0029_A0029M-05* . West Conshohocken, PA: ASTM International.

ASTM Standard A615. (2008). *Standard Specification for Deformed and Plain Carbon-Steel Bars for Concrete Reinforcement , DOI: 10.1520/A0615_A0615M-08B* . West Conshohocken, PA: ASTM International.

ASTM Standard D2216. (2005). *Standard Test Methods for Laboratory Determination of Water (Moisture) Content of Soil and Rock by Mass , DOI: 10.1520/D2216-05* . West Conshohocken, PA: ASTM International.

ASTM Standard D422. (2007). *Standard Test Method for Particle-Size Analysis of Soils , DOI: 10.1520/D0422-63R07* . West Conshohocken, PA: ASTM International.

ASTM Standard D4318. (2005). *Standard Test Methods for Liquid Limit, Plastic Limit, and Plasticity Index of Soils , DOI: 10.1520/D4318-05* . West Conshohocken, PA: ASTM International.

Beard, M., Lowe, M., & Cawley, P. (2001). Inspection of Rockbolts using Guided Ultrasonic Waves. *Review of Progress in Quantitative Nondestructive Evaluation* , 1156-1163.

Bray, D. E., & Stanley, R. K. (1989). *Nondestructive Evaluation.* New York: CRC Press.

Davies, R. (1948). A Critical Study of the Hopkinson Pressure Bar. *Phil. Transactions* , 375-457.

Esser, A. J., & Dingeldein, J. E. (2007). Failure of Tieback Wall Anchors Due to Corrosion. *Geo-Denver 2007*, (pp. 1-10). Denver.

Hudson, G. (1943). Dispersion of Elastic Waves in Solid Circular Cylinders. *Physics Review* , 46-51.

Kolsky, B. (1963). *Stress Waves in Solids.* New York: Dover Publications Inc.

Krautkramer, J., & Krautkramer, H. (1990). *Ultrasonic Testing of Materials.* Berlin: Springer-Verlag.

Light, G. M., & Joshi, N. R. (1987). Ultrasonic Waveguide Technique for Detection of Simulated Corrosion Wastages. *Nondestructive Testing Communications* , 13-27.

Main, L. G. (1988). *Vibrations and Waves in Physics.* New York: Cambridge University Press.

Niles, G. B. (1996). In Situ Method for Inspecting Anchor Rods for Section Loss Using the Cylindrically Guided Wave Technique. *IEEE Transactions of Power Delivery* , 1601-1605.

Pochhammer, J. (1876). About the reproduction speeds of small vibrations in an infinite isotropic circular cylinder. *Journal of Pure and Applied Math* , 324-336.

Pollock, D. G. (1997). *Reliability Assessment of Timber Connections Through Ultrasonic Inspection of Bolts.* Texas A&M University.

US Army Corps of Engineers. (1994, March 31). Retrieved January 18, 2009, from Design of Sheet Pile Walls: http://140.194.76.129/publications/eng-manuals/em1110-2-2504/

Williams Form Engineering Corp. (2008). Retrieved April 2, 2009, from Tie Rod Information: http://www.williamsform.com/